

UNIVERSITY OF GLASGOW

CHEMISTRY DEPARTMENT

ELECTRON PARAMAGNETIC RESONANCE SPECTROSCOPY OF
SOME COMPLEXES OF MANGANESE(VI) AND RHENIUM(VI)

being

A thesis submitted in part fulfilment of the requirements

for the

DEGREE OF DOCTOR OF PHILOSOPHY

by

ALI HUSAIN HUMOOD AL-MOWALI

October, 1974

ProQuest Number: 11018019

All rights reserved

INFORMATION TO ALL USERS

The quality of this reproduction is dependent upon the quality of the copy submitted.

In the unlikely event that the author did not send a complete manuscript and there are missing pages, these will be noted. Also, if material had to be removed, a note will indicate the deletion.



ProQuest 11018019

Published by ProQuest LLC (2018). Copyright of the Dissertation is held by the Author.

All rights reserved.

This work is protected against unauthorized copying under Title 17, United States Code
Microform Edition © ProQuest LLC.

ProQuest LLC.
789 East Eisenhower Parkway
P.O. Box 1346
Ann Arbor, MI 48106 – 1346

ELECTRON PARAMAGNETIC RESONANCE SPECTROSCOPY OF SOME
COMPLEXES OF MANGANESE(VI) AND RHENIUM(VI)

Summary

This thesis is subdivided into six main parts, which are summarised separately below.

Part I

The principles of electron paramagnetic resonance spectroscopy are discussed in this introductory section, with particular reference to transition metal complexes of the type studied in this work.

Part II

This section describes a study of rhenium oxychloride, ReOCl_4 , and some of its adducts $\text{ReOCl}_4 \cdot 2\text{C}_4\text{H}_8$, $\text{ReOCl}_4 \cdot \text{OPCl}_3$, $\text{ReOCl}_4 \cdot \text{NCCH}_3$ and $[(\text{C}_6\text{H}_5)_4\text{As}] [\text{ReOCl}_5]$. The X-band e.p.r. spectra of ReOCl_4 and its adducts have been recorded in solution at 290K and in magnetically dilute glasses at 77K, and these spectra are analysed in detail. The spin Hamiltonian parameters A_0 , g_0 , A , B , Q' , g_{11} and g_1 have been extracted from these spectra. These parameters, and data obtained from visible-u.v. spectra have been used to obtain quantitative descriptions of the bonding in these compounds in terms of molecular orbital models. From

extended Huckel L.C.A.O. molecular orbital calculations, carried out on the compound ReOCl_4 , the metal ion spin-orbit coupling constant and the parameter P are estimated to be about 2400 cm^{-1} and 0.033 cm^{-1} respectively. Spin Hamiltonian parameters are listed for each substance and are equated to the atomic orbital coefficients in some of the molecular orbitals involved in bonding in these molecules, and a good agreement is obtained between the values obtained in this way and those derived from the molecular orbital calculations. The unpaired electron lies in a molecular orbital which involves the metal ion $5d_{xy}$ orbital and it is strongly delocalised (33%) on to the chlorine ligands. g_{11} is greater than g_1 and this is shown to be essentially due to charge-transfer mixing by spin-orbit coupling at the chlorine atoms. The changes in the spin Hamiltonian parameters when a sixth ligand is added to ReOCl_4 are accounted for.

Part III

In this section a detailed study has been made of electron paramagnetic relaxation phenomena in solutions of ReOCl_4 in chloroform. This has enabled the separate contributions from spin-rotational interactions, from g-tensor anisotropy, from hyperfine coupling anisotropy, and from unresolved chlorine hyperfine coupling, to the observed e.p.r. linewidths to be evaluated. These results have been used to estimate the size of the chlorine isotropic hyperfine coupling constant and then

the extent of delocalisation of the unpaired electron available in the complex on to the chlorine ligands. In this way it has been shown that the extent of delocalisation of the unpaired electron on to chlorine groups in ReOCl_4 is about 21%. This result is in reasonable agreement with the deduction made from the analysis of the spin Hamiltonian parameters obtained in Part II.

Part IV

This section describes a study of the six-coordinated trigonal-prismatic complexes, $\text{Re}(\text{S}_2\text{C}_2\text{Ph}_2)_3$ and $\text{Re}(\text{S}_2\text{C}_6\text{H}_3\text{CH}_3)_3$. The e.p.r. spectra of these complexes have been recorded in solution at 298K and in magnetically dilute glasses at 77K. These e.p.r. spectra are quite different from those that have been obtained from the other rhenium complexes that have been studied in part II. Each trigonal pyramidal rhenium complex shows a single electron resonance signal in both magnetically concentrated solid and in solution at room temperature. The spectra of magnetically dilute glasses at 77K show small g-tensor anisotropy and vanishingly small rhenium nuclear hyperfine coupling. The small g-tensor anisotropy is very characteristic of sulphur-containing organic radicals and the vanishing small rhenium nuclear hyperfine coupling, almost certainly a direct dipolar coupling, sets an upper limit of the order of 0.1% to the rhenium contribution to the molecular orbital containing the unpaired electron in these complexes. The e.p.r. spectra show that the unpaired electron in these complexes is in a non-bonding molecular orbital

derived from the ligand π -orbitals.

E.P.R. properties, electronic absorption spectra, voltammetric properties, the magnetic properties of ions derived from $\text{Re}(\text{S}_2\text{C}_2\text{Ph}_2)_3$, and the unusually high electrical conductivities exhibited by the solids, are all consistent with an electronic ground state configuration $(3a'_1)^2(4e')^4(2a'_2)^1$ for these complexes.

Part V

This section describes a study of the octacyanorhenium complexes. E.p.r. spectra of magnetically undiluted polycrystalline $[\text{Ph}_4\text{As}]_2[\text{Re}(\text{CN})_8]$ have been recorded at room temperature and at 77K. The spectra are characteristic of an unpaired electron moving in an axially symmetric orbital in which the hyperfine coupling A is greater than B, and the g-tensor components are almost identical. Five different arrangements of the cyanide ligands around the rhenium atom have been considered. They are: a cube, a square antiprism, a dodecahedron, a trigonal prism with ligands in the centres of the two end faces and a trigonal prism with ligands centred on two side faces. Only the dodecahedron structure is consistent with the e.p.r. results for the paramagnetic complex $[\text{Ph}_4\text{As}]_2[\text{Re}(\text{CN})_8]$. The small size of the rhenium hyperfine coupling and the small

anisotropy in the g-tensor components of this complex indicate that the rhenium d-orbitals must be very mixed with the cyanide orbitals in the formation of the complex.

The infra-red spectra of the complexes, $K_3\text{Re}(\text{CN})_8$, and $[\text{Ph}_4\text{As}]_2 [\text{Re}(\text{CN})_8]$ have been recorded in solid phase at room temperature. The infra-red spectrum of $K_3\text{Re}(\text{CN})_8$ contains two strong sharp bands and two weak bands in $\text{C}\equiv\text{N}$ stretching region. Since the dodecahedron with D_{2d} symmetry has two strong infra-red active $\text{C}\equiv\text{N}$ stretching modes and two weak modes, therefore, the infra-red spectrum of $K_3\text{Re}(\text{CN})_8$ is consistent with this structure. The infra-red spectrum of $[\text{Ph}_4\text{As}]_2 [\text{Re}(\text{CN})_8]$ is not well resolved and shows superposition of several bands, so that it is not possible to get information from this spectrum about the actual structure of this complex.

Part VI

This section describes a study of the distorted tetrahedral complex of dichlorodioxomanganese(VI), MnO_2Cl_2 .

The X-band e.p.r. spectra of magnetically dilute solutions of MnO_2Cl_2 in CCl_4 have been recorded at 77K and at 298K, and are analysed in detail. The spin-orbit coupling constant and the parameter P for the manganese ion in this compound are estimated to be 248 cm^{-1} and 0.0172 cm^{-1} respectively. At 77K, MnO_2Cl_2 rotates about its X-axis in CCl_4 solution.

Spin Hamiltonian parameters are listed for 298K, for 77K, and for the rigid molecule, and are equated to the atomic orbital coefficients in the molecular orbitals involved in bonding in this molecule. The unpaired electron lies in the metal ion $3d_{x^2-y^2}$ orbital mixed with a small amount (8%) of the $3d_{z^2}$ orbital, and it is strongly (55%) delocalised on to the ligands. One of the principal components of the g-tensor, g_{xx} is larger than the spin-only value, a situation unusual in d^1 complexes. This is shown to be due to relatively large spin-orbit coupling at the chlorine atoms. It is pointed out that principal values of the g-tensor may be used to distinguish distorted tetrahedral complexes which are stretched along their z-axes from the corresponding complexes compressed in this direction, provided that spin-orbit interactions at the ligands are relatively large.

Acknowledgements

I would like to express my gratitude to my Supervisor, Dr. A. L. Porte, for his constant guidance and patient supervision throughout this work.

I thank Professor G. A. Sim in whose laboratories this work was carried out.

I would also like to thank all my colleagues for their helpful discussions and comments.

Finally, I would like to express my thanks to the University of Basrah for studyleave, during the tenure of which this work was carried out.

TABLE OF CONTENTS

PART I

	<u>Page</u>
<u>INTRODUCTION</u>	
1. Magnetic properties of electrons and nuclei	1
2. The Zeeman interaction	4
3. The resonance condition in electron paramagnetic resonance	5
4. The hyperfine interaction	7
5. The Spin Hamiltonian	10
6. Electron paramagnetic resonance in bulk matter	12
7. The Bloch equations and lineshapes in magnetic resonance spectroscopy	17
8. Sources of linebroadening	26
9. Electron paramagnetic resonance studies and electronic structure	27
10. Experimental aspects	33

PART II

AN ELECTRON PARAMAGNETIC RESONANCE STUDY OF THE ELECTRONIC STRUCTURE OF RHENIUM OXYCHLORIDE, ReOCl_4 , AND SOME OF ITS ADDUCTS

1. Introduction	36
2. Experimental	37
3. Analysis of e.p.r. spectra	39
4. U.v-visible spectra of rhenium oxychloride and its adducts	50
5. Extended Hückel molecular orbital calculations of rhenium oxychloride and its adducts	51
6. Results and discussion of molecular orbital calculations	62
7. Equations relating the spin Hamiltonian parameters to the molecular orbital coefficients in rhenium oxychloride	68

	<u>Page</u>
8. Molecular orbital coefficients and bonding in rhenium oxychloride and its adducts	72
9. Summary of part II	76

PART III

ELECTRON PARAMAGNETIC RESONANCE LINEWIDTH STUDIES OF ReOCl_4 IN SOLUTION

1. Introduction	80
2. Mechanisms of electron spin relaxation in solutions of transition metal complexes	81
3. Experimental	91
4. Results and discussion	92
5. Summary of part III	101

PART IV

THE ELECTRONIC GROUND STATES OF THE TRIGONAL-PRISMATIC RHENIUM COMPLEXES, TRIS(CIS-1,2-DIPHENYLETHENE-1,2-DITHIOLATO)RHENIUM, $\text{Re}(\text{C}_2\text{S}_2\text{Ph}_2)_3$, AND TRIS(TOLUENE-3,4-DITHIOLATO)RHENIUM, $\text{Re}(\text{S}_2\text{C}_6\text{H}_3\text{CH}_3)_3$.

1. Introduction	104
2. Experimental	107
3. Analysis of the e.p.r. spectra	108
4. The electronic spectra of $\text{Re}(\text{S}_2\text{C}_2\text{Ph}_2)$ and $\text{Re}(\text{S}_2\text{C}_6\text{H}_3\text{CH}_3)_3$	111
5. Molecular orbitals in tris(dithiolato)-rhenium complexes	117
6. Results and discussion	124
7. Summary of part IV	131

PART VELECTRON PARAMAGNETIC RESONANCE AND OPTICAL SPECTRA
OF THE OCTACYANORHENIUM COMPLEXES

1. Introduction	134
2. Experimental	136
3. Analysis of the e.p.r. spectra of $[\text{Ph}_4\text{As}]_2[\text{Re}(\text{CN})_8]$	138
4. Visible-u.v. spectra of $[\text{Ph}_4\text{As}]_2[\text{Re}(\text{CN})_8]$ and $\text{K}_3\text{Re}(\text{CN})_8$	139
5. Infra-red spectra of $\text{K}_3\text{Re}(\text{CN})_8$ and $[\text{Ph}_4\text{As}]_2[\text{Re}(\text{CN})_8]$	141
6. Theory	148
7. Results and discussion	154
8. Summary of part V	158

PART VIAN ELECTRON PARAMAGNETIC RESONANCE STUDY OF
DICHLORODIOXOMANGANESE(VI), MnO_2Cl_2 .

1. Introduction	161
2. Experimental	162
3. Analysis of the e.p.r. spectra	163
4. Extended Hückel molecular orbital calculation of MnO_2Cl_2	169
5. Equations relating the spin Hamiltonian parameters to the molecular orbital coefficients in MnO_2Cl_2	179
6. Molecular orbital coefficients and bonding in MnO_2Cl_2	185
7. Summary of part VI	189

APPENDIX A

THE SPIN HAMILTONIAN

192

APPENDIX B

EIGENVALUES OF THE SPIN HAMILTONIAN

201

APPENDIX C

LINE SHAPES FOR ELECTRON PARAMAGNETIC RESONANCE
SPECTRA OF MAGNETICALLY DILUTE GLASSES OR
POLYCRYSTALLINE SAMPLES

212

Preface

This thesis is concerned with electron paramagnetic resonance phenomena in complexes of manganese(VI) and rhenium(VI), and with the relationships that connect these phenomena with the symmetry properties and the electron distributions within the complexes that were investigated.

The thesis is concerned with several shapes of complex and it is subdivided into six parts. Part I is concerned with the principles of electron paramagnetic resonance spectroscopy. Part II describes studies of the rhenium(VI) ion in square pyramidal and in axially distorted octahedral environments, and it shows how electron paramagnetic resonance measurements of these can be combined with molecular orbital calculations to obtain detail quantitative information about the electron distribution and about the nature of bonding within these complexes. Part III is concerned with measurements of linewidths of electron paramagnetic resonance spectra of ReOCl_4 in chloroform solution. These measurements cover a range of temperature, and they also have been used to obtain information about the electronic distribution in this compound. Part IV and Part V are concerned with studies of the rhenium(VI) ion in six-coordinate trigonal-prismatic complexes and in eight-coordinate dodecahedral complexes respectively, and they show that the electron paramagnetic resonance measurements can be used to deduce the natures of the

electronic ground states in these complexes. Part VI describes a similar study of the manganese(VI) ion in the distorted tetrahedral molecule, MnO_2Cl_2 .

The work described in this thesis is original, and was carried out in partial fulfilment of the requirements for the degree of Ph.D. in the University of Glasgow.

October, 1974

A.H.H. Al-Mowali.

1.

PART 1

INTRODUCTION

1.1 Magnetic properties of electrons and nuclei

Electrons, protons and neutrons undergo various kinds of closed-loop like motion: they possess angular momentum and an associated magnetic moment. The angular momentum, \underline{G} , associated with any of these particles may be written in the form

$$\underline{G}^2 = G_x G_x + G_y G_y + G_z G_z \quad \dots\dots 1.1$$

where G_x , G_y and G_z are its components along three mutually perpendicular axes x , y and z . The properties of angular momentum operators in quantum mechanics show that the square of the total angular momentum is given by

$$\underline{G}^2 = G(G+1)\hbar^2 \quad \dots\dots 1.2$$

where G , the total angular momentum quantum number, may be an integer or half-integer and $\hbar = (\text{Planck's constant}) \times (2\pi)^{-1}$. The component of the total angular momentum in the z -axis direction is similarly shown to be

$$G_z = m_G \hbar \quad \dots\dots 1.3$$

where $m_G = G, (G-1), \dots\dots, -G$.

The angular momentum of an isolated electron arises as a result of its intrinsic spin, defined by the quantum

number s , and its orbital motion defined by the quantum number l . The spin quantum numbers of the electron, proton and neutron all have values of one half. Since nuclei are compounded out of protons and neutrons it follows that the total angular momentum of a nucleus is made up of contributions from individual nucleons, and the actual value of a nuclear spin quantum number, I , can be $0, \frac{1}{2}, 1, \frac{3}{2}, \dots$ depending on the way in which the spin and orbital angular momenta of the nucleons involved are coupled together.

When a charged particle has an angular momentum, it will possess a permanent magnetic dipole moment. Both the orbital and spin angular momentum contribute to the magnetic moment of the electron. The magnitude of the magnetic moment is proportional to the magnitude of the angular momentum, $\mu = \gamma_e G$, the constant of proportionality, γ_e being known as the magnetogyric ratio, and is defined by

$$\gamma_e = \frac{g_e e}{2mc} \quad \dots\dots 1.4$$

where e and m are the charge and the mass of the electron respectively, c is the velocity of light, and g_e is the electronic g factor which equals 1 and 2.00232 for the electron orbital and spin angular momenta respectively. For a single electron in an isolated atom where the spin and orbital angular momenta are coupled together, the total angular momentum is

$$G = [j(j+1)]^{\frac{1}{2}} \hbar \quad \dots\dots 1.5$$

where $j = l + s$, and the g factor is

$$g_j = 1 + \left[\frac{j(j+1) + s(s+1) - l(l+1)}{2j(j+1)} \right] \dots\dots 1.6$$

In chemically interesting situations atoms are not isolated. Then the electron's orbital is perturbed by the asymmetric electric field caused by the presence of neighbouring atoms. Such fields uncouple the spin and orbital angular momenta, and if the electric fields are large then the orbital contribution to the electronic angular momentum is almost completely removed, and the g -factor is very nearly the spin-only value, 2.00232. In cases where the ground state spin eigenfunction has only a second order contribution from orbital paramagnetism, the electronic magnetic moment may be written as

$$\mu = -g_{\text{eff}} \left[s(s+1) \right]^{\frac{1}{2}} e\hbar (2mc)^{-1} \dots\dots 1.7$$

where the orbital contribution is taken in to the effective g factor and the magnetic moment is assumed to arise from the spin of the electron only. g_{eff} is a tensor quantity.

The magnetic moment of the nucleus may similarly be related to its angular momentum

$$\mu_N = \gamma_N G_N \dots\dots 1.8$$

where the nuclear magnetogyric ratio, γ_N , is defined by

$$\gamma_N = \frac{g_N e}{2Mc} \dots\dots 1.9$$

where e and M are respectively the charge and mass of the proton and c is the velocity of light. g_N , the nuclear g -factor, is a constant for each nucleus. The

orbital and spin angular momenta of the nucleus are not considered separately and their resultant is described by the particular value of g_N for the nucleus in question. 1.8 may be written in the form

$$\mu_N = \frac{g_N e}{2Mc} \hbar \underline{I} \quad \dots\dots 1.10$$

where $\underline{I}^2 = I(I+1)$

1.2 The Zeeman interaction

When an applied magnetic field, H , interacts with a magnetic dipole moment μ the energy of the dipole is altered by an amount

$$\mathcal{H} = - \mu \cdot \underline{H} \quad \dots\dots 1.11$$

when the magnetic field is assumed to lie along the z-axis direction, and μ is the magnetic dipole moment of an unpaired electron then 1.11 becomes

$$\begin{aligned} \mathcal{H} &= - (\mu_e)_z H \\ &= (g_e)_z S_z H \beta_e \end{aligned} \quad \dots\dots 1.12$$

where β_e , the electronic Bohr magneton, is a constant equal to $e\hbar(2mc)^{-1}$, and S_z is the spin operator defining the z-axis component of the electron's angular momentum. In an applied magnetic field, the value of S_z can be either $+\frac{1}{2}$ or $-\frac{1}{2}$, which correspond to alignment of the electronic magnetic moment roughly parallel and antiparallel respectively, to the direction of the applied field.

The eigenvalues of equation 1.12 are just multiples of the eigenvalues of S_z , and are given by

$$\begin{aligned} E &= g_e \beta_e H m_s \\ &= \pm \frac{1}{2} g_e \beta_e H \end{aligned} \quad \dots 1.13$$

with the lower state corresponding to the $m_s = -\frac{1}{2}$ eigenvalue of S_z .

Similarly, the interaction of a nuclear magnetic moment with a steady magnetic field applied in the z-axis direction is given by

$$\begin{aligned} \mathcal{H} &= -\mu_N \cdot \underline{H} \\ &= -\gamma_N \hbar \underline{I} \cdot \underline{H} \\ &= -\gamma_N \hbar I_z H \end{aligned} \quad \dots 1.14$$

where I_z is the nuclear spin operator along the z-axis direction. The interaction energy E is given by the eigenvalues of this Hamiltonian

$$E = -\gamma_N \hbar m_I H \quad \dots 1.15$$

where $m_I = I, (I-1), \dots, -I$.

1.3 The resonance condition in electron paramagnetic resonance

In order to study the transitions between electronic Zeeman energy levels an interaction which can effect transitions between them is needed. The interaction most

commonly used for this purpose consists of that which arises when a small alternating magnetic field is applied at right angles to the static field. The Hamiltonian which represents this interaction is given by

$$\mathcal{H}'(t) = g_e \beta_e \left[S_x H_x(t) + S_y H_y(t) \right] \dots 1.16$$

where $H_x(t)$, $H_y(t)$ are the x and y components of the alternating field, $2H_1 \cos \omega t$, where ω is the angular frequency of this field. It turns out that S_z can only connect states with $\Delta m_s = 0$ whereas S_x and S_y can connect only states with $\Delta m_s = \pm 1$. Hence why in order to cause transitions between the energy levels, the alternating field is applied in the xy plane. If this condition is obeyed then transitions between adjacent energy levels only are allowed. Transitions, in accordance with the selection rule $\Delta m_s = \pm 1$, will be induced only when the energy of the applied alternating field is equal to the energy separation between adjacent levels, i.e. when

$$\begin{aligned} \Delta E &= \hbar \omega \\ &= h\nu \dots 1.17 \\ &= g_e \beta_e H \end{aligned}$$

and so
$$\omega = g_e \beta_e H (\hbar)^{-1} \dots 1.18$$

For an applied field of 3×10^3 gauss it turns out that the resonance frequency of an electron ($g_e \simeq 2.0023$) is about 9000 MHz, corresponding to a wave length of

about 3 cm, i.e. electron paramagnetic resonance transitions in fields of the order of 3000 gauss fall in the microwave region of the spectrum.

1.4 The hyperfine interaction

If an unpaired electron is in the vicinity of a nucleus which has a magnetic moment, the magnetic dipoles of the electron and the nucleus may couple together. In a steady magnetic field, the perturbation of the electronic Zeeman energy levels caused by the hyperfine coupling may be looked on as arising from the presence of an extra magnetic field due to the nucleus, and whose magnitude depends on the magnetic dipole moment of the nucleus. The single transition which would be observed in the absence of hyperfine coupling is then split into $(2I+1)$ approximately equally spaced transitions which obey the selection rules $\Delta m_s = \pm 1$, $\Delta m_I = 0$. The electron-nuclear hyperfine interaction is, in general, represented by a contribution, \mathcal{H}_{IS} , to the spin Hamiltonian of the form

$$\mathcal{H}_{IS} = \underline{I} \cdot \underline{A} \cdot \underline{S} \quad \dots 1.19$$

where \underline{A} is a symmetric tensor, the hyperfine coupling tensor. The hyperfine tensor \underline{A} , can always be reduced to a diagonal form by choosing as axes the principal axes x , y and z , and the hyperfine coupling is then written

$$\mathcal{H}_{IS} = A_{xx} S_x I_x + A_{yy} S_y I_y + A_{zz} S_z I_z \quad \dots 1.20$$

Very often the principal axes system of this hyperfine tensor coincides with that of the g-tensor, and if this condition is fulfilled then the analysis of an electron paramagnetic resonance spectrum is considerably simplified. The interaction between the unpaired electron and the nucleus arises in three quite distinct ways. These are briefly outlined below

(a) An isotropic interaction, the Fermi contact interaction, arises when the unpaired electron resides in an atomic orbital which has a finite spin density at the nucleus concerned, i.e. when the electron is in an orbital of s-type or with s-character, or when there is significant polarisation of the paired s electron about the nucleus by the unpaired electron. This interaction may be represented by

$$\mathcal{H}_c = \frac{8\pi}{3} g_e g_N \beta_e \beta_N \delta(r_n) \underline{I} \cdot \underline{S} \quad \dots\dots 1.21$$

where $\delta(r_n)$ is the Dirac delta function which, integrated over the electronic wavefunction, gives the square of the value of the wavefunction at the nucleus.

$$\int \delta(r_n) \Psi^2(\mathbf{r}) d\mathbf{r} = \Psi^2(r_n) \quad \dots\dots 1.22$$

r_n is a nuclear coordinate.

(b) An anisotropic dipolar coupling arises from the dipolar coupling between the magnetic moments of the electron and the nucleus. This interaction is essentially the classical interaction of two dipoles $\underline{\mu}_e$ and $\underline{\mu}_N$ separated by a distance \underline{r} . In a strong magnetic field,

the electron and nuclear spin vectors, \underline{I} and \underline{S} are fully decoupled. The Hamiltonian representing the energy of dipolar interaction may be written as

$$\mathcal{H}_{\text{dipolar}} = - \frac{g_e \beta_e g_N \beta_N}{r^3} \left[\underline{I} \cdot \underline{S} - \frac{3(\underline{I} \cdot \underline{r})(\underline{S} \cdot \underline{r})}{r^2} \right] \quad \dots\dots 1.23$$

The anisotropy arises from the orientation dependence of the vector \underline{r} . 1.23 can usefully be rewritten in the form

$$\mathcal{H}_{\text{dipolar}} = g_e \beta_e g_N \beta_N \left\langle \frac{1-3 \cos^2(\theta)}{r^3} \right\rangle_{\text{av}} \underline{I} \cdot \underline{S} \quad \dots\dots 1.24$$

where θ is the angle between the vector connecting the dipoles and the magnetic field direction. In an atom or molecule r and θ are not constant because of the orbital motion of the electron, and so the orientation dependent term includes a spatial average over the whole orbital occupied by the unpaired electron. When the unpaired electron distribution is spherically symmetric or when the orientation dependent term has a spherically symmetric time average, as is the case for example in solution due to the Brownian motion, then the dipole contribution to the hyperfine coupling is zero.

(c) The third contribution to hyperfine coupling concerns the dipolar interaction of the orbital magnetic moment of the electron with the nuclear magnetic moment. This is fairly small in many transition metal complexes.

A nucleus with spin quantum number I greater than $\frac{1}{2}$ can also possess an electric-quadrupole moment, which interacts with the electric field gradients produced at the nucleus by the surrounding electrons or other charges. This interaction results in shifts in the energy levels and it may make normally forbidden transitions with

$\Delta m_I = \pm 2$ become weakly allowed with both electron and nuclear spins changing simultaneously. The quadrupole interaction does not cause any change in the position of the resonance lines when the steady magnetic field lies parallel to the symmetry axis of the crystal, but it does cause such changes when the magnetic field is not parallel to the z-axis, and in addition the resulting nuclear hyperfine lines are then unequally spaced. The spin Hamiltonian representing this interaction can be written

$$\mathcal{H}_Q = \underline{I} \cdot \underline{P} \cdot \underline{I} \quad \dots\dots 1.25$$

where P is the quadrupole coupling tensor.

1.5 The spin Hamiltonian

For the complexes whose electron paramagnetic resonance spectra will be discussed in this work, one unpaired electron interacts with one nucleus and the orbital contribution to the magnetic moment of the electron is small. It is therefore possible to represent the behaviour of the energy levels by the following Hamiltonian which has only spin operators

$$\mathcal{H} = \beta_e \underline{H} \cdot \underline{g} \cdot \underline{S} + \underline{S} \cdot \underline{A} \cdot \underline{I} + \underline{I} \cdot \underline{P} \cdot \underline{I} \quad \dots\dots 1.26$$

The advantage of the spin Hamiltonian, which was first introduced by Abragam and Pryce, is that a complete description of the experimental data can be presented by giving the magnitudes of the coefficients of the terms in equation 1.26, together with the direction of the appropriate principal axes relative to the crystal axes when anisotropy is present.

The direct interaction of the nuclear spin with the magnetic field is normally one or two orders of magnitude less than that between the nuclear and electronic spins, so that it has been ignored in equation 1.26.

If it is possible to choose a system where the x, y and z axes are principal axes, which simultaneously diagonalise the g, A and P tensors, then the spin Hamiltonian can be written in the form

$$\mathcal{H} = \sum_i (\beta_e g_{ii} H_i S_i + A_{ii} S_i I_i + P_{ii} I_i^2) \dots 1.27$$

where the summation is over the principal axes coordinates. In solutions where the rotation of the system averages out the anisotropic contribution to the various tensors, the spin Hamiltonian becomes

$$\mathcal{H} = g_0 \beta_e \underline{H} \cdot \underline{S} + A_0 \underline{S} \cdot \underline{I} \dots 1.28$$

$$\text{where } g_0 = \frac{1}{3} \sum_i g_{ii} \text{ and } A_0 = \frac{1}{3} \sum_i A_{ii} \dots 1.29$$

Since the quadrupole tensor is traceless, there is no contribution from this in equation 1.28, and the eigenvalues of the resultant Hamiltonian 1.28 are given by

$$E_{m_S, m_I} = g_0 \beta_e m_S H + A_0 m_I m_S \quad \dots\dots 1.30$$

provided nuclear hyperfine interactions are small compared with the interaction between the electron and the applied magnetic field.

1.6 Electron paramagnetic resonance in bulk matter

In practice observations of electron paramagnetic resonance are made on bulk matter i.e. on liquids, solids and gases containing a large number of spins, and not on isolated spins. We must therefore consider what happens to the spins in a macroscopic sample when they are subjected to both steady and oscillating magnetic fields. For simplicity consider a sample in which all paramagnetic molecules are identical and have spin quantum numbers $s = \frac{1}{2}$ in the solid or liquid state. The material in which the unpaired electrons are embedded is usually called the "lattice" whether it be solid or liquid or gas. When this sample is subjected to a steady magnetic field \underline{H} , along the z-axis direction, the spins will tend initially to distribute themselves over the two possible energy states, separated in energy by $g_e \beta_e H$. Hyperfine interactions are neglected in order to simplify the analysis. Application of an oscillating magnetic field in a direction perpendicular to the steady field, causes transitions between the two energy levels to take place. The oscillating field is equally likely to produce transitions up from the lower $\{-\frac{1}{2}\}$ level to the upper $\{+\frac{1}{2}\}$ level which results in absorption of radiation energy, or down from the $\{+\frac{1}{2}\}$ level to the $\{-\frac{1}{2}\}$ level by stimulated emission, which results in

emission of energy, and we can only detect absorption of energy from the radiation field if the population of the lower level exceeds that of the upper level.

At thermal equilibrium the distribution of the spins between the two allowed energy levels is given by the Boltzmann formula.

$$\frac{n_l}{n_u} = e^{\frac{\Delta E}{kT}} = e^{g_e \beta_e H/kT} \quad \dots \quad 1.31$$

where n_l and n_u are the numbers of spins in the lower and upper levels, respectively, k is the Boltzmann constant and T is the absolute temperature. If Δn is the population difference between the lower and upper states and $g_e \beta_e H/kT$ is small.

$$\Delta n = n_u \frac{g_e \beta_e H}{kT} \approx \frac{1}{2} \frac{g_e \beta_e H}{kT} N \quad \dots \quad 1.32$$

where N is the total number of unpaired spins in the two levels.

The net absorption of microwave energy is due to this small excess (Δn) in the lower level and corresponds to the transfer of some of the excess population in the lower level to the upper level. Therefore, if the unpaired spins were isolated from their surroundings, the two levels would rapidly become equally populated and the absorption of microwave energy would cease. The fact that magnetic resonance can be observed while radiation is applied at low power levels means that there must be other mechanisms by which energy absorbed and stored in the upper state can be dissipated in such a

manner as to permit the spins to return to the ground state. Such mechanisms are called relaxation processes.

The decrease in the population difference with absorption of microwave energy may be described by imagining the spin temperature, T_S , steadily rising as the microwave energy is absorbed, while the temperature of the lattice remains unaltered. Interactions between the spin system and the lattice will tend to bring the two systems into thermal equilibrium but the resultant temperature will be close to that of the lattice since the heat capacity of the spin system is negligible compared with that of the lattice. Therefore the spin-lattice interactions reduce the spin temperature much below $T_S = \infty$, i.e. they increase the population of the lower level. When spin-lattice interaction is present the upward transition probabilities are no longer equal to the downward transition probabilities. If the upward and downward transition probabilities are denoted w_1 and w_2 respectively, with $w_1 \neq w_2$, the rate of change of population of the lower state is given by the equation

$$\frac{dn_1}{dt} = n_u w_2 - n_l w_1 \quad \dots\dots 1.33$$

when thermal equilibrium has been established,

$$\frac{dn_1}{dt} = 0$$

and if the equilibrium populations are n_l^0 and n_u^0 , then

$$\frac{n_u^0}{n_1^0} = \frac{w_1}{w_2} \quad \dots\dots 1.34$$

By the use of equation 1.31, it now follows that

$$\frac{w_1}{w_2} = \exp(-\Delta E/kT) \quad \dots\dots 1.35$$

If Δn and N are expressed in terms of n_u and n_1 , then

$$\frac{d\Delta n}{dt} = -\Delta n (w_2 + w_1) + N (w_2 - w_1) \quad \dots\dots 1.36$$

Rearrangement yields

$$\frac{d\Delta n}{dt} = -\left(\frac{\Delta n - \Delta n_0}{T_1}\right) \quad \dots\dots 1.37$$

Where

$$\Delta n_0 = N \left(\frac{w_2 - w_1}{w_2 + w_1}\right) \quad \text{and} \quad T_1 = \frac{1}{w_1 + w_2}$$

Δn_0 is the population difference at thermal equilibrium and T_1 is called the spin-relaxation time, or longitudinal relaxation time, and it has dimensions of time.

The complete behaviour of the spin system in a normal electron paramagnetic resonance experiment can be described by including the effect of induced transitions which arise in the presence of a microwave field. If we denote the absorption and stimulated emission probabilities by P , then the rate of change of the population difference due to these processes is

$$\frac{d\Delta n}{dt} = -2P \Delta n \quad \dots\dots 1.38$$

and the rate of absorption of energy from the microwave field is

$$\frac{dE}{dt} = \Delta n P \Delta E \quad \dots\dots 1.39$$

The total rate of change of the population difference is the sum of the rates due to the combined effects of the radiation and spin-lattice relaxation,

$$\frac{d \Delta n}{dt} = -2P \Delta n - (\Delta n - \Delta n_0) T_1^{-1} \dots\dots 1.40$$

At thermal equilibrium $\frac{d \Delta n}{dt} = 0,$

$$\therefore \Delta n = \frac{\Delta n_0}{1 + 2PT_1}$$

$$\text{and } \frac{dE}{dt} = \Delta n_0 \Delta E P (1 + 2PT_1)^{-1} \dots\dots 1.41$$

Equation 1.41 indicates that provided $2PT_1 \ll 1$, the electron paramagnetic absorption signal is not liable to become saturated.

As a result of relaxation, the spin states have a finite lifetime and the shape of the resonance absorption line cannot be represented by a δ function. If the lifetime is controlled by spin-lattice relaxation the linewidth is of the order of T_1^{-1} but in practice this is rarely so since there exist other relaxation processes which broaden the lines by varying the relative energies of the spin levels, rather than their lifetimes. Such processes are characterised by a relaxation time T_2 , called the spin-spin relaxation time or transverse relaxation time. T_1 and T_2 are closely related since any interaction which can decrease the lifetimes of spin states may also modulate the energy levels.

The total linewidth $(T_2')^{-1}$ generally consists of two contributions; the first arises from spin-lattice relaxation and equals $(2T_1)^{-1}$, and the second results from spin-spin relaxation and is equal to $(2T_2)^{-1}$.

1.7 The Bloch equations and lineshapes in magnetic resonance spectroscopy

In order to complete our macroscopic description of spins and to discuss the lineshapes of electron paramagnetic resonance it is necessary to describe the dynamic behaviour of a collection of spins in a magnetic field. Consider first the bulk magnetic moment vector \underline{M} which is the resultant sum of the magnetic moment vectors of the individual electrons at a certain temperature. If all magnetic fields are suddenly switched off then, spin-lattice relaxation causes the population difference to decay exponentially to equilibrium, and the rate of change is

$$\frac{d \Delta n}{dt} = - \frac{\Delta n}{T_1} \quad \dots \quad 1.42$$

Since the z-component of bulk magnetic moment, M_z , is proportional to the excess population of spins in the lower level, the rate of decay of M_z to zero is therefore governed by the spin-lattice relaxation equation

$$\frac{dM_z}{dt} = - \frac{M_z}{T_1} \quad \dots \quad 1.43$$

M_x and M_y , the x and y components of \underline{M} , obey the same decay equation as M_z since there is no physical

distinction between the x, y and z axes directions in the absence of the applied field.

If a steady magnetic field is now applied along the z-axis direction, M_z tends to approach a steady value M_0 , while M_x and M_y still decay exponentially to zero with different characteristic time, T_2 . If the effects of precession are ignored then the rates of decay are given by

$$\frac{dM_z}{dt} = - \frac{M_z - M_0}{T_1}$$

$$\frac{dM_x}{dt} = - \frac{M_x}{T_2} \quad \dots\dots 1.44$$

$$\frac{dM_y}{dt} = - \frac{M_y}{T_2}$$

However, in the presence of an applied field, H_0 , along the z-axis direction is exerted a torque on the bulk magnetization, causing it to precess about H_0 with an angular frequency ω_0 according to the equation

$$\frac{d\mathbf{M}}{dt} = \gamma_0 (\mathbf{M} \times \mathbf{H}_0) \quad \dots\dots 1.45$$

The angular frequency ω_0 , is called the Larmor frequency, and the resultant precessional motion is known as the Larmor precession. The direction of precession depends on the sign of the magnetogyric ratio, and since γ is negative for the electron, the electronic spins therefore precess anticlockwise about the magnetic field

direction H_0 .

If the relaxation effects 1.44 are added to equation 1.45, then the equations of motion for the three components become

$$\frac{dM_x}{dt} = -\omega_0 M_y - \frac{M_x}{T_2}$$

$$\frac{dM_y}{dt} = \omega_0 M_x - \frac{M_y}{T_2}$$

..... 1.46

$$\frac{dM_z}{dt} = -\frac{M_z - M_0}{T_1}$$

These equations are called Bloch equations. They describe a damped precession of the spins, in which the rotating transverse component of \underline{M} decays to zero with characteristic time T_2 , and the longitudinal component M_z relaxes toward its equilibrium value M_0 with a characteristic decay time T_1 .

So far, we have only considered electron spins in the fixed field H_0 along the z-axis direction. If a circularly polarised magnetic field \underline{H}_1 rotating in the xy plane in the same direction as the Larmor precession, with a uniform angular velocity ω , which need not be equal to the resonance frequency ω_0 , is now applied to this system, then the Bloch equations become

$$\frac{dM_x}{dt} = \gamma_e (M_z H_1 \sin \omega t - H_0 M_y) - \frac{M_x}{T_2}$$

$$\frac{dM_y}{dt} = \gamma_e (H_0 M_x - M_z H_1 \cos \omega t) - \frac{M_y}{T_2} \quad \dots 1.47$$

$$\frac{dM_z}{dt} = \gamma_e (M_y H_1 \cos \omega t - M_x H_1 \sin \omega t) - \frac{M_z - M_0}{T_1}$$

where the rotating component of \underline{H}_1 in the xy plane is

$$\underline{H}_1 = i H_1 \cos \omega t + j H_1 \sin \omega t$$

i and j are unit vectors along the x and y axes respectively.

To solve equations 1.47 it is convenient to transform the frame of reference from fixed axes, x, y and z to a set of axes imagined to rotate with the \underline{H}_1 field, at an angular velocity ω about the z-axis. In the rotating frame, both H_0 and H_1 are fixed. We may then resolve the components of \underline{M} on the xy plane into components u and v, which are along and perpendicular to the direction of \underline{H}_1 , respectively, and they are often called in-phase and out-of-phase components of \underline{M} . The relations between u and v are

$$u = M_x \cos \omega t + M_y \sin \omega t.$$

.... 1.48

$$v = M_x \sin \omega t - M_y \cos \omega t$$

If we substitute equations 1.48 in the Bloch equations, we obtain a new set for the three components u, v and M_z referred to rotating axes

$$\frac{du}{dt} = (\omega_0 - \omega) v - \frac{u}{T_2}$$

$$\frac{dv}{dt} = -(\omega_0 - \omega) u + \gamma_e M_z H_1 - \frac{v}{T_2} \quad \dots 1.49$$

$$\frac{dM_z}{dt} = -\gamma_e H_1 v - \frac{M_z - M_0}{T_1}$$

$\omega_0 - \omega$ is a measure of how far we are off the peak of resonance.

The last equation is particularly significant, since it shows that the changes of M_z which reflect the changes in the energy of the spin system, are associated only with v , the out-of-phase component, and not with u .

This means that the absorption signals will be associated with the measurement of v . The component u will be associated with dispersion-mode signals.

If the microwave field, H_1 , has been applied for a sufficiently long time, then a steady state is reached and in that case the solutions of the Bloch equations are obtained by setting all the time-derivatives equal to zero. Then we obtain

$$u = M_0 \frac{\gamma_e H_1 T_2^2 (\omega_0 - \omega)}{1 + \gamma_e^2 H_1^2 T_1 T_2 + T_2^2 (\omega_0 - \omega)^2}$$

$$v = M_0 \frac{\gamma_e H_1 T_2}{1 + \gamma_e^2 H_1^2 T_1 T_2 + T_2^2 (\omega_0 - \omega)^2} \quad \dots 1.50$$

$$M_z = M_0 \frac{1 + T_2^2 (\omega_0 - \omega)^2}{1 + T_2^2 (\omega_0 - \omega)^2 + \gamma_e^2 H_1^2 T_1 T_2}$$

From these equations we can obtain the transverse components of the magnetization in the static laboratory coordinate system

$$M_x = \frac{1}{2} M_0 \gamma_e T_2 \frac{T_2(\omega_0 - \omega)2H_1 \cos \omega t + 2H_1 \sin \omega t}{1 + T_2^2(\omega_0 - \omega)^2 + \gamma_e^2 H_1^2 T_1 T_2} \dots 1.51$$

$$M_y = \frac{1}{2} M_0 \gamma_e T_2 \frac{T_2(\omega_0 - \omega)2H_1 \sin \omega t - 2H_1 \cos \omega t}{1 + T_2^2(\omega_0 - \omega)^2 + \gamma_e^2 H_1^2 T_1 T_2}$$

The results of these equations show that the magnetization has a constant component in the direction of the applied static magnetic field, and a rotating component in the xy plane. Although we have only solved the equations in a rotating field H_1 , in experimental electron paramagnetic resonance spectroscopy the perturbing field is an oscillating linearly polarized field. The solution of these equations in an oscillating field is almost the same since a linearly polarized field of strength $2H_1 \cos \omega t$ in the x-direction can be regarded as the sum of two counter-rotating fields of magnitude H_1 with Cartesian components $(H_1 \cos \omega t, -H_1 \sin \omega t, 0)$ and $(H_1 \cos \omega t, H_1 \sin \omega t, 0)$. Only the field which rotates in an anticlockwise sense can induce transitions, the effect of the other field rotating in the opposite direction will be negligibly small.

The effect of the linear field can be conveniently described in terms of susceptibilities χ' and χ'' ,

often referred to as Bloch susceptibilities. Thus the field $2H_1 \cos \omega t$ produces an in-phase magnetization, $M' = 2 \chi' H_1 \cos \omega t$, and an out-of-phase magnetization $M'' = 2 \chi'' H_1 \sin \omega t$. Since M_x and M_y contain both in-phase and out-of-phase components, we define a complex susceptibility by

$$\chi = \chi' - i \chi'' \quad \dots 1.52$$

M_x is then taken to be the real component of magnetization

$$M_x = \text{Re}(\chi 2H_1 e^{i\omega t})$$

$$\therefore M_x = \chi' 2H_1 \cos \omega t + \chi'' 2H_1 \sin \omega t \quad \dots 1.53$$

Comparing equations 1.53 with 1.51 we get, for the complex susceptibilities

$$\chi' = \frac{1}{2} \chi_0 \omega_0 \frac{T_2^2 (\omega_0 - \omega)}{1 + T_2^2 (\omega_0 - \omega)^2 + \gamma_{\theta}^2 H_1^2 T_1 T_2} \quad \dots 1.54$$

$$\chi'' = \frac{1}{2} \chi_0 \omega_0 \frac{T_2}{1 + T_2^2 (\omega_0 - \omega)^2 + \gamma_{\theta}^2 H_1^2 T_1 T_2} \quad \dots 1.55$$

Note that $\chi_0 H_0 = M_0$

It is obvious that in-phase and out-of-phase magnetization components u and v relate to χ' and χ'' respectively

$$u = 2 \chi' H_1$$

$$v = 2 \chi'' H_1$$

Let us now turn to a consideration of the power absorbed by the sample from the H_1 field. When the frequency of H_1 passes through the resonance, χ' changes sign so that \underline{M} is 90° out of phase with the microwave field at the high frequencies while χ'' shows very large increase near resonance, and this causes a strong absorption of energy. For an x-polarized microwave field the mean rate of energy absorption per unit volume of sample, A, is given by

$$\begin{aligned}
 A &= \overline{H_x \frac{dM_x}{dt}} \\
 &= \frac{2M_0 \gamma_e T_2 \omega H_1^2}{1 + \gamma_e^2 H_1^2 T_1 T_2 + T_2^2 (\omega_0 - \omega)^2} \left[\overline{\cos^2 \omega t - T_2 (\omega_0 - \omega)^2 \sin \omega t \cos \omega t} \right] \\
 &\dots\dots 1.56
 \end{aligned}$$

It can be readily shown that

$$\begin{aligned}
 \overline{\cos^2 \omega t} &= \frac{1}{2} \quad \text{and} \quad \overline{\sin \omega t \cos \omega t} = 0 \\
 \therefore A &= \frac{\gamma_e \omega H_1^2 M_0 T_2}{1 + T_2^2 (\omega_0 - \omega)^2 + \gamma_e^2 H_1^2 T_1 T_2} \dots\dots 1.57
 \end{aligned}$$

Comparing equation 1.57 with equation 1.55 we see that the power absorbed is readily expressed in term of the out-of-phase Bloch susceptibility

$$A = 2 \omega H_1^2 \chi'' \dots\dots 1.58$$

If H_1 is deliberately made sufficiently small so

that $\gamma_e^2 H_1^2 T_1 T_2 \ll 1$, then the normalised absorption line is Lorentzian in shape, i.e. of the form

$$g(\omega) = \frac{T_2}{\pi} \frac{1}{1 + T_2^2 (\omega - \omega_0)^2} \quad \dots 1.59$$

The term $\gamma_e^2 H_1^2 T_1 T_2$ becomes important when H_1 or T_1 is large, and the lineshape is then no longer Lorentzian. This effect is called saturation and it relatively weakens the centre of the absorption line, and causes apparent broadening. By a suitable modification of the experimental conditions, we can observe either the absorption mode which is related to χ'' , or the dispersion mode which is related to χ' . The absorption and dispersion shapes predicted from the Bloch equations are shown in Figure 1.1.

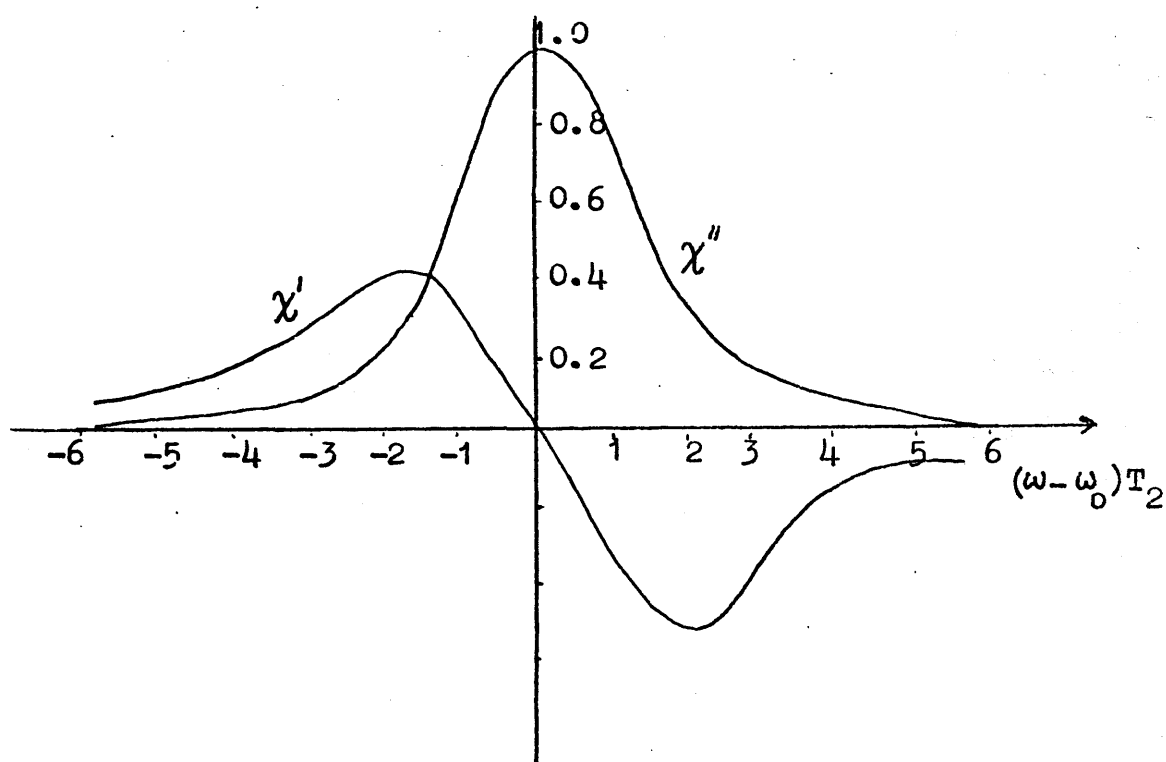


Figure 1.1 Dispersion and absorption lineshapes derived from the Bloch equation.

1.8 Sources of linebroadening

In addition to the natural linewidths described above, various additional effects may also contribute to the widths of electron paramagnetic resonance spectral lines. The relative importance of these sources depends on the particular system under discussion.

In magnetically concentrated crystals, where the neighbouring electron spins are close enough, the unpaired electron can jump rapidly from one molecule to another. If the rate of jumping is large, the effect is similar to what we would expect if the electron were free to move throughout the crystal. This has the effect of averaging out any hyperfine interactions and gives rise to a narrow line. When the rate of jumping is not sufficient enough to average out hyperfine interactions, then jumping may produce a very broad line. For this reason electron paramagnetic resonance studies are usually carried out on magnetically dilute systems, e.g. in solutions, or using crystals of a diamagnetic host, into which the paramagnetic species are doped. In solutions the important contributions to the absorption linewidths of transition metal complexes are outlined below.

- (a) Anisotropic interactions, which arise when the tumbling rate of a paramagnetic complex in solution is not rapid enough to completely average out the g and A tensors, cause fluctuating magnetic fields which produce linebroadening.
- (b) When a complex rotates in solution, the motion of its electron and its nuclei produce magnetic fields which can interact with the magnetic moment of the unpaired electron. Since the magnitudes and directions of these fields are time-dependent this also causes broadening of the resonance spectra.
- (c) Unresolved hyperfine interactions may exist in the complex which are not large enough to cause splitting of the component lines, but which are large enough to cause broadening of the linewidths.

These are the important sources in systems with one unpaired electron. Other sources may be dominant in other species, in which case each system must be individually considered.

1.9 Electron paramagnetic resonance studies and electronic structure

The electronic structures of the complexes to be discussed in this thesis are described in terms of the molecular orbital method in its LCAO (linear combinations of atomic orbitals) form. The electronic states of the molecule are described in terms of products of one-electron

wavefunctions which are formed from a linear combination of the atomic orbitals of the individual atoms which make up the complex, i.e. the molecular orbitals Ψ_j are of the form

$$\Psi_j = \sum_i c_{ij} \phi_i \quad \dots 1.60$$

where ϕ_i are appropriate atomic orbitals.

The molecular orbitals of many transition metal complexes such as the complexes studied here, are formed from nd , $(n+1)s$ and $(n+1)p$ orbitals of a central metal ion and s and p orbitals of ligands. In the formation of molecular orbitals by taking linear combinations of the combining atomic orbitals, the symmetry properties of the system must be taken into account.

Consider the simplest possible situation, where a metal and a ligand orbital combine. This combination produces two molecular orbitals Ψ^* and Ψ at energies above and below those of the component atomic orbitals respectively.

$$\Psi = a \phi_M + b \phi_L \quad \dots 1.61$$

$$\Psi^* = a^* \phi_M - b^* \phi_L$$

where ϕ_M is a metal ion orbital and ϕ_L is a ligand orbital. The molecular orbital energy levels are shown diagrammatically in Figure 1.2.

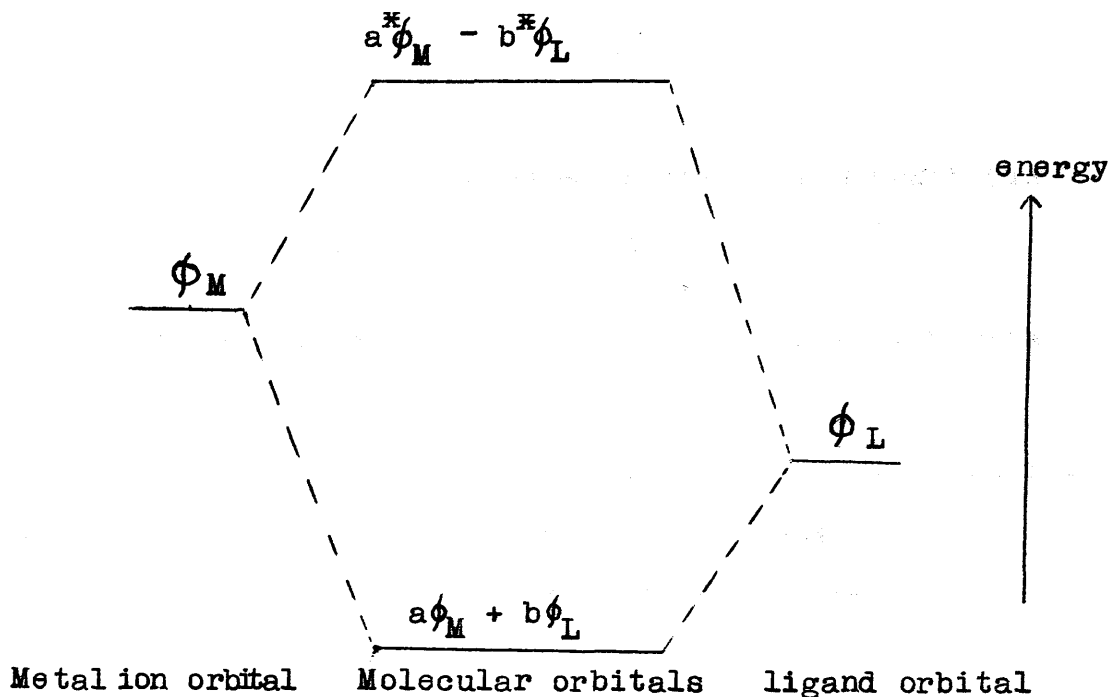


Figure 1.2

The coefficients in the wavefunctions must obey the normalization and orthogonality requirements

$$a^2 + 2abS + b^2 = 1$$

$$a^2 - 2a^*b^*S + b^{*2} = 1 \quad \dots 1.62$$

$$aa^* - bb^* + S(ab^* - ab^*) = 0$$

where the overlap integral $S = \int \phi_M \phi_L \, d\tau$

ψ^* is the antibonding orbital which is often mainly metal ion orbital in character, and often contains no electrons in the ground state of the molecule, while

ψ is the bonding orbital, which is often mainly ligand orbital in character, and is usually occupied in

the ground state. An unpaired electron in an anti-bonding orbital will effectively spend a portion of its time near the ligand atom if there is appreciable mixing of the two basis orbitals.

Electron paramagnetic studies of transition metal ions yield very detailed information about the distribution of electrons in transition metal complexes. This information can be derived in two ways. First, it is possible to estimate the degree of delocalisation of an unpaired electron away from a metal nucleus from the size of the metal hyperfine coupling, since the magnitude of the hyperfine coupling depends on the distance of the electron from the nucleus. This may lead to some information about the distribution of the unpaired electron in the molecular orbital it occupies in the ground state of the complex. In cases where the hyperfine coupling with the ligand magnetic nucleus is not large enough to cause splitting, because the separation between the lines is less than the component linewidths, the size of the ligand hyperfine coupling can be estimated by analysis of the linewidths of the electron paramagnetic resonance spectra at different temperatures. Second, it is also possible to derive information about the electron distribution from the size of the orbital contribution to the effective paramagnetic moment, as reflected in the deviation of the principal values of the g -tensor from the spin-only value.

The unpaired d-electrons in an isolated transition metal-ion possess orbital angular momentum in addition to the spin momentum. When the transition metal ion is in a complex, the electric field caused by the surrounding ligands tends to force the unpaired electron to occupy an orbital which has no orbital angular momentum associated with it. Orbital angular momentum may, however, be reinstated by spin-orbit coupling. The spin-orbit coupling originates in the interaction between the spin of the electron and the magnetic field generated by the motion of the electron in the electric field of the nucleus. The magnitude of the spin-orbit coupling increases with increasing atomic number of the nucleus involved, and decreases rapidly with the distance of the electron from the nucleus. This coupling causes considerable mixing of the characters of some excited states into the orbital containing the unpaired electron, and it leads to a reintroduction of a certain amount of orbital magnetic moment. These excited states are produced either by promoting the unpaired electron into the empty anti-bonding orbitals or by promoting an electron from the filled bonding orbitals into the orbital containing the unpaired electron.

The degree of the orbital contribution to paramagnetism depends on the degree of localisation of the electron on the metal ion in the ground and excited states. Thus if the degree of the electron localisation in the

ground state is known, from the hyperfine coupling for instance, it is possible to use the spin-orbit coupling effect to study the electron distribution in the excited states, in this case in the empty antibonding and filled bonding molecular orbitals.

If the coefficients of the antibonding molecular orbital are known, it is possible to obtain the coefficients of the bonding molecular orbital by using the Mulliken gross-population analysis. Consider first our two-molecular orbitals example. In this analysis we split up the term $2abS$ equally between the metal and ligand atoms and define the one-electron populations on the metal and ligand atoms in the bonding and antibonding orbitals as follows

$$\begin{aligned}
 P_M &= a^2 + abS & P_L &= b^2 + abS \\
 P_M^* &= a^{*2} - a^*b^*S & P_L^* &= b^{*2} - a^*b^*S
 \end{aligned}
 \quad \dots 1.63$$

From equations 1.63 we can show that

$$\begin{aligned}
 P_M + P_L &= 1 & P_M^* + P_L^* &= 1 \\
 P_M + P_M^* &= 1 & P_L + P_L^* &= 1 \dots 1.64
 \end{aligned}$$

Thus, knowing the orbital population in the antibonding molecular orbitals, the population in the bonding orbitals can be deduced through the use of equation 1.64.

1.10 Experimental aspects

The apparatus used for the observation of electron paramagnetic resonance spectra is by now well established and is discussed in numerous texts. All the electron paramagnetic resonance spectra discussed in this work were recorded on a Decca X-3 spectrometer, operating in the X-band region at a frequency of 9270 MHz., combined with a Newport instruments 11-in magnet system. The resonance fields were calibrated by standard ^1H n.m.r. techniques, and the calibration system itself was checked with a reference of a finely powdered sample of diphenyl picrylhydrazyl, whose g-factor is known accurately (2.00366).

The measurement of e.p.r. spectra of the samples at room temperature were carried out in spectrosoil quartz tubes, while at 77K, spectra were obtained by placing the samples in a long-tailed dewar, the spectrosoil quartz tail of which was inserted into the sample cavity, and then pouring liquid nitrogen on top of it. The measurement of the spectra over a range of temperatures was carried out by means of a flow system. For cooling, a stream of gaseous nitrogen was passed through a coil immersed in a bath of liquid nitrogen and then passed over the sample in the cavity; for heating, the gaseous nitrogen was passed over an electrically heated coil before reaching the sample.

Temperature was measured with a copper-constantan thermocouple together with a digital voltmeter and the temperature of the sample could be held within $\pm 1\text{K}$ for

a period of at least one hour.

More detailed investigation of electron paramagnetic phenomena of complexes of the d^1 ions manganese (VI) and rhenium (VI) will now be described.

Rhenium (VI) in a square pyramidal environment found in ReOCl_4 , and the axially distorted octahedral environment found in the adducts of ReOCl_4 , is first considered.

References to Part 1

The treatment of the theory in Part 1 of this thesis has been based on the following sources.

1. A. Carrington and A.D. McLachlan, "Introduction to Magnetic Resonance", Harper and Row, New York, 1967.
2. C.P. Slichter, "Principles of Magnetic Resonance", Harper and Row, New York, 1963.
3. B.R. McGarvey, "Transition Metal Chemistry", R.L. Carlin ed., Edward Arnold, London, 1966, 3,90.
4. A. Abragam and B. Bleaney, "Electron Paramagnetic Resonance of Transition Ions", Clarendon Press, Oxford, 1970.
5. N.M. Atherton, "Electron Spin Resonance", Ellis Horwood, London, 1973.
6. P.B. Ayscough, "Electron Spin Resonance in Chemistry", Methuen, London, 1967.
7. J.D. Memory, "Quantum Theory of Magnetic Resonance Parameters", McGraw-Hill, New York, 1968.
8. C.J. Ballhausen and H.B. Gray, "Molecular Orbital Theory" W.A. Benjamin and Co., New York, 1965.

PART II

AN ELECTRON PARAMAGNETIC RESONANCE STUDY OF THE ELECTRONIC STRUCTURE OF RHENIUM OXYCHLORIDE, ReOCl_4 , AND SOME OF ITS ADDUCTS

2.1 Introduction

Detailed investigations of electronic spectra, of electron paramagnetic resonance spectra, and of the relationships connecting these branches of spectroscopy with bonding, have been made for d^1 complexes derived from the oxy-ions of vanadium, niobium, chromium, molybdenum and tungsten ^{1,2}. The relatively simple magnetic and optical properties which arise from the single unpaired electron and the approximately C_{4v} symmetry have made these systems of particular interest.

The electronic structure of these complexes have been described in terms of a molecular orbital model and it seems to be most appropriate for the description of the bonding. A semiempirical LCAO-MO method has been used by Ballhausen and Gray ³ on the complex $\text{VO}(\text{H}_2\text{O})_5^{2+}$ and Gray and Hare ⁴ on $(\text{MOCl}_5)^{2-}$, where $M = \text{Cr}$ or Mo , from which they are able to predict the relative energies of the molecular orbitals in the complexes and they obtained a reasonable fit for the optical spectra. In these calculations, they found that the unpaired electron was in a non-bonding molecular orbital localised completely on the central metal ion.

On the basis of electron paramagnetic resonance studies of bromo oxo-anion complexes of molybdenum and tungsten, Kon and Sharpless⁵ showed that the bromine hyperfine coupling observed in the e.p.r. spectrum can be explained in terms of in-plane π bonding between the four halogens in the XY plane and the transition metal ion. Further evidence that metal-halogen interactions cannot be neglected has been provided by Harner and Tyree⁶.

Much less information is available for the corresponding compounds of the hexivalent states of the group VIIa elements. In this context, in the case of rhenium (VI), electron paramagnetic resonance absorption has only been observed in magnetically concentrated samples containing the rhenate ion⁷, ReO_4^{2-} , and in rhenium oxychloride and some of its adducts^{8,9}, but detailed analyses of these last observations have not been reported. It was therefore decided to study the electron paramagnetic resonance spectra obtained from glasses which contain rhenium oxychloride and its adducts in order to obtain information about the spin-Hamiltonian parameters, and thence use these parameters to obtain detailed quantitative information about the electronic distribution and bonding within these compounds.

2.2 Experimental

Rhenium oxychloride and its adducts $\text{ReOCl}_4\text{O}_2\text{C}_4\text{H}_8$, $\text{ReOCl}_4\text{OPCl}_3$, $\text{ReOCl}_4\text{NCCH}_3$ and $\left[(\text{C}_6\text{H}_5)_4\text{As}\right] \left[\text{ReOCl}_5\right]$ were

prepared by the following methods.

I. ReOCl_4 , was prepared ¹⁰ by reacting rhenium metal powder with purified sulphuryl chloride inside an evacuated sealed tube held at 340°C for three days. After allowing the reaction mixture to cool to room temperature excess SO_2Cl_2 was distilled off under vacuum at 273K and the volatile dark red-brown ReOCl_4 was separated from unreacted rhenium metal by subliming it in vacuum at 290K.

II. $\text{ReOCl}_4\text{O}_2\text{C}_4\text{H}_8$, was prepared by distillation of purified dioxane on to the re-sublimed product of ReOCl_4 in a vacuum line at room temperature. The solution produced is dark purple-red in colour.

III. $\text{ReOCl}_4\text{POCl}_3$, was prepared ¹¹ by mixing re-sublimed ReOCl_4 with purified POCl_3 in sealed glass apparatus fitted with break-seals and attached to a vacuum line. After allowing the reaction mixture to cool to ice-temperature excess POCl_3 was distilled off. The red product of $\text{ReOCl}_4\text{POCl}_3$ was purified by sublimation.

IV. $\text{ReOCl}_4\text{NCCH}_3$, was prepared ¹² by distillation of an excess of anhydrous acetonitrile on to re-sublimed ReOCl_4 in a vacuum line at room temperature. An orange-brown solution and solid formed. After allowing the reaction mixture to stand for an hour, the excess of acetonitrile was distilled off and the remaining solid was pumped for one hour at room temperature.

V. $[(C_6H_5)_4As][ReOCl_5]$ was prepared ¹² on the vacuum line by mixing a purified solution of $ReOCl_4$ in chloroform with a solution of tetraphenylarsonium chloride in the same solvent. The product precipitated out on standing at room temperature as small red-brown crystals. These were filtered off, washed several times with chloroform, and then pumped in vacuo to remove excess chloroform.

Because of the sensitivity of these compounds to moisture, all the solvents and reagents were purified, dried and degassed beforehand, and the compounds themselves were stored and handled in a nitrogen-filled dry box. The purity of $ReOCl_4$ and its adducts was checked by infrared measurements in Nujolmull and in solution and the observed I.R. frequencies for these compounds were in good agreement with previous observations ^{11,12,13,14}. The e.p.r. spectra of thoroughly out-gassed $10^{-3}M$ solutions of each compound were examined at 290K and in glasses at 77K in a Decca X-3 e.p.r. spectrometer. Visible u.v. absorption spectra of solutions of each compound were recorded on Unicam SP700C and 800 spectrophotometers, using matched 1-cm quartz cells.

2.3 Analysis of the e.p.r. spectra

The e.p.r. spectra of $ReOCl_4$ and its adducts in solutions show six lines due to the interaction of one unpaired electron with an applied magnetic field and with one rhenium nucleus; nuclear spin-quantum numbers,

I, for Re^{185} (natural abundance 37.07%) and Re^{187} (natural abundance 62.93%) are both $5/2$. The magnetic dipole moments of these isotopes differ by only 1% so that we have not been able to resolve any rhenium isotopic fine structure. A typical solution spectrum, in this case for ReOCl_4 in CCl_4 at 290K, is shown in Figure 2.2. The separation between successive lines in the spectrum are not equal, due to the effect of the second-order term in the equations describing the positions of the resonance fields, and the heights of the lines in the spectrum are not equal, although the area under each peak is the same. Rotation of the complex in the solution averages out the anisotropic contributions to the spectrum better for some lines than for others, hence the variation in linewidth.

As shown in Appendix A, expressions for the observed resonance fields can be obtained by solving a spin Hamiltonian of the form ¹⁵

$$\mathcal{H} = g_0 \beta_e \underline{H} \cdot \underline{S} + A_0 \underline{S} \cdot \underline{I} \quad \dots\dots 2.1$$

where g_0 and A_0 are the isotropic g-factor and hyperfine coupling constant. The expression for the allowed transitions of the form $\Delta m_I = 0$, $\Delta m_S = \pm 1$ obtained ¹⁵ by solving this Hamiltonian can be written

$$H = h \nu_0 (g_0 \beta_e)^{-1} - hc (g_0 \beta_e)^{-1} A_0 m_I - hc^2 (2g_0 \beta_e \nu_0)^{-1} A_0^2 \times \left[I(I+1) - m_I^2 \right] \quad \dots\dots 2.2$$

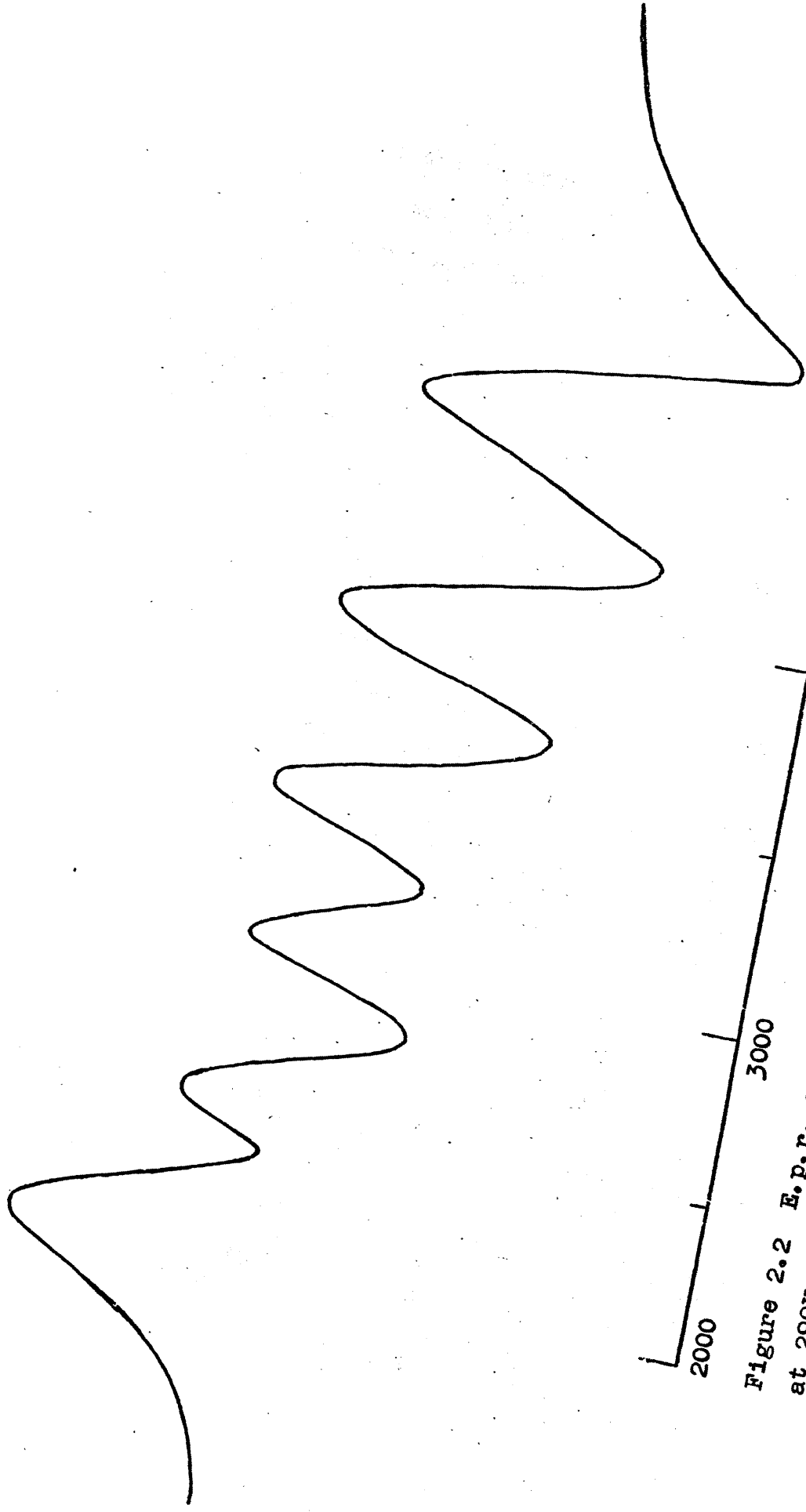


Figure 2.2 E.p.r. spectrum of a 10^{-3} M solution of ReOCl_4 in CCl_4 solution at 290K.

where the hyperfine coupling A_0 is in cm^{-1} . Thus by using equation 2.2, the value of g_0 and A_0 can be obtained from the observed values of the resonance fields in the spectra. g_0 and A_0 values for ReOCl_4 and its adducts are listed in Table 2.1.

The e.p.r. spectra obtained from magnetically dilute glasses of ReOCl_4 and its adducts are very well resolved as shown in Figure 2.3 for ReOCl_4 in dioxane. It is possible to distinguish peaks in the spectra corresponding to the case where the applied magnetic field lies along each of the principal axes of the compounds. For the compounds of this type, which have C_{4v} symmetry, the principal axes are those shown in Figure 2.1 below.

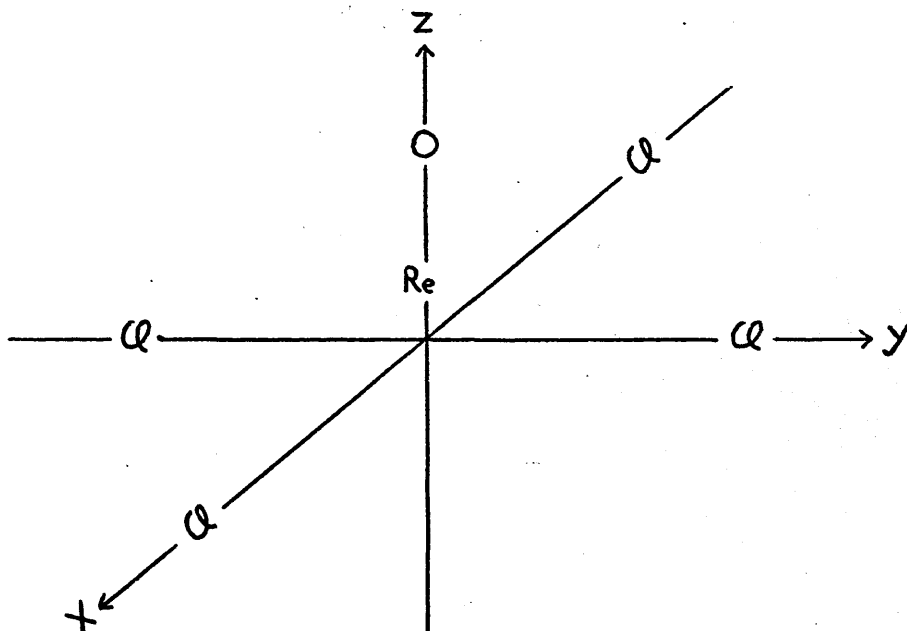


Figure 2.1

Table 2.1

Isotropic spin-Hamiltonian parameters for rhenium compounds in solution at 290K. The A_0 values are in units of cm^{-1} . Limits of error are $g_0 \pm 0.005$, $A_0 \pm 0.0005 \text{ cm}^{-1}$.

<u>Compound</u>	<u>Solvent</u>	<u>A_0</u>	<u>g_0</u>
ReOCl_4	CCl_4	-0.0422	1.793
$\text{ReOCl}_4 \cdot \text{O}_2 \cdot \text{C}_4\text{H}_8$	dioxane	-0.0415	1.800
$\text{ReOCl}_4 \cdot \text{NCCH}_3$	nitromethane	-0.0409	1.808
$\text{ReOCl}_4 \cdot \text{OPCl}_3$	POCl_3	-0.0397	1.814
$[(\text{C}_6\text{H}_5)_4\text{As}] [\text{ReOCl}_5]$	dioxane	-0.0390	1.820

These spectra at 77K are all characteristic of one unpaired electron moving in an axially symmetric orbital so that as shown in Appendix A the spin Hamiltonian has the form ¹⁵

$$\mathcal{H} = g_{11} \beta_e H_z S_z + g_{\perp} \beta_e (H_x S_x + H_y S_y) + A S_z I_z + B (S_x I_x + S_y I_y) + Q' \left[I_z^2 - \frac{1}{3} I(I+1) \right] \quad \dots 2.3$$

where g_{11} and g_{\perp} denote the electron g values parallel and perpendicular to the symmetry axis (z -axis) of the molecule, respectively; A and B are the nuclear hyperfine coupling parallel and perpendicular to the symmetry axis, respectively; $H_{x,y,z}$ are the components of the magnetic field vector; and Q' is related to nuclear quadrupole coupling constant eqQ by the equation

$$Q' = \frac{3eqQ}{4I(I+1)}$$

As shown in Appendix B, the general expression for the allowed transitions of the form $\Delta m_I = 0$, $\Delta m_S = \pm 1$, where the applied magnetic field lies at an angle θ to the symmetry axis is given by ¹⁶

$$\begin{aligned} H = H^0 &- K m_I - \frac{B^2 g_{\perp}^2}{4H g^2} \left[\frac{A^2 g_{11}^2 + K^2 g^2}{K^2 g^2} \right] \left[I(I+1) - m_I^2 \right] \\ &- \frac{1}{2H} \left[\frac{A^2 g_{11}^2 - B^2 g_{\perp}^2}{K g^2} \right]^2 \left[\frac{g_{11} g_{\perp}}{g^2} \right]^2 \sin^2 \theta \cos^2 \theta m_I^2 \\ &+ \frac{2Q'^2 g_{\perp}^2 \cos^2 \theta \sin^2 \theta}{K g^2} \left[\frac{A B g_{11}^2 g_{\perp}^2}{K^2 g^4} \right]^2 m_I \left[4I(I+1) - 8m_I^2 - 1 \right] \\ &- \frac{Q'^2 g_{\perp}^2 \sin^4 \theta}{2K g^2} \left[\frac{B g_{\perp}^2}{K g^2} \right]^4 m_I \left[2I(I+1) - 2m_I^2 - 1 \right] \end{aligned}$$

..... 2.4

45.

The equation 2.4 has two important cases. At $\theta = 0^\circ$ (parallel orientation), $g = g_{11}$, $K = A$, and only the first three terms contribute to the lines position. Hence the quadrupole terms do not contribute in this case. In the perpendicular orientation case ($\theta = 90^\circ$), $g = g_1$, $K = B$, and the second-order hyperfine interaction becomes more important and the quadrupole interaction contributes to the line position. Thus the values of g_{11} , g_1 , A, B and Q' can be obtained from equation 2.4 by analysing the e.p.r. spectra at these two orientations. The estimation of these parameters was accomplished with the help of a computer programme, whereby it was possible to simulate the spectrum. The program involved an iterative procedure, whereby the computer was supplied with a set of resonant fields $H_y = H_x$, and H_z for each m_I value as estimated from the spectrum. The computer then plotted a set of Kneubühl curves of the type described in Appendix C, added them together, broadened them, and plotted the first derivative of the spectrum. The lineshape was assumed to be Gaussian¹⁷, and the computer was also supplied with a broadening parameter β . The values of the resonant fields supplied, and the value of β , were then varied until the best fit between the observed and calculated spectra was obtained. The observed and calculated spectra of ReOCl_4 in CCl_4 and in dioxane are shown in Figure 2.3. The values of the resonant fields corresponding to the best fit were then used with equation 2.4 to calculate the values of g_{11} , g_1 ,

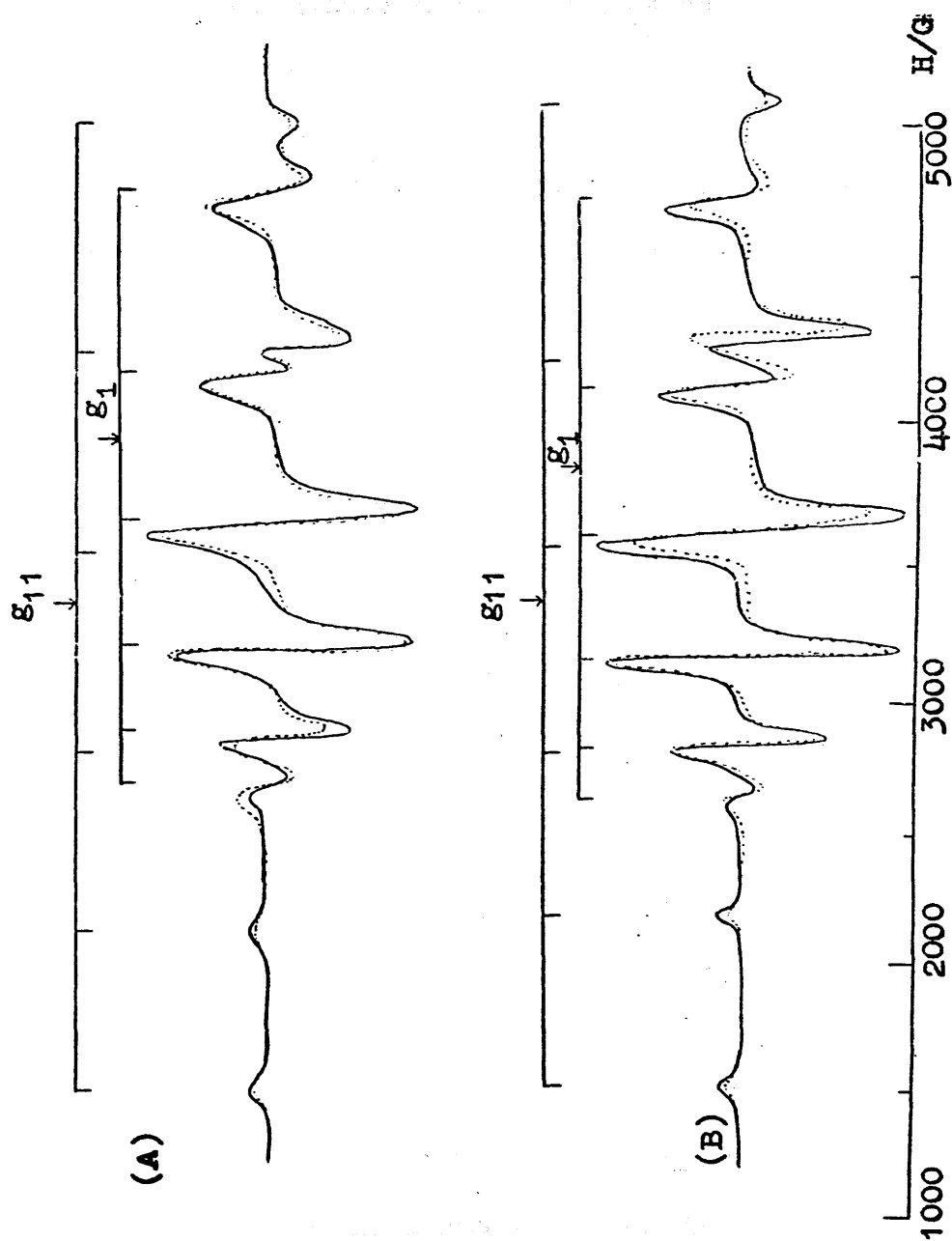


Figure 2.3. observed (full line) and calculated (dotted line) e.p.r. spectra of 10^{-3} M-solutions of ReOCl_4 in CCl_4 , A, and $\text{ReOCl}_4\text{O}_2\text{C}_4\text{H}_8$ in dioxane, B, at 77K.

A, B and Q' for each compound. These parameters are listed in Table 2.2, where A, B and Q' are expressed in cm^{-1} .

The forms of the contributions to the polycrystalline spectrum originating from complexes in which $m_I = 3/2$ puzzled as until it was realised that for these species the relative magnitudes of the spin-Hamiltonian parameters are such that the resonant field values do not vary smoothly as the orientations of these molecules in the applied magnetic field are altered. As in the case already reported for some copper (II) complexes^{18,19}, discontinuities therefore appear in the Kneubühl function $S(H)$ for $m_I = 3/2$, in addition to those that are observed when the magnetic field lies along the principal axes directions. For ReOCl_4 in dioxane, $S(H)$ for $m_I = 3/2$ is shown in Figure 2.4.

From these analyses g_{11} turns out to be greater than g_1 , a situation which is unusual in d^1 species subjected to a tetragonal ligand field and this as will be explained later is shown to be essentially due to charge-transfer^{5,20,21} mixing by spin-orbit coupling at the chlorine atoms. The analyses show that A and B must have the same sign since the isotropic coupling, A_0 , obtained from the solution spectra serves as a useful check to the relative sign to these parameters which are equated by the approximate relationship

$$A_0 \approx \frac{A+2B}{3} \quad \dots \quad 2.5$$

Table 2.2

Spin Hamiltonian parameters for rhenium oxychloride and its "adducts" at 77K. All hyperfine tensor components are in units of cm^{-1} . Limits of error are g_{11} and g_1 and $\langle g \rangle$, ± 0.004 , A, Band(A) $\pm 0.0004 \text{ cm}^{-1}$, $Q' = \pm 0.0001 \text{ cm}^{-1}$.

Compound	Solvent	g_{11}	g_1	A	B	Q'	$\langle g \rangle$	$\langle A \rangle$
ReOCl_4	CCl_4	1.974	1.708	-0.0636	-0.0323	± 0.0020	1.796	-0.0419
$\text{ReOCl}_4 \cdot 2\text{C}_6\text{H}_6$	dioxane	1.968	1.720	-0.0630	-0.0320	± 0.0020	1.803	-0.0417
$\text{ReOCl}_4 \cdot \text{NCCH}_3$	nitromethane	1.970	1.732	-0.0621	-0.0315	± 0.0020	1.811	-0.0406
$\text{ReOCl}_4 \cdot \text{OPCl}_3$	POCl_3	1.970	1.734	-0.0616	-0.0308	± 0.0019	1.813	-0.0397
$[(\text{C}_6\text{H}_5)_4\text{As}][\text{ReOCl}_5]$	dioxane	1.975	1.740	-0.0609	-0.0305	± 0.0020	1.818	-0.0392

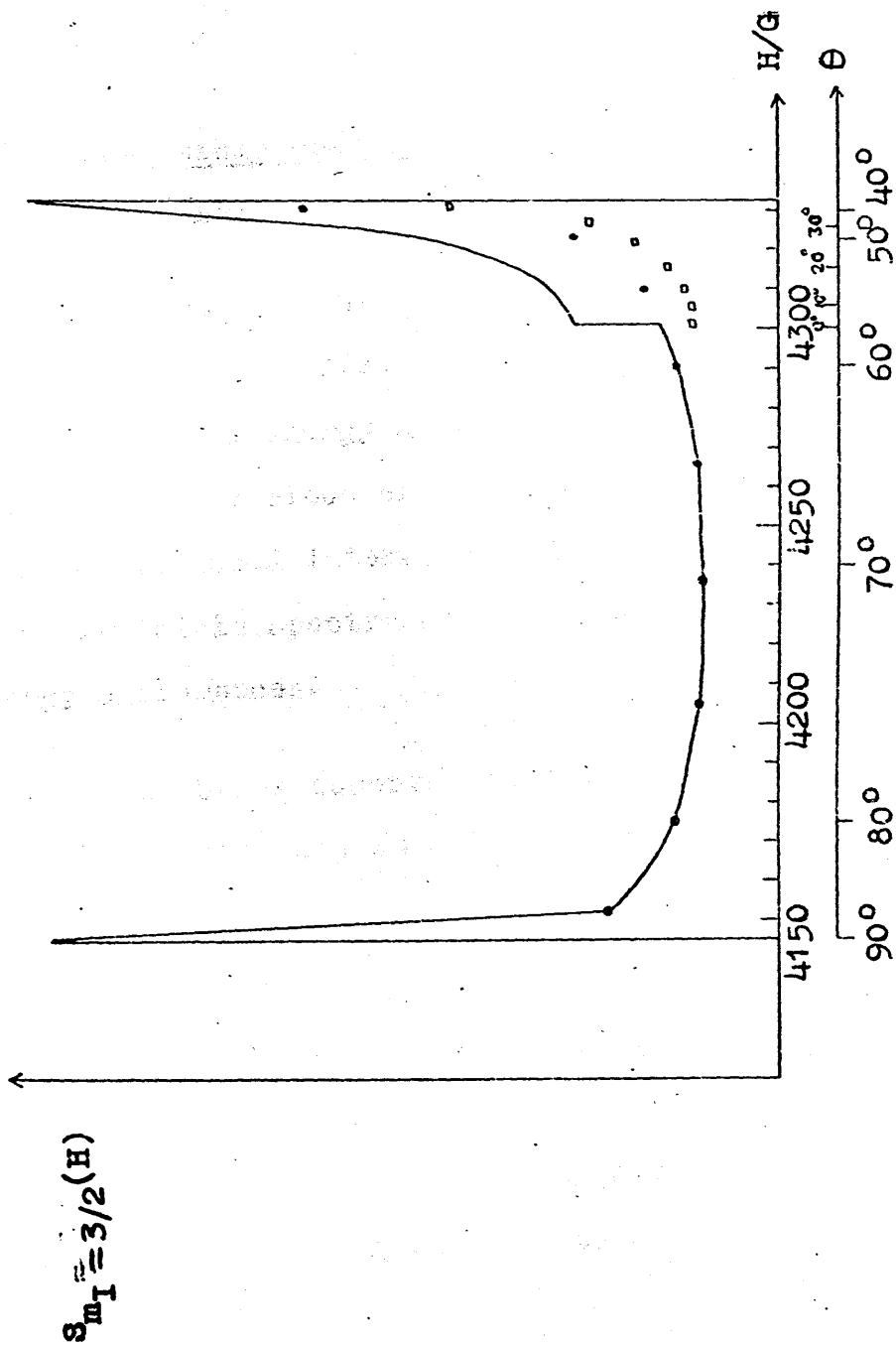


Figure 2.4. The Kneubühl curve $S_{m_I}(H)$ for ReOCl_4 when $m_I = 3/2$. θ is the angle between the applied magnetic field and the molecular C_4 axis, and H is the corresponding resonant field.

□ denote contributions from molecules for which $0^\circ \leq \theta \leq 35^\circ$. \circ denote contributions for which $40^\circ \leq \theta \leq 90^\circ$. — is the resultant $S_{m_I}(H)$ function.

The theoretical treatment which will be discussed later shows that the signs of A and B in these compounds are negative. Since forbidden transitions have not been observed the sign of Q' cannot be obtained from these spectra.

2.4 U.v-visible spectra of rhenium oxychloride and its adducts

In describing the electronic structure of rhenium compounds by using electron paramagnetic resonance techniques, the energy differences between the ground state and the various excited states must be known, as will be discussed later. The band maxima observed in u.v.-visible spectra can often be equated to these energy differences.

The various bands observed in the u.v-visible spectra of rhenium compounds in solution can be summarised as follows.

- a) ReOCl_4 in CCl_4 shows weak absorption at 12800 cm^{-1} which, from its position and intensity is almost certainly a d-d transition, involving the transfer of the unpaired electron to an empty antibonding orbital. This band is shifted to lower energy in the case of the six coordinated adducts.
- b) ReOCl_4 in CCl_4 shows a weak transition again at 17500 cm^{-1} . This is almost certainly a d-d transition, involving the transfer of the unpaired electron to another empty

antibonding orbital. In the case of the six coordinated adducts this band is shifted slightly to lower energy.

c) ReOCl_4 in CCl_4 shows a strong absorption band at 23800 cm^{-1} . This is assignable to the first charge-transfer band, involving excitation of an electron from a filled orbital to the orbital containing the unpaired electron. This band is not sensitive to addition of an extra ligand to the sixth coordination position of ReOCl_4 .

d) Other bands which appear in the u.v.-region (29000 - 32000 cm^{-1}) for these compounds may be assigned to other charge transfers.

From the above it was shown that the addition of an extra ligand to the sixth coordination position of ReOCl_4 has a considerable effect on the first band in the spectra and little effect on the second. The third band which is assigned to be charge-transfer no considerable effects have been noticed.

The frequency of the band maxima in the u.v.-visible spectra of the compounds are shown in Table 2.3 and example of the spectrum of ReOCl_4 in CCl_4 is given in Figure 2.5.

2.5 Extended Hückel molecular orbital calculations of rhenium oxychloride and its adducts.

In order to use the spin-Hamiltonian parameters to obtain detailed information about the electronic distributions in these compounds, estimates of the values

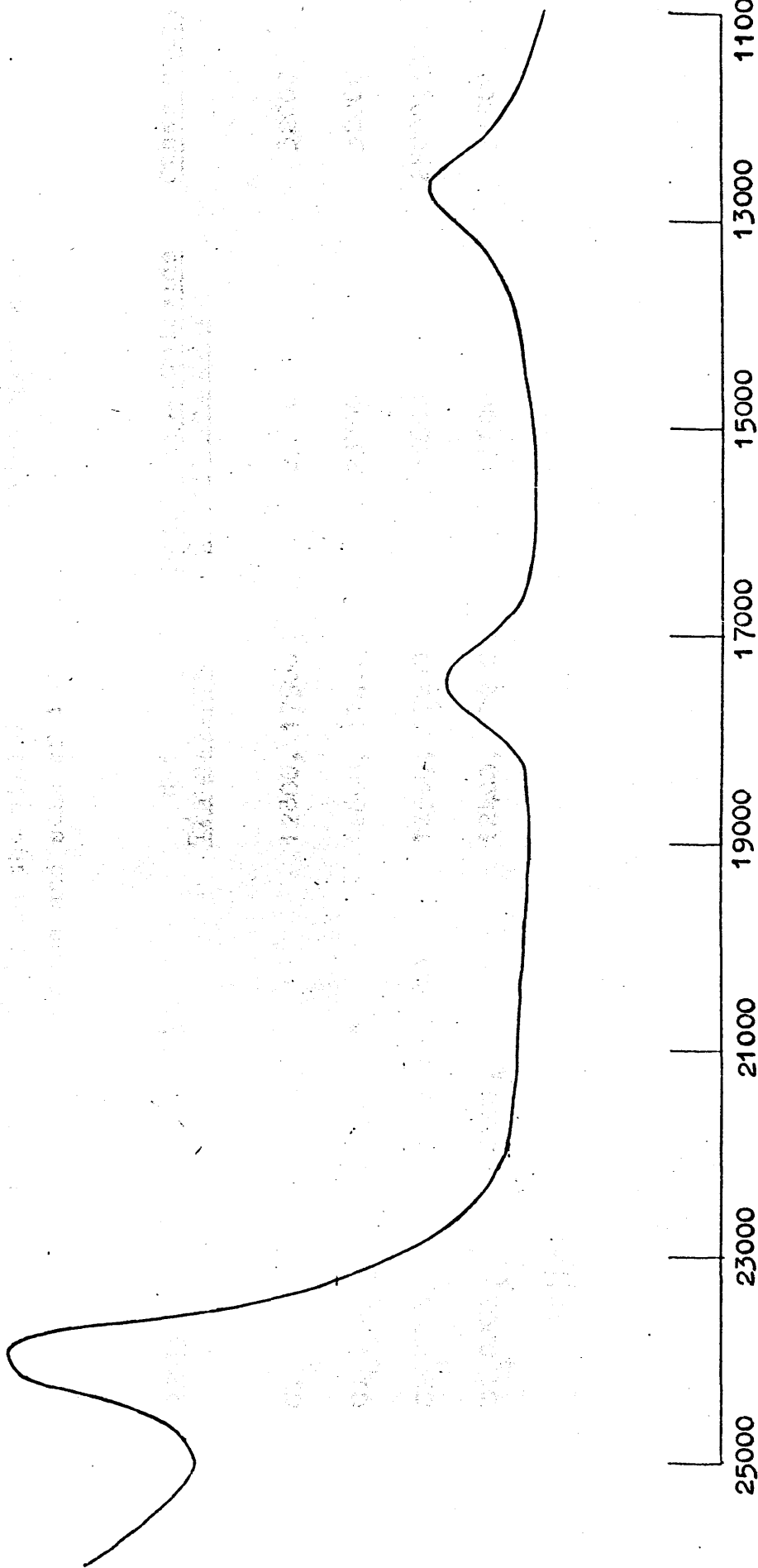


Figure 2.5 U.v.-visible spectrum of ReOCl_4 in CCl_4 at 290K.

Table 2.3

Band maxima (cm^{-1}) in the visible -u.v. absorption spectra of rhenium oxychloride and some of its "adducts".

<u>Compound</u>	<u>Solvent</u>	<u>d-d Transitions</u>	<u>Metal ion ← Chloride Charge transfer</u>	<u>Other bands</u>
ReOCl_4	CCl_4	12800, 17500	23800	32000
$\text{ReOCl}_4 \cdot 2\text{C}_4\text{H}_8$	dioxane	12600, 17400	23700	32000
$\text{ReOCl}_4 \cdot \text{NCCH}_3$	nitromethane	12500, 17200	23600	25000, 31200
$\text{ReOCl}_4 \cdot \text{POCl}_3$	POCl_3	12400, 17200	23600	31500
$[(\text{C}_6\text{H}_5)_4\text{As}][\text{ReOCl}_5]$	dioxane	12000, 17000	23600	29000

of the spin-orbit coupling constant ξ , and the parameter $P = 2.0023 g_N \beta_e \beta_N \langle \Psi | r^{-3} | \Psi \rangle$ for the rhenium ion with the appropriate charge were needed. To do this an extended Hückel molecular orbital calculation was carried out on ReOCl_4 .

The general method used for the calculation can be summarised as follows.

- a) The metal ion and ligand orbitals are assigned to the various irreducible representations of the point group of the molecule, which is assumed to be C_{4v} .
- b) The overlap integrals between the central metal ion and the ligand orbitals are calculated. Hence the group overlap integrals between the metal ion orbitals and ligand orbitals of the various symmetry types are calculated.
- c) The coulomb integrals for the various atomic orbitals are approximated as valence-state ionisation energies. The valence-state ionisation energy is a function of the charge and the configuration of the atom in the molecule in question.
- d) The resonance integrals between the two orbitals on different atoms are assumed to be functions of the coulomb integrals of the two orbitals as well as of the overlap integrals between them.
- e) The molecular orbitals of the compound are assumed to be a linear combination of the central metal ion atomic orbitals and the ligand group orbitals of the same symmetry.

f) From the known values of coulomb integrals H_{ii} , resonance integrals H_{ij} and the overlap integrals S_{ij} , the secular determinant can be solved and the eigenvalues and eigenfunctions obtained.

g) The electrons available to the compound are fed into the molecular orbitals according to the Aufbau principle. A population analysis is carried out, and the charge and configuration of the metal ion are obtained.

h) The computed metal ion charge and orbital populations are then used to estimate new H_{ii} values and the cycle of calculations are then repeated until the input and output charges are identical.

The dimensions used in our molecular orbital calculations were obtained from Edwards' X-ray analysis²² of ReOCl_4 . This shows that the molecule is a square pyramid with C_{4v} symmetry, the four chlorine atoms forming the base of the pyramid and the rhenium atom is raised 0.59 \AA above the plane containing the four chlorine atoms. The Re-O bond length is 1.63 \AA , the Re-Cl bond length is 2.26 \AA and the O-Re-Cl bond angle is 105° . By using the coordinate system shown in Figure 2.6, molecular orbitals in this compound may be described in terms of basis orbitals derived from

- i) the 5d, 6s and 6p orbitals of the rhenium ion,
- ii) the chloride ion 3s and 3p orbitals and,
- iii) the oxide ion 2s and 2p orbitals.

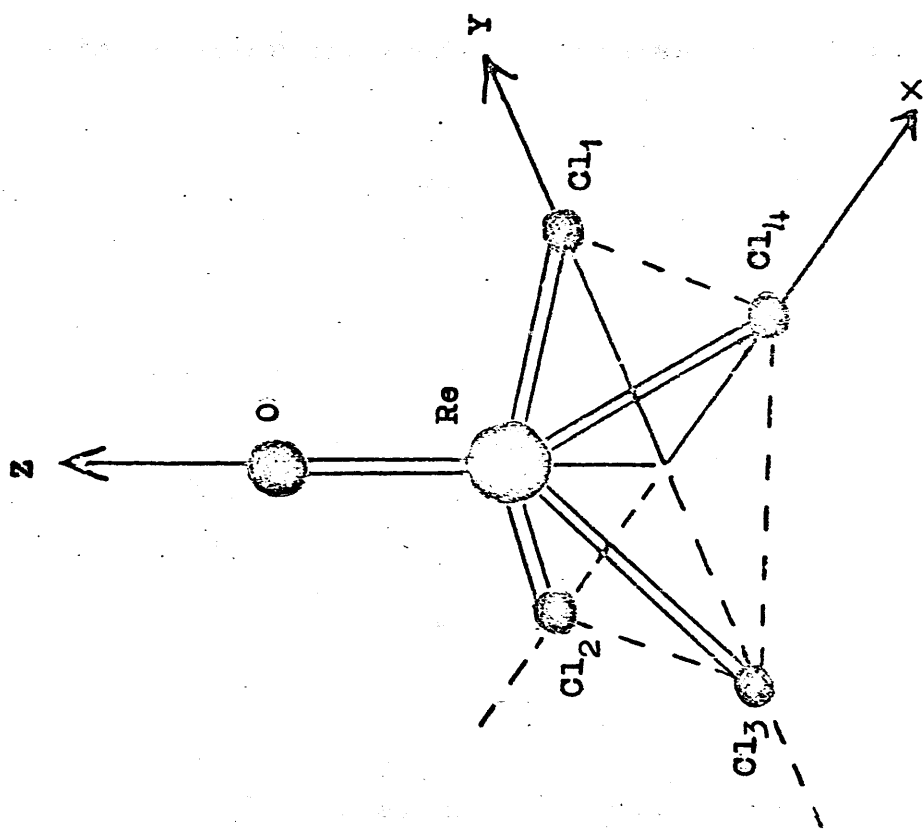


Figure 2.6 Coordinate system of rhenium oxychloride.

In the C_{4v} group, these twenty-nine basis orbitals can themselves be grouped as shown in Table 2.4.

Slater-type atomic orbitals of the kind described by Cusachs et al. ^{23,24} were used to estimate the overlap integrals between basis orbitals. These are single exponents of the form $Nr^{n-1}e^{-\xi r}$, in which the value of the principal quantum number n , and the orbital exponent ξ , are chosen to give the best agreement with the overlap properties of Clementi's multi-exponent wave functions ^{25,26}. The best value of ξ and n for the various atoms are given below.

Rhenium	6s	n=6	$\xi = 2.5$
"	6p	n=6	$\xi = 2.2$
"	5d	n=5	$\xi = 2.92$
Chlorine	3s	n=3	$\xi = 2.2$
"	3p	n=3	$\xi = 1.82$
Oxygen	2s	n=2	$\xi = 2.2$
"	2p	n=2	$\xi = 1.95$

The group overlap integrals obtained using these values are listed in Table 2.5. The ionisation energies for the rhenium ion atomic orbitals were obtained using the method of Cotton and Harris ^{27,28} while the corresponding energies for chlorine 3s and 3p orbitals and for oxygen 2s and 2p orbitals were taken from reference 29.

The resonance integrals were calculated using the Wolfsberg-Helmholtz ³⁰ approximation

$$H_{ij} = 0.95 [H_{ii} + H_{jj}] S_{ij} \quad \dots \quad 2.6$$

Table 2.4

Metal and ligand orbitals for the molecular orbital of ReOCl_4

	A_1	A_2
Rhenium ion orbitals	$6s; 6p_z; 5d_{z^2}$	-
Chloride ion orbitals	$3s(A_1) = \frac{1}{2} [3s_1 + 3s_2 + 3s_3 + 3s_4]$ $3p_z(A_1) = \frac{1}{2} [3p_{z1} + 3p_{z2} + 3p_{z3} + 3p_{z4}]$ $3p_x(A_1) = \frac{1}{2} [-3p_{y1} + 3p_{x2} + 3p_{y3} - 3p_{x4}]$	$3p(A_2) = \frac{1}{2} [3p_{x1} + 3p_{y2} - 3p_{x3} - 3p_{y4}]$
Oxide ion orbitals	$2s; 2p_z$	-
	B_1	B_2
Rhenium ion orbitals	$5d_{x^2-y^2}$	$5d_{xy}$
Chloride ion orbitals	$3p_z(B_1) = \frac{1}{2} [3s_1 - 3s_2 + 3s_3 - 3s_4]$ $3p_z(B_1) = \frac{1}{2} [3p_{z1} - 3p_{z2} + 3p_{z3} - 3p_{z4}]$ $3p_x(B_1) = \frac{1}{2} [3p_{y1} + 3p_{x2} - 3p_{y3} - 3p_{x4}]$	$3p(B_2) = \frac{1}{2} [3p_{x1} - 3p_{y2} - 3p_{x3} + 3p_{y4}]$
Oxide ion orbital	-	-

E

Rhenium ion orbitals

$$6p_x; 6p_y; 5d_{xz}; 5d_{yz}$$

Chloride ion orbitals

$$3s_1(E) = \frac{1}{\sqrt{2}} [3s_1 - 3s_3]$$

$$3s_2(E) = \frac{1}{\sqrt{2}} [3s_2 - 3s_4]$$

$$3p_{xz}(E) = \frac{1}{\sqrt{2}} [3p_{z_2} - 3p_{z_4}]$$

$$3p_{yz}(E) = \frac{1}{\sqrt{2}} [3p_{z_1} - 3p_{z_3}]$$

$$3p_{\pi x}(E) = \frac{1}{\sqrt{2}} [3p_{x_1} + 3p_{x_3}]$$

$$3p_{\sigma x}(E) = \frac{1}{\sqrt{2}} [3p_{x_2} + 3p_{x_4}]$$

$$3p_{\sigma y}(E) = \frac{1}{\sqrt{2}} [3p_{y_1} + 3p_{y_3}]$$

$$3p_{\pi y}(E) = \frac{1}{\sqrt{2}} [3p_{y_2} + 3p_{y_4}]$$

Oxide ion orbitals

$$2p_x; 2p_y$$

Table 2.5 (contd.)

E symmetry

	$3s_1(E)$	$3s_2(E)$	$3p_{yz}(E)$	$3p_{xz}(E)$	$3p_{\pi x}(E)$	$3p_{\sigma x}(E)$	$3p_{\sigma y}(E)$	$3p_{\pi y}(E)$	$2p_x$	$2p_y$
$6p_y$	0.505	0.000	0.194	0.000	0.000	0.000	-0.478	0.241	0.000	0.222
$6p_x$	0.000	-0.506	0.000	-0.194	0.241	-0.478	0.000	0.000	0.222	0.000
$5d_{xz}$	0.000	0.051	0.000	-0.051	-0.023	0.101	0.000	0.000	0.146	0.000
$5d_{yz}$	-0.051	0.000	0.051	0.000	0.000	0.000	0.101	-0.023	0.000	0.146

3.6 Results and discussion of molecular orbital calculations

As indicated above, the cycle of molecular orbital calculations were repeated until the input and output charges coincided. The most important results of the molecular orbital calculations of ReOCl_4 are listed below.

(1) The final estimated electronic configuration and charge at the rhenium atom turned out to be $\text{Re}(\text{-----}5d^{4.880} \quad 6s^{0.714} \quad 6p^{0.939})$ and + 0.476, respectively. The overall charges in the molecule in units of protonic charge are distributed as follows

Atom	Re	O	Cl
Charge	+0.476	-0.431	-0.011

The final eigenvalues and eigenfunctions are listed in Table 2.6 and the resultant energy level diagram is shown in Figure 2.7.

(2) The unpaired electron is in the antibonding molecular orbital B_2 numbered 21 in Figure 2.7 and starred in Table 2.6. This orbital is compounded out of the $5d_{xy}$ orbital of rhenium and chlorine $3p_x$ and $3p_y$ orbitals, and it is about 35% delocalised on to the chlorine atoms. This agrees with the qualitative deduction made earlier from the g -tensor values about the ligand orbital contributions to the molecular orbital containing the unpaired electron.

Table 2.6

Energy levels and atomic orbital coefficients in the LCAO molecular orbital description of ReOCl_4 . Molecular orbitals are in symmetry classes appropriate to the C_{4v} group. Energies are in units of eV. The unpaired electron is in the starred B_2 orbital.

<u>A_1 symmetry</u>		<u>Atomic orbital coefficients</u>							
Orbital	Energy	6s	6p _z	5d _{z²}	3s(A_1)	3p _z (A_1)	3p _x (A_1)	2s	2p _z
1	-31.21	0.139	0.077	0.091	0.032	-0.024	-0.011	0.888	0.035
2	-25.93	0.200	-0.063	-0.063	0.884	0.004	-0.036	-0.096	0.001
6	-15.50	0.234	0.015	-0.394	-0.246	0.079	0.674	-0.003	0.110
10	-13.90	0.192	-0.098	0.386	-0.127	0.227	0.198	-0.160	-0.721
14	-12.95	-0.011	0.125	-0.086	0.032	0.929	-0.166	-0.048	0.163
25	- 8.5	0.065	-0.429	0.744	-0.071	0.166	0.243	0.014	0.594
28	33.4	-0.417	1.352	0.703	0.539	-0.345	0.918	-0.738	0.403
29	51.2	1.679	0.387	0.082	-0.694	-0.415	-0.975	-0.835	0.574

Table 2.5 (Contd.)

<u>A₂ symmetry</u>		<u>Atomic orbital coefficients</u>		
Orbital	Energy	3p(A ₂)		
18	-12.80	1.000		
<u>B₁ symmetry</u>		<u>Atomic orbital coefficients</u>		
Orbital	Energy	5d _{x²-y²}	3s(B ₁)	3p _z (B ₁)
5	-25.14	-0.103	0.981	-0.001
7	-14.35	-0.549	-0.141	0.270
17	-12.80	0.000	0.000	0.928
24	- 8.92	0.870	0.187	0.268
<u>B₂ symmetry</u>		<u>Atomic orbital coefficients</u>		
Orbital	Energy	5d _{xy}	3p(B ₂)	
11	-13.80	-0.603	-0.729	
21 [±]	-11.01	0.807	-0.696	

Table 2.6 (contd.)

Orbital	Energy	Atomic orbital coefficients							
		6p _x or 6p _y	5d _{xz} or 5d _{yz}	3s ₂ (E) or 3s ₁ (E)	3p _{xz} (E) or 3p _{yz} (E)	3p _x (E) or 3p _y (E)	3p _{πx} (E) or 3p _{πy} (E)	3p _{πx} (E) or 3p _{πy} (E)	2px or 2py
3,4	-25.30	+0.127	+0.037	+0.930	-0.013	+0.034	+0.017	+0.015	
8,9	-14.13	-0.000	+0.619	+0.062	+0.233	+0.461	-0.104	+0.431	
12,13	-13.41	+0.204	+0.122	+0.136	+0.429	+0.582	+0.351	+0.301	
15,16	-12.80	0.000	0.000	0.000	+0.273	0.000	+0.899	0.000	
19,20	-12.66	+0.036	+0.122	+0.014	+0.789	-0.296	-0.127	+0.502	
22,23	-9.79	+0.048	+0.786	+0.035	+0.216	-0.307	+0.051	-0.681	
26,27	+31.0	+1.627	-0.103	+0.901	+0.349	+0.888	-0.443	-0.388	

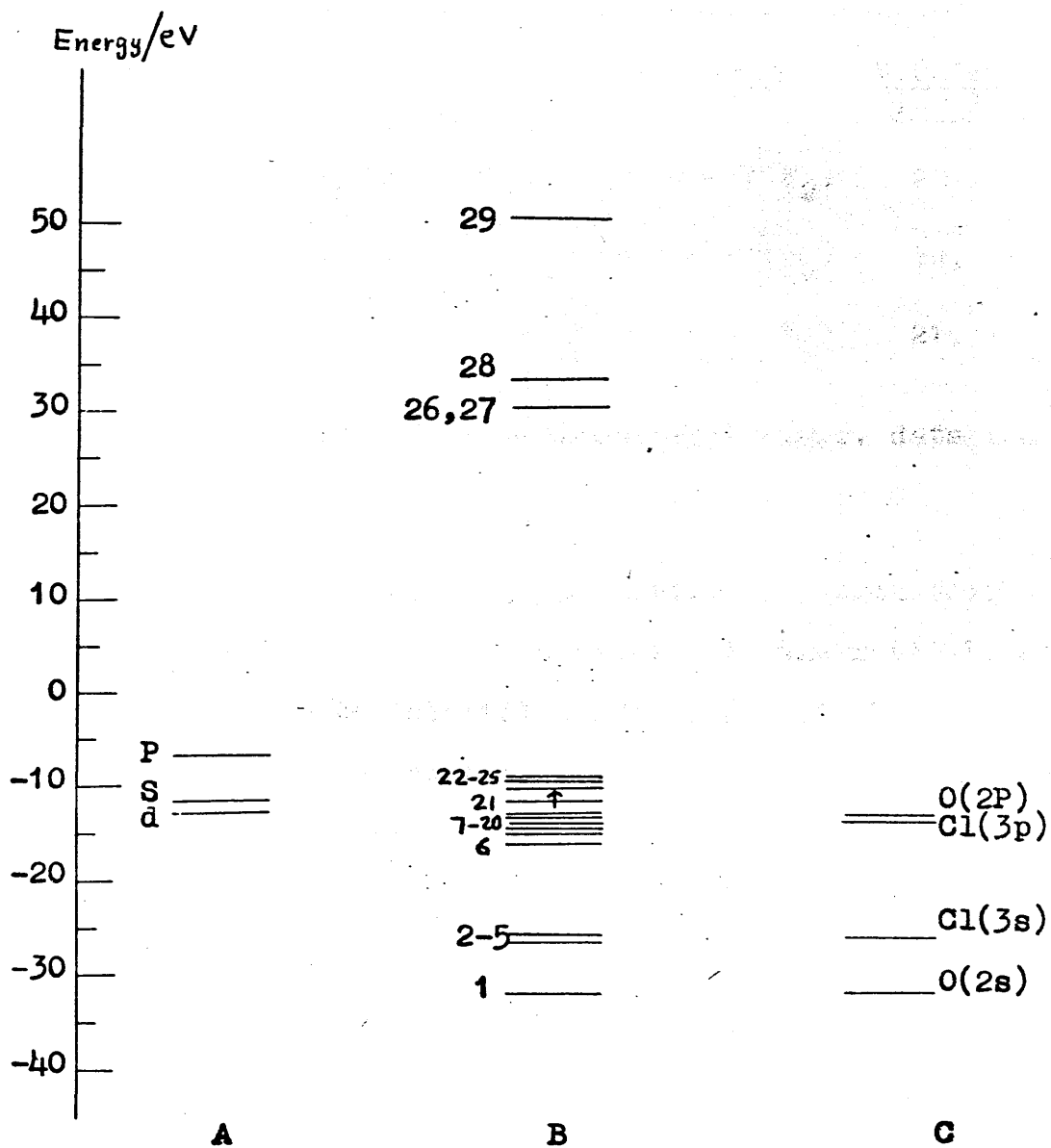


Figure 2.7 Molecular orbital energy-level diagram for ReOCl_4 : A, metal-ion orbitals; B, molecular orbitals; and C ligand orbitals.

(3) If the electron-electron repulsions are ignored, the band maxima in the visible-u.v. absorption spectra listed in Table 2.3 can be equated to the separation of the energy levels in the molecular orbital diagram. These bands should be assigned in the following way.

<u>Band maxima (cm⁻¹)</u>	<u>Transition</u>	<u>M.O. levels involved</u>
12800	$\Psi^*(E) \leftarrow \Psi^*(B_2)$	22, 21
17500	$\Psi^*(B_1) \leftarrow \Psi^*(B_2)$	24, 21
23800	$\Psi^*(B_2) \leftarrow \Psi(B_1)$	21, 7

These assignments are consistent with e.p.r. data and with the positions and intensities of the bands.

(4) The molecular orbital calculation suggests that there is a high degree of covalency in the metal-ligand bonds. The metal orbital coefficients of the anti-bonding molecular orbitals 21, 24 and 22 estimated from this calculation are

$$\begin{array}{ccc} \underline{\beta_2} & \underline{\beta_1} & \underline{e_{xz}} \\ 0.807 & 0.869 & 0.786 \end{array}$$

where β_2 , β_1 and e_{xz} are the coefficients of rhenium d_{xy} , $d_{x^2-y^2}$ and d_{xz} orbitals respectively. These coefficients will be estimated independently from e.p.r. data later.

(5) Knowing the ionic charge of the central metal ion, the value of the spin-orbit coupling constant ζ for rhenium in ReOCl_4 can be estimated from Figure 2.8 which obtains when the free-ion values of the spin-orbit coupling constant¹ for rhenium are plotted against ionic charge. Since spin-orbit coupling constants for the third transition series are only approximately known, and since we do not have enough information to enable us to estimate the effects of change in configuration on these values, we have used the value of $\zeta = 2400 \text{ cm}^{-1}$, obtained directly from Figure 2.8, for $\text{Re}^{0.476}$ in rhenium oxychloride. The spin-orbit coupling constant for chlorine in ReOCl_4 was assumed to be identical with the value for the free atom²⁰ ($\zeta_{\text{Cl}} = 587 \text{ cm}^{-1}$). The P value of 0.033 cm^{-1} was obtained by interpolating between the values of 0.032 cm^{-1} for Re^0 (----- $5d^5 6s^2$) and 0.050 cm^{-1} for Re^{+6} (----- $5d^1$), which were derived from the value of $\langle r^{-3} \rangle$ given by McMillan and Halpern^{1,31}.

2.7 Equations relating the spin-Hamiltonian parameters to the molecular orbital coefficients in rhenium oxychloride

As can be seen from the energy level diagram of the molecular orbitals the unpaired electron is located in a B_2 antibonding molecular orbital. If the spin-orbit coupling is ignored then this orbital has the form

$$\Psi^*(B_2) = \beta_2 d_{xy} + \beta_2^{(1)} 3p_{(B_2)} \quad \dots \quad 2.7$$

but when spin-orbit interactions are considered then mixing of excited states into the ground state of the molecule must be taken into account. These excited states are produced either by promoting the unpaired electron into an empty antibonding orbital of B_1 or of E symmetry which is immediately above $\Psi^*(B_2)$ in Figure 2.7, or by promoting an electron from the filled bonding orbitals of B_1 or of E symmetry into $\Psi^*(B_2)$: only mixing of the molecular orbitals numbered 7, 22, 23 and 24 need be considered in this context. The molecular orbital calculations show that in these compounds ligand s orbitals contribute little to the magnetically important molecular orbitals so that these may be written in the forms

$$\Psi(B_1) = \beta_1 d_{x^2-y^2} + \beta_1^{(1)} 3p_{\sigma} [B_1] + \beta_1^{(11)} 3p_z [B_1]$$

$$\Psi(E_{xz}) = e_{xz} d_{xz} + e_{xz}^{(1)} 3p_{xz} [E] + e_{xz}^{(11)} 3p_{\sigma x} [E] + e_{xz}^{(111)} 2p_x [E] \quad \dots \quad 2.8$$

$$\Psi(E_{yz}) = e_{yz} d_{yz} + e_{yz}^{(1)} 3p_{yz} [E] + e_{yz}^{(11)} 3p_{\sigma y} [E] + e_{yz}^{(111)} 2p_y [E]$$

If the matrix elements of true Zeeman and hyperfine Hamiltonian are equated to the corresponding matrix elements of the spin Hamiltonian as described in Appendix A, equations relating the spin-Hamiltonian

parameters to the molecular orbital coefficients for the compounds are obtained. Thus mixing of the orbitals (2.7) and (2.8) under the influence of spin-orbit coupling at the rhenium and chlorine atoms, along with Zeeman interaction and hyperfine interactions, then leads to the relationships (2.9) - (2.13) for the principal components of the g- and hyperfine coupling tensors ^{21,32}.

$$g_{11} = 2.0023 \pm \left[\frac{2 \xi_{\text{Re}}}{|\Delta E(B_1)|} \left[2\beta_1 \beta_2 - \beta_1^{(1)} \beta_2^{(1)} \right] V_{\text{Cl}} \right] \\ \times \left[2\beta_1 \beta_2 - \beta_1^{(1)} \beta_2^{(1)} \right] \dots\dots 2.9$$

where orbitals 7 and 24 contribute to the sum, and the positive sign refers to orbital 7 and the negative sign to orbital 24.

$$V_{\text{Cl}} = \left(\xi_{\text{Cl}} / \xi_{\text{Re}} \right)$$

$$g_1 = 2.0023 - \frac{2 \xi_{\text{Re}}}{|\Delta E(E)|} \left[\beta_2 e_{xz} + \beta_2^{(1)} e_{xz}^{(1)} \right]^2 \\ \dots\dots 2.10$$

where the second term is due to mixing of orbital 22.

g_{11} is greater than g_1 in ReOCl_4 and therefore in equation (2.9) we have allowed for mixing of states obtained by exciting bonding electrons but we have not considered similar effects in equation (2.10).

$$A = P \left[-K - \frac{4}{7} B_2^2 \pm 8 \xi_{\text{Re}} B_2^2 \left(\sum \frac{B_1^2}{|\Delta E(B_1)|} \right) - \frac{6}{7} \frac{\xi_{\text{Re}} B_2^2 e_{xz}^2}{|\Delta E(E)|} \right] \quad \dots 2.11$$

where orbitals 7 and 24 contribute to the sum, the positive sign referring to orbital 7, and the negative sign to orbital 24. Orbital 22 contributes to the last term in (2.11).

$$B = P \left[-K + \frac{2}{7} B_2^2 - \frac{11}{7} \frac{\xi_{\text{Re}} B_2^2 e_{xz}^2}{|\Delta E(E)|} \right] \quad \dots 2.12$$

$$\langle A \rangle = -PK - (2.0023 - \langle g \rangle) P \quad \dots 2.13$$

K is the isotropic contribution to the hyperfine constant due to polarisation of the inner electron spin density by the unpaired d-electron.

2.8 Molecular orbital coefficients and bonding in rhenium oxychloride and its adducts.

The spin Hamiltonian parameters and the assignments of the band maxima in the u.v.-visible spectra of the compounds now enable the values of the isotropic contact term K, and the molecular orbital coefficients B_2 , B_1 and e_{xz} to be estimated by using equations (2.9) - (2.13). Parameters obtained in this way for ReOCl_4 and its adducts are listed in Table 2.7.

Since the molecular orbital that contains the unpaired electron, has zero electron spin density at the rhenium nucleus and does not mix with the metal 6s orbital in

Table 2.7

K values and molecular orbital coefficients for ReOCl_4 and some of its "adducts".

Molecular orbital		21	24	22
	K	$ B_2 $	$ B_1 $	$ e_{xz} $
ReOCl_4	1.064	0.820	0.780	0.920
$\text{ReOCl}_4 \cdot \text{O}_2 \text{C}_4\text{H}_8$	1.063	0.814	0.782	0.913
$\text{ReOCl}_4 \cdot \text{NCCH}_3$	1.041	0.809	0.781	0.907
$\text{ReOCl}_4 \cdot \text{OPCl}_3$	1.012	0.808	0.781	0.906
$[(\text{C}_6\text{H}_5)_4\text{As}][\text{ReOCl}_5]$	1.004	0.805	0.780	0.903

C_{4v} symmetry, there is no direct way of putting unpaired electron density on the nucleus. The non zero values of the isotropic contact term K , must then arise from the spin polarization mechanism³³. The values of β_2 in Table 2.7 indicate the degree of delocalisation of the unpaired electron in these compounds on to the ligands and show that in each case the unpaired electron is about 33% delocalised on to the chlorine atoms. We have not been able to resolve chlorine hyperfine coupling in these spectra but linewidth measurements which we have carried out are consistent with about 21% delocalisation in this orbital. The value of 0.82 for β_2 in ReOCl_4 is in excellent agreement with the value obtained from the molecular orbital calculations.

The β_1 and e_{xz} values in Table 2.7, which reflect the bonding of the metal ion $d_{x^2-y^2}$ and d_{xz} or d_{yz} orbitals respectively with the ligand orbitals defined by equation 2.8 are in good agreement with values obtained from the molecular orbital calculation. These values show again an appreciable degree of covalency in the metal-ligand bonds. Thus there is a good correlation between the coefficients obtained from electron paramagnetic resonance and those from molecular orbital calculations.

Addition of an extra ligand to the sixth coordination position of ReOCl_4 has no measureable effect on sigma bonding to the metal ion $5d_{x^2-y^2}$ orbital, and it has little effect on the transition energies $|\Delta E (B_1)|$.

Hence coordinating a sixth ligand does not alter g_1 . On the other hand, in the case of in-plane π -bonding to the metal-ion $5d_{xy}$ orbital, and of out-of-plane π -bonding to the metal ion $5d_{xz}$ and $5d_{yz}$ orbitals, the sixth ligand does cause very small additional drifts of electrons away from the central metal ion, and also increases the magnitudes of the transition energies $|\Delta E(E)|$. The additional ligand therefore noticeably increases the magnitude of g_1 and reduces the magnitudes of the magnetic hyperfine tensor components. This ligand should presumably have the greatest influence on sigma bonding to the metal ion $5d_{z^2}$ orbital, but this involves molecular orbitals of A_1 symmetry which are inaccessible to us since they do not affect the paramagnetic properties of these compounds.

2.9 Summary of Part II

X-band e.p.r. spectra of ReOCl_4 and of the adducts $\text{ReOCl}_4 \cdot \text{O}_2\text{C}_2\text{H}_4$, $\text{ReOCl}_4 \cdot \text{NCCH}_3$, $\text{ReOCl}_4 \cdot \text{OPCl}_3$ and $\text{ReOCl}_4 \cdot \text{O}_2\text{C}_2\text{H}_4$, $\text{ReOCl}_4 \cdot \text{NCCH}_3$, $\text{ReOCl}_4 \cdot \text{OPCl}_3$ and $[(\text{C}_6\text{H}_5)_4\text{As}][\text{ReOCl}_5]$ have been recorded at 290K, and in magnetically dilute glasses at 77K and these spectra are analysed in detail. The spin-Hamiltonian parameters A_0 , g_0 , A , B , Q' , g_{11} and g_1 have been extracted from these spectra. These parameters, and data obtained from visible-u.v. spectra have been used to obtain quantitative descriptions of the bonding of these compounds in terms of molecular orbital models. From extended Hückel L.C.A.O. molecular orbital calculations, carried out on the compound ReOCl_4 , the metal ion spin-orbit coupling constant and the parameter P are estimated to be about 2400 cm^{-1} and 0.033 cm^{-1} respectively. Spin Hamiltonian parameters are listed for each substance and are equated to the atomic orbital coefficients in some of the molecular orbitals involved in bonding in these molecules, and a good agreement is obtained between the values obtained in this way and those derived from the molecular orbital calculations. The unpaired electron lies in a molecular orbital which involves the metal ion $5d_{xy}$ orbital and it is strongly delocalised (33%) on to the chlorine ligands. g_{11} is greater than g_1 and this is shown to be essentially due to charge-transfer mixing by spin-orbit coupling at the chlorine atoms. The changes in the spin Hamiltonian parameters when a sixth ligand is added to ReOCl_4 are accounted for.

Information about the extent of delocalisation on to the ligands can also be obtained by detailed analysis of the e.p.r. linewidths in solution, as will be shown in the next section of this thesis.

References to Part II

1. A.B. Goodman and J.B. Raynor, "Adv.Inorg.Chem. and Radiochem.", H.J. Emeleus and A.G. Sharpe, eds., Academic Press, London, 1970, 13, and references therein.
2. J.R. Shock and M.T. Rogers, J.Chem.Phys., 1973, 58,3356.
3. C.J. Ballhausen and H.B.Gray, Inorg.Chem., 1962, 1, 111.
4. H.B.Gray and C.R. Hare, Inorg.Chem., 1962, 1, 363.
5. H.Kon and N.E. Sharpless, J.Phys.Chem., 1966, 70,105.
6. S.M. Horner and S.Y. Tyree, Jr., Inorg.Nucl.Chem. Letters, 1965, 1, 43.
7. A.Carrington, D.J.E. Ingram and M.C.R.Symons, J.Chem.Soc., 1956, 4710.
8. N.S. Garifyanov, Zh.Exsp.Teor.Fiz., 1963, 45, 1819;
Soviet Phys.JETP(English Translation)1964,18,1246.
9. N.S. Garifyanov, Izvest.Akad.Nauk.S.S.S.R., Ser.Khim,1968,1902.
10. D.A. Edwards and A.A. Woolf, J.Chem.Soc. A, 1966, 91.
11. A. Guest and C.J.L. Lock, Can.J.Chem., 1971, 49, 603.
12. B.R.Brisdon and D.A.Edwards, Inorg.Chem., 1968, 7,1898.
13. K.W. Bagnall, D.Brown and R.Colton, J.Chem.Soc.,1964,3017.
14. C.G.Barraclough and D.J. Kew, Aust.J.Chem., 1972,25,27.
15. A.Abragam and M.H.L.Pryce, Proc.Roy.Soc.(A),1951,205,135.
16. L.D.Rollmann and S.I.Chan, "Electron Spin Resonance of Metal Complexes", T.F.Yen ed., Adam Hilger Ltd., London, 1969, 175.
17. L.Petrarkis, J.Chem.Ed., 1967, 44, 432.
18. R.Neiman and D. Kivelson, J.Chem.Phys., 1961, 35, 156.
19. H.R. Gersmann and J.D.Swalen, J.Chem.Phys.,1962,36,3221.

- 19.
20. H.Kon and N.E. Sharpless, J.Chem.Phys., 1965, 42, 906.
 21. K. DeArmond, B.B.Garrett, and H.S. Gutowsky, J.Chem. Phys., 1965, 42, 1019.
 22. A.J. Edwards, J.Chem.Soc., Dalton, 1972, 582.
 23. L.C. Cusachs, B.L. Trus, D.G. Carroll and S.P. McGlynn, Internat. J.Quantum Chemistry, 1967, 1, 423.
 24. L.C. Cusachs, and J.H. Corrington, "Sigma Molecular Orbital Theory", O. Sinanoglu and K.W. Wiberg, Yale University Press, 1970, 256.
 25. E. Clementi, "Table of Atomic Functions", I.B.M. Corporation Development Lab. Report, 1965; I.B.M. J.Res.Dev., 1965, 9, 2.
 26. E. Clementi, D.L. Raimondi and W.P. Reinhardi, J.Chem.Phys., 1967, 43, 1300.
 27. F.A. Cotton and C.E. Harris, Inorg. Chem., 1967, 6, 369, 376.
 28. F.A. Cotton and C.B. Harris, Inorg.Chem., 1967, 6, 924.
 29. C.J. Ballhausen and H.B.Gray, "Molecular Orbital Theory", W.A.Benjamin and Co., New York, 1965.
 30. M.Wolfsberg and L.Helmholtz, J.Chem.Phys., 1952, 20, 837.
 31. J.A.McMillan and T.Halpern, J.Chem.Phys., 1971, 55, 33.
 32. A.H. Maki and B.R. McGarvey, J.Chem.Phys., 1958, 29, 31.
 33. B.R.McGarvey, J.Chem.Phys., 1967, 71, 51.

PART IIIELECTRON PARAMAGNETIC RESONANCE LINEWIDTH STUDIES OF
ReOCl₄ IN SOLUTION3.1 Introduction

In the study of the electronic structure of ReOCl₄ and its adducts, as described in detail in part II, the unpaired electron in the complexes was found in an antibonding molecular orbital compounded out of the 5d_{xy} orbital of rhenium, and chlorine 3p_x and 3p_y orbitals, and it is about 33% delocalised on to the chlorine atoms. This kind of information was obtained essentially from the analysis of the spin-dipolar interaction of the magnetic moment of the unpaired electron with the magnetic moment of ^{the} rhenium nucleus. It is possible to obtain similar information about the delocalisation of the unpaired electron on to the chlorine ligands from the size of the chlorine nuclear hyperfine interaction in these complexes. We have not been able to resolve chlorine hyperfine coupling in the e.p.r. spectra due to the interaction of the unpaired electron with the chlorine ligand nuclei. However it is still possible to estimate the size of the isotropic hyperfine coupling from the contribution which it makes to the width of the lines in the e.p.r. spectra of these complexes in solution. It was therefore decided to analyse in detail the e.p.r. linewidths of ReOCl₄ in chloroform as a function of temperature in

order to separate the unresolved ligand hyperfine structure contribution from the other various effects which contribute to the linewidths. The estimated value of the chlorine hyperfine coupling obtained in this way is then used to estimate independently the extent of delocalisation of the unpaired electron on to the chlorine ligand orbitals. This result is then compared with the values obtained from the analysis of the spin Hamiltonian described in Part II.

3.2 Mechanisms of electron spin relaxation in solutions of transition metal complexes

As mentioned in Part I, there are several varieties of magnetic interactions which influence the linewidths of paramagnetic ions in solution. The standard procedure for examining the behaviour of such a system is to write down the appropriate Hamiltonian for the system to be discussed and solve for the time-independent and time-dependent components.

$$\mathcal{H} = \mathcal{H}_0 + \mathcal{H}(t) \quad \dots\dots 3.1$$

\mathcal{H}_0 is time-independent and determines the sharp line spectrum. $\mathcal{H}(t)$ is time-dependent with zero field average. The effect of $\mathcal{H}(t)$ is to cause the eigenfunctions, and hence the properties, of the system to be a function of time, i.e. it is the time-dependent terms in the Hamiltonian which cause relaxation.

The magnetic terms in the Hamiltonian for one unpaired electron moving in an axially symmetric orbital and interacting with one nucleus such as in ReOCl_4 can be written in the form ¹

$$\mathcal{H} = g_r \beta_e H_r S_r + g_p \beta_e H_p S_p + g_q \beta_e H_q S_q + A_r S_r I_r + A_p S_p I_p + A_q S_q I_q$$

..... 3.2

where p, q, r are a set of orthogonal unit vectors fixed in the complex, r being the unit vector parallel to the symmetry axis. In a tetragonal complex,

$$g_r = g_{11} \neq g_p = g_q = g_{\perp}$$

$$\text{and } A_r = A \neq A_p = A_q = B$$

In solution the complex undergoes rotational motion and the Brownian motions tend to average out the anisotropic contributions to the g and hyperfine tensors. In most cases the rotational motion of the complex is not fast enough to average out completely the anisotropic contributions to g and hyperfine tensors, and the fluctuating magnetic field which this produces causes broadening of the e.p.r. linewidths.

If the solutions of the paramagnetic ions are made sufficiently dilute, then the contributions of magnetic dipolar interactions, exchange interactions and intramolecular vibrations to the linewidths are so small as to be negligible.

A relaxation mechanism in liquids in the presence of anisotropic Zeeman and hyperfine interactions was first proposed by McConnell¹. He assumed that the ion and its ligand group, can be considered as a unit even in solution, the group of molecules tumbling as a whole. Thus the spin Hamiltonian 3.2 can be used as the appropriate Hamiltonian for the tumbling microcrystal. It is necessary to transform the Hamiltonian 3.2 to the new coordinate system x, y, z , fixed in the laboratory which is defined by the direction z of the magnetic field H_0 and the angles θ and ϕ . The transformed Hamiltonian may be considered as compounded from two terms, \mathcal{H}_0 and $\mathcal{H}(t)$.

$$\mathcal{H}_0 = g_0 \beta_e H_0 S_z + A_0 \underline{S} \cdot \underline{I} \quad \dots 3.3$$

where $g_0 = \frac{1}{3} (g_{11} + 2g_1)$, and $A_0 = \frac{1}{3} (A + 2B)$

$$\begin{aligned} \text{and } \mathcal{H}(t) = & \left[\Delta g \beta_e H_0 + b I_z \right] \left[\cos^2 \theta(t) - \frac{1}{3} \right] S_z + \frac{1}{2} \left[\Delta g \beta_e H_0 + b I_z \right] \\ & \times \left[\sin \theta(t) \cos \theta(t) \right] \left[S_+ e^{-i\phi(t)} + S_- e^{i\phi(t)} \right] \\ & - \frac{1}{4} b \left[\cos^2 \theta(t) - \frac{1}{3} \right] \left[S_+ I_- + S_- I_+ \right] \\ & + \frac{1}{4} b \left[\sin^2 \theta(t) \right] \left[I_+ S_+ e^{-2i\phi(t)} + I_- S_- e^{2i\phi(t)} \right] \\ & + \frac{1}{2} b \left[\sin \theta(t) \cos \theta(t) \right] \left[I_+ e^{-i\phi(t)} + I_- e^{i\phi(t)} \right] S_z \\ & \dots \dots 3.4 \end{aligned}$$

where $b = A - B$, and θ and ϕ are the polar and azimuthal angles of the micro-crystalline symmetry axis (r) relative to the laboratory x, y, z axes. Because of the Brownian motion, the angles θ and ϕ are functions of time so

that all terms in $\mathcal{H}(t)$ are all averaged to zero over a sphere and the centre of gravity of each of the hyperfine multiplet resonances is obtained from the eigenvalues of \mathcal{H}_0 .

Electron spin-lattice relaxation, with characteristic time T_1 , arises from the second, third and fourth terms in 3.4 containing the electron spin raising and lowering operators, obtained by

$$S_{\pm} = S_x \pm iS_y \quad \dots 3.5$$

Nuclear relaxation arises from the third, fourth and fifth terms. Another contribution to the broadening of electron resonance comes from the first and the last term in equation 3.4, but the characteristic time for this process is taken as T_2 . McConnell¹ used the Hamiltonian 3.4 to calculate relaxation times T_1 and T_2 but the complete solution of this Hamiltonian was not attempted. Instead he assumes that

$\Delta g \beta_e H_0 \gg |b|$ so that the last three terms in equation 3.4 may be neglected. This implies neglect of nuclear spin-lattice relaxation, so that the time-dependence of matrix elements of I_z in the first two terms is also neglected. With these conditions McConnell showed that

$$\frac{1}{T_1} \geq (8\pi^2/15)(\Delta g \beta_e H_0 + bI_z)^2 h^{-2} \tau_c (1 + 4\pi^2 \nu_0^2 \tau_c)^{-1}$$

.... 3.6

$$\left(\frac{1}{T_2}\right)^2 \geq (32\pi/45)(\Delta g \beta_e H_0 + bI_z)^2 h^{-2} \tan^{-1}(2\tau_c/T_2)$$

.... 3.7

where ν_0 is the frequency at which the resonance is observed and τ_c is the correlation time for the angular functions $[\cos^2 \theta(t) - \frac{1}{3}]$ and $[\sin \theta(t) \cos \theta(t)]$ of the microcrystal orientation. The most interesting aspect of these results is the dependence of the linewidths for the individual hyperfine lines on the magnetic quantum number m_I (i.e. I_z).

McGarvey² discusses the linewidths of several paramagnetic ions in solution in terms of the microcrystalline model. He considers two contributions to the linewidths of paramagnetic ions in solution. The first of these is that due to the tumbling of the microcrystal in solution, i.e. the mechanism discussed by McConnell. The second arises from relaxation processes involving spin-orbit coupling with excited states: when the symmetry of the crystalline field about the ion in the microcrystal is such as to permit a low-lying excited state to interact, this can result in an efficient relaxation process which may be dominant.

S.A. Al'tshuler and K.A. Valiev³ have criticised the McConnell-McGarvey theory of the linewidths in e.p.r. spectra of transition metal ion complexes on the grounds that this theory is based on experiments carried out at

a single frequency only, and at a single temperature, and they state that B.M. Kozyrev^{4,5} has carried out series of experiments on different transition metal ions in solution at different temperature and over a wide range of frequency. The experimental results of Kozyrev show that the dependence of longitudinal relaxation times on temperature and on the applied magnetic field direction is completely at variance with McConnell's theory. Al'tshuler and Valiev believe that T_1 is defined by the vibrations within the complex rather than by rotations of the complex.

The results of Al'tshuler and Valiev, however, are not substantiated by Kivelson and co-workers⁶⁻¹⁰. Kivelson⁶ has developed in great detail the theory of linewidths of free radicals in diamagnetically diluted crystals and in dilute liquid solutions, considering the case in which the orbital magnetism has been essentially quenched. Nuclear quadrupole moments, zero field splitting, anisotropic Zeeman terms, and intramolecular electron-nuclear dipolar interactions, as well as motional and exchange effects are considered in this theory.

Rogers and Pake¹¹ have studied the e.p.r. spectrum of the vanadyl ion in solution at two frequencies and at different temperatures, and their results appear to support McConnell's mechanism.

Atkins, Wilson and Kivelson ⁷⁻¹⁰ have discussed the relations between linewidths and temperature, viscosity and magnetic field for the vanadyl and cupric acetylacetonates. They find that in addition to the effects of motional modulation of anisotropic g and hyperfine tensors already discussed, there is a residual linewidth which is independent of m_I and only very weakly dependent on H_0 . This residual contribution is a linear function of T/η , where η is the viscosity. This residual linewidth is ascribed to a spin-rotational interaction. When a complex rotates in solution, the electrons do not follow ^{7,12} precisely the motion of the nuclei and this imbalance of rotating charge generates a magnetic moment which can interact with both the nuclear and electronic spins in the molecule. The magnitude of the interaction, which is anisotropic and therefore tensorial, is measured by the spin-rotational coupling tensor $C(t)$. This interaction can be written as

$$\mathcal{H}(t) = \underline{J}(t) \cdot C(t) \cdot \underline{S} \quad \dots\dots 3.8$$

where $\underline{J}(t)$ is the rotational angular momentum operator for the molecule. The interaction will comprise a relaxation mechanism if the interaction is modulated and in solution there are two ways in which this can happen. First, the rotational angular moment can be modulated as the molecule brushes against its neighbours in solution, and second, the spin-rotational coupling

can be modulated as the molecule changes its orientation through more violent encounters, but in fact the modulation of rotational angular momentum by molecular collisions in solution is the more important relaxing mechanism.

The density matrix approach¹³⁻¹⁹ seems to be the best approach for treating the theoretical aspect of electron spin relaxation. In this approach, the eigenfunctions of the Hamiltonian \mathcal{H} of equation 3.1 are expanded as a linear combination of the eigenfunctions of \mathcal{H}_0 , of the form

$$\Psi = \sum_i c_i \phi_i \quad \dots 3.9$$

The time-dependence of the eigenfunctions Ψ is thus contained in the coefficients c_i . The expectation value of any operator O is given by

$$\langle O \rangle = \sum_{i,j} c_i^* c_j \langle \phi_i | O | \phi_j \rangle \quad \dots 3.10$$

If an operator ρ is defined such that

$$\rho_{i,j} = \langle \phi_i | \rho | \phi_j \rangle = c_j^* c_i \quad \dots 3.11$$

then

$$\langle O \rangle = \sum_{i,j} \langle \phi_j | \rho | \phi_i \rangle \langle \phi_i | O | \phi_j \rangle = \text{Tr } \rho O \quad \dots 3.12$$

The elements of the operator ρ constitute what is known as the density matrix. By differentiating this equation, the time-dependence of the operator ρ can be obtained

$$\frac{d \langle O \rangle}{dt} = \sum_{i,j} \frac{d \rho_{ji}}{dt} \langle \phi_i | O | \phi_j \rangle \quad \dots 3.13$$

Thus the problem of obtaining an expression for the time-dependence of any property of the system reduces to deriving an equation describing the time-dependence of the elements of the density matrix, i.e. of the product $c_j c_i$. Redfield^{16,19} derived such an expression for the time-dependence of ρ_{ij} as function of $\mathcal{H}(t)$ by using time-dependent perturbation theory. Using the Redfield expression it is possible to derive an expression for the transverse relaxation time T_2 . The T_2 value can then be related to the peak-to-peak linewidth ΔH for the first derivative of a Lorentzian line by the relation

$$\Delta H = \frac{2}{T_2 \sqrt{3}} \quad \dots 3.14$$

Kivelson⁶ used these theoretical grounds to derive a polynomial relation for the total linewidth of the hyperfine lines in e.p.r. spectra. If the width of the hyperfine line corresponding to the nuclear quantum number, m_I , is defined as ΔH , then the linewidth in the complexes studied here can be written in the form^{7,20,21}

$$\Delta H = \alpha + \alpha' + \alpha'' + \beta m_I + \gamma m_I^2 + \delta m_I^3 \quad \dots 3.15$$

where the parameters α'' , β , γ and δ are given by

$$\alpha'' = (\tau_c/360)(\pi \sqrt{3}g \beta_e / \hbar)^{-1} \left\{ 8(H_0 \Delta\gamma)^2 [4+3(1+\omega_0^2 \tau_c^2)^{-1}] \right. \\ \left. + 9I(I+1)b^2 [3+7(1+\omega_0^2 \tau_c^2)^{-1}] \right\}$$

$$\beta = (\tau_c/15)(\pi \sqrt{3}g \beta_e / \hbar)^{-1} b H_0 \Delta\gamma [4+3(1+\omega_0^2 \tau_c^2)^{-1}]$$

.... 3.16

$$\gamma = (\tau_c/40)(\pi \sqrt{3}g \beta_e / \hbar)^{-1} [5 - (1+\omega_0^2 \tau_c^2)^{-1}] b^2$$

$$\delta = (\tau_c/10)(\pi \sqrt{3}g \beta_e / \hbar)^{-1} (b^2 \langle A \rangle / \hbar \omega_0)$$

where $\Delta\gamma$ and b are now re-defined by

$$\Delta\gamma = (g_{11} - g_1) \beta_e / \hbar \quad \text{and} \quad b = 2(A-B)/3\hbar$$

In the above expressions the hyperfine coupling constants are in units of ergs, and the linewidths in gauss. α'' arises from the modulation of the anisotropic hyperfine tensor and the anisotropic g-factor; γ and δ terms arise from the modulation of the anisotropic hyperfine tensor; β arises from cross term dependent on modulation both the anisotropic hyperfine tensor and the anisotropic g-factor; the α' term is the contribution from the spin-rotational interaction; and α is the contribution from the unresolved hyperfine coupling, plus any other small contributions which have not been considered above.

The parameter τ_c is the tumbling or reorientation correlation time, and it is a measure of the rate at

which the complex rotates in solution and it is given approximately by ^{22,23}

$$\tau_c \cong \frac{4\pi \eta a_0^3}{3KT} \quad \dots 3.17$$

where η is the coefficient of viscosity of the solvent and a_0 is the molecular radius of the equivalent rotating sphere.

3.3 Experimental

ReOCl_4 was prepared by the method described in Part II and the linewidths of ReOCl_4 in thoroughly out-gassed chloroform were measured as function of temperature. Observations were made over a broad temperature range, from 230 to 295K. The temperature was measured with a copper-constantan thermocouple linked to a digital voltmeter and was varied using the gas flow system described in the introductory chapter. The temperature gradient during recording of the spectrum did not exceed 1° . The chloroform solvent, was repeatedly fractionated and purified with P_2O_5 and the dissolved oxygen was removed by degassing, employing successive freezing and thawing of the solution.

The viscosity coefficients η of the chloroform as a function of temperature were taken from the International Critical Tables ²⁴. The values for low temperatures were obtained by extrapolation, using the formula

given with the tables.

In order to keep intermolecular interactions from affecting the linewidths of the e.p.r. spectrum, the solution concentrations were reduced until the linewidths ceased to depend on the concentration. This was achieved to $10^{-3}M$.

The e.p.r. spectra of $ReOCl_4$ in liquid chloroform at two temperatures are shown in Figure 3.1.

3.4 Results and discussion

In order to estimate the value of the isotropic hyperfine coupling of the chlorine ligands, it is necessary to calculate all the other contributions to the linewidths of the e.p.r. spectra. To do this the linewidths of the e.p.r. spectra are fitted using a least squares procedure to the polynomial formula 3.15 and the parameters $\alpha + \alpha' + \alpha''$, β , γ and δ are obtained. The values of these parameters at different temperatures are listed in Table 3.1.

According to the theory discussed in 3.2, the parameter γ should be proportional to \mathcal{H}/T , so it is necessary to check that before using γ in further calculations. This parameter is plotted as a function of \mathcal{H}/T in Figure 3.2, and it can be seen from the graph that γ provided a good straight line, passing close to the origin, in a good agreement with the theory. From this figure the least squares fit of γ is given by

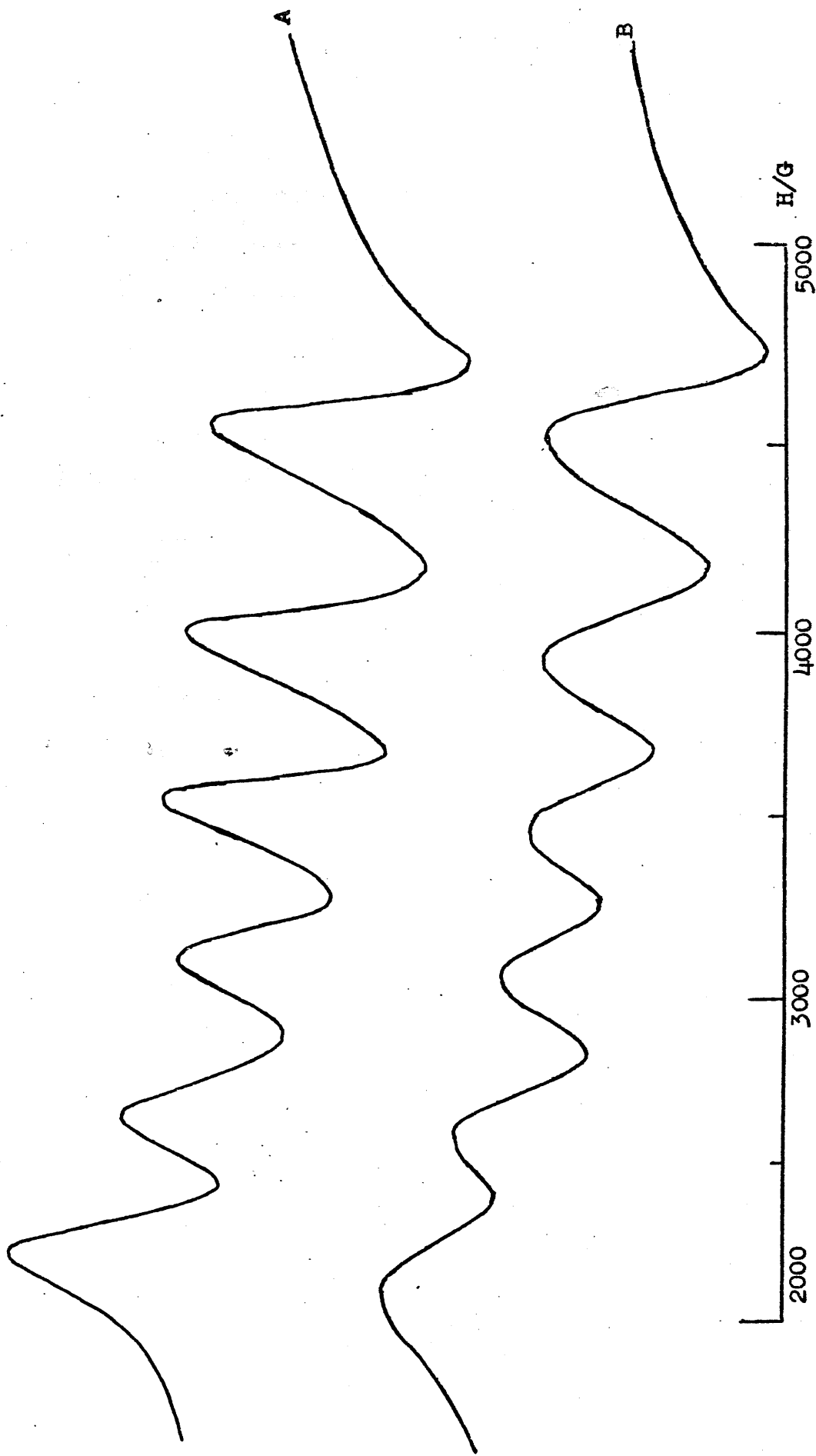


Figure 3.1 E.p.r. spectra of 10^{-3} M solution of ReOCl_4 in chloroform at 274K, A, and at 230K, B.

Table 3.1

Parameters obtained from the least-squares fit of the e.p.r. linewidths of the complex ReOCl_4 in chloroform solution as function of m_I ; all values are in units of gauss.

<u>Temperature (K)</u>	<u>$\alpha + \alpha' + \alpha''$</u>	<u>β</u>	<u>γ</u>	<u>δ</u>
295	196	-8.2	2.8	-0.14
290	193.6	-8.8	3.05	-0.16
284	203	-9.2	3.35	-0.19
274	203.4	-9.5	3.6	-0.23
257	218.6	-9.3	4.16	-0.24
240	233	-9.6	4.87	-0.26
230	226	-10	5.1	-0.30

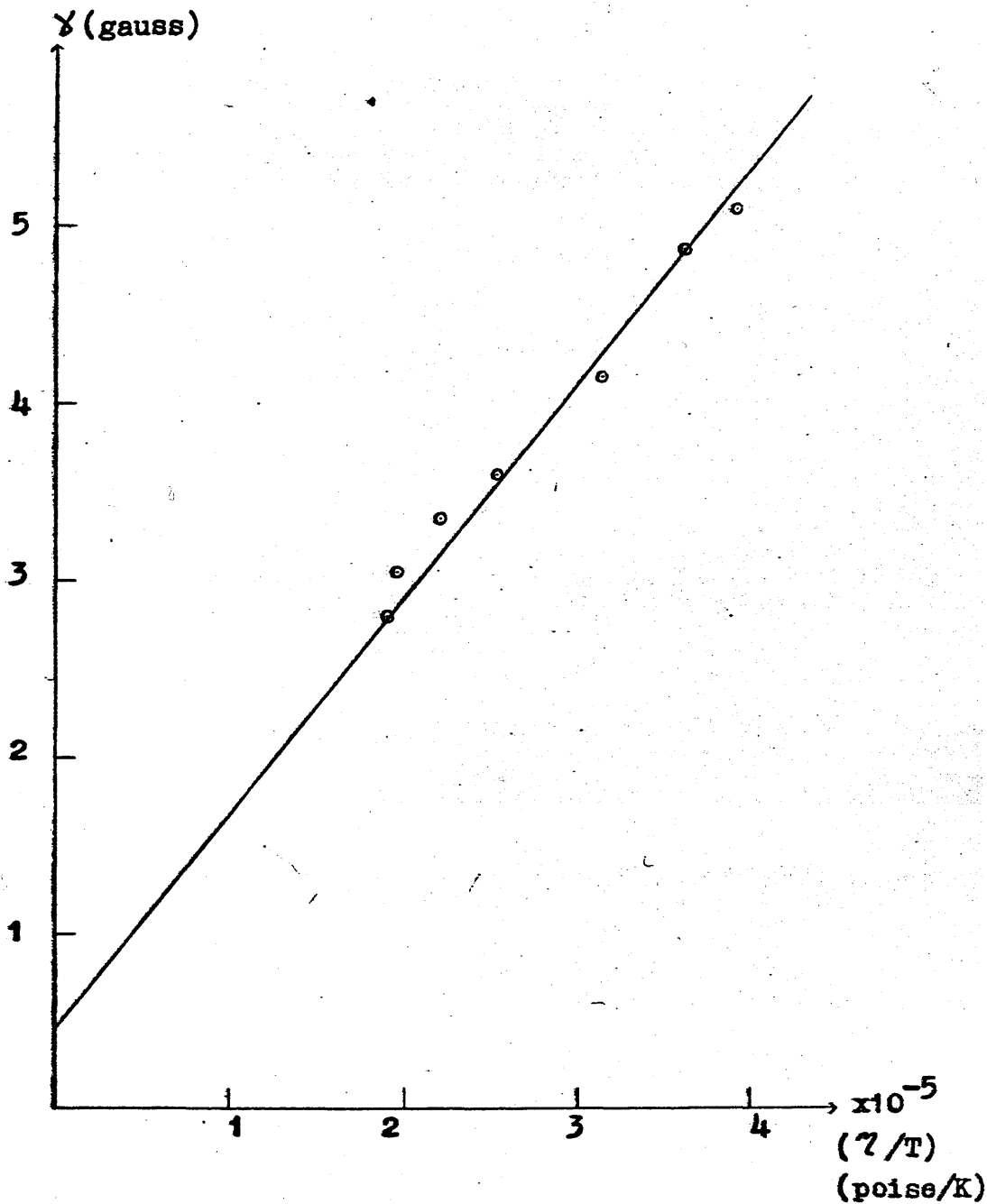


Figure 3.2 Δ (gauss) vs η/T (poise/K) for ReOCl_4

$$\gamma = 0.49 + 125000 \gamma/T$$

By using the spin Hamiltonian parameters obtained in Part II together with the values of γ at each temperature, the rotational correlation times, τ_c , can be calculated from equations 3.16. The values of τ_c then used to calculate α'' again from equations 3.16. Thus the values of the residual linewidth $\alpha + \alpha'$, could then be calculated since the values of $\alpha + \alpha' + \alpha''$ were already known. The values of τ_c and $\alpha + \alpha'$ obtained in this way together with the effective molecular radius, a_0 , obtained from equation 3.17 are listed in Table 3.3.

Since the values of α' are proportional to γ/T , the contribution of the chlorine nuclear hyperfine structure, α , to the linewidth can be obtained by fitting the values of $\alpha + \alpha'$ to an equation of the form

$$\alpha + \alpha' = \alpha + KT/\gamma$$

where K is constant, and the resulting least squares fit, which is shown graphically in Figure 3.3 is given by

$$\alpha + \alpha' = 18 + 0.0015 T/\gamma$$

As shown in Figure 3.3, the contribution to the linewidths from unresolved chlorine nuclear hyperfine structure is 18 gauss.

Table 3.2

Values of the viscosity (η), η/T and T/η for chloroform at various temperatures. Values of η are in units of poise, and were obtained by interpolation of the values given in the international critical tables ²⁴.

<u>Temperature</u>	<u>η</u>	<u>η/T</u>	<u>T/η</u>
295	5.60×10^{-3}	1.90×10^{-5}	52678
290	5.69×10^{-3}	1.96×10^{-5}	50966
284	6.23×10^{-3}	2.20×10^{-5}	45586
274	6.96×10^{-3}	2.54×10^{-5}	39368
257	8.04×10^{-3}	3.13×10^{-5}	31965
240	8.62×10^{-3}	3.60×10^{-5}	27842
230	8.99×10^{-3}	3.90×10^{-5}	25584

Table 3.3

Values of residual linewidths ($\alpha + \alpha'$), in gauss, correlation times (τ_c) in seconds, and the molecular radius (a_0) in angstroms for the complex ReOCl_4 at various temperatures.

<u>Temperature</u>	<u>$\alpha + \alpha'$</u>	<u>τ_c</u>	<u>a_0</u>
295	100	4.202×10^{-11}	4.15
290	89	4.577×10^{-11}	4.22
284	88	5.027×10^{-11}	4.20
274	80	5.402×10^{-11}	4.10
257	76	6.24×10^{-11}	4.01
240	66	7.308×10^{-11}	4.04
230	51	7.65×10^{-11}	3.99

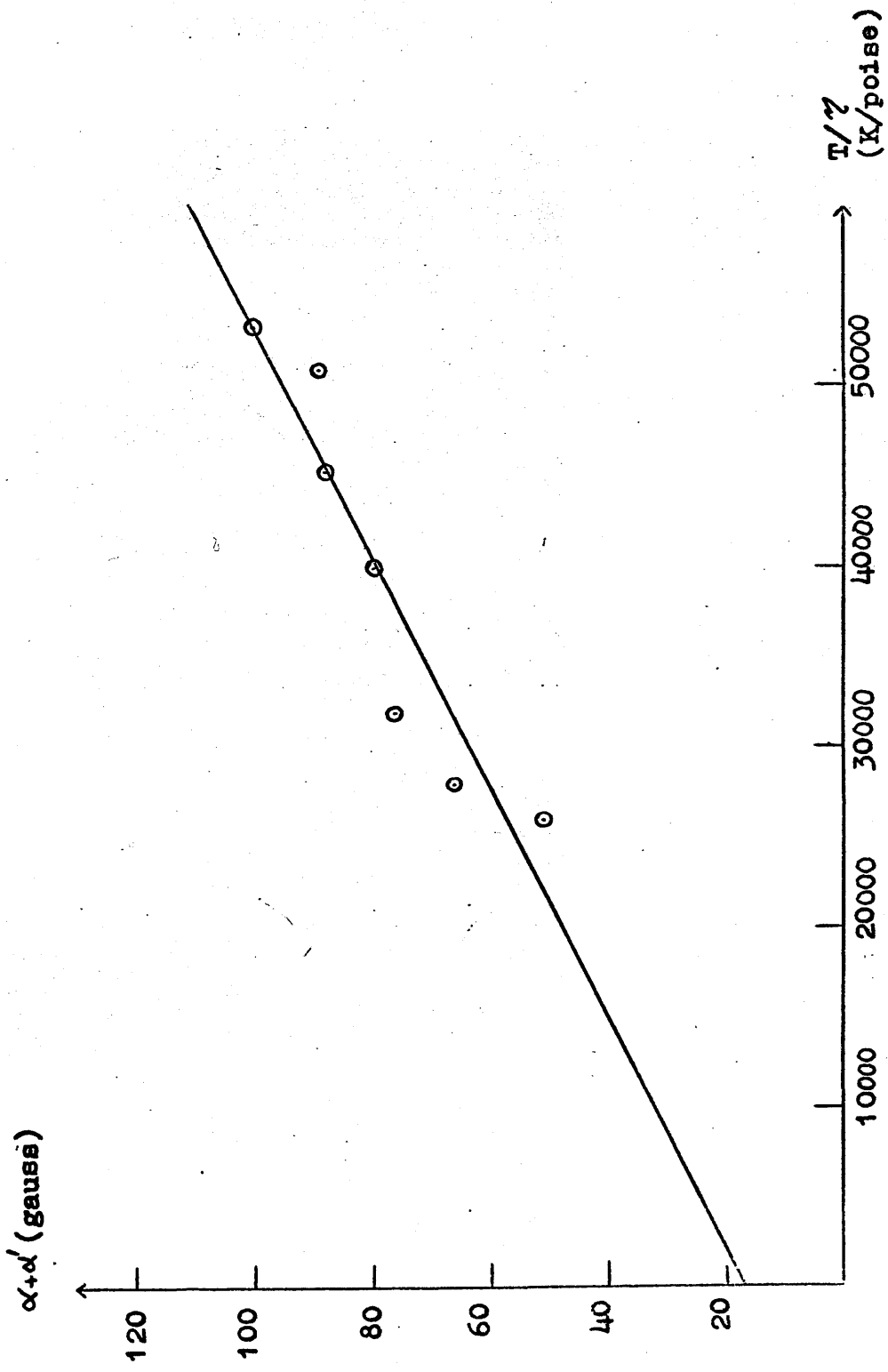


Figure 3.3. $\alpha + \alpha'$ (gauss) vs T/η (K/poise) for ReOCl_4 .

Each of the lines in the e.p.r. spectra of the oxychloride consists of an unresolved 1:2:3:4:5:6:7:6:5:4:3:2:1 multiplet, and so to estimate the size of the chlorine hyperfine coupling which would give rise to a particular contribution to the linewidths, a computer programme has been used which plotted out the single line arising from the superposition of the thirteen peaks of this type. The spacing between the constituent peaks was simply varied until the width of the single composite line was larger than that of the constituent lines by 18 gauss. In this way the chlorine nuclear hyperfine coupling was estimated to be 15 gauss. Now this value could be used to estimate the extent of delocalisation of the unpaired electron available in the complex on to chlorine ligands.

By setting the value of the chlorine isotropic coupling constant roughly equal to the largest principal value of the chlorine spin-dipolar interaction $\frac{4}{7} P \beta_2^{*2}(1)$, where $\beta_2^{*2}(1)$ is the coefficient of the chlorine P-orbital in the molecular orbital containing the unpaired electron, and $\frac{4}{7}P$ is the largest principal value of the spin-dipolar interaction for one electron in a chlorine P-orbital, which is estimated to be 90 gauss²⁵⁻²⁹, the value of $\beta_2^{*2}(1)$ was estimated to be 0.167, corresponding to a delocalisation of the unpaired electron in the complex of about 21%. Thus the linewidth analysis of ReOCl_4 confirms that the unpaired electron is in a metal ion orbital and delocalised by about 21% on to the chlorine atoms, in reasonable agreement with the conclusions reached from the analysis of the spin Hamiltonian parameters discussed in Part II.

3.5 Summary of Part III

In this section a detailed study has been made of electron paramagnetic relaxation phenomena in solutions of ReOCl_4 in chloroform. This has enabled the separate contributions from spin-rotational interactions, from g -tensor anisotropy, from hyperfine coupling anisotropy, and from unresolved chlorine hyperfine coupling, to the observed e.p.r. linewidths to be evaluated. These results have been used to estimate the size of the chlorine isotropic hyperfine coupling constant and then the extent of delocalisation of the unpaired electron available in the complex on to the chlorine ligands. In this way it has been shown that the extent of delocalisation of the unpaired electron on to chlorine groups in ReOCl_4 is about 21%. This result is in reasonable agreement with the deductions made from the analysis of the spin-Hamiltonian parameters obtained in Part II.

The magnetic properties and the electronic ground state of the rhenium (VI) ion in trigonal-prismatic complexes will be considered in the next section of this thesis.

References to Part III

1. H.M. McConnell, J.Chem.Phys., 1956, 25, 709.
2. B.R. McGarvey, J.Phys.Chem., 1957, 61, 1232.
3. S.A. Al'tshuler and K.A. Valiev, Soviet Physics J.E.T.P., 1959, 35, 661.
4. S.A. Al'tshuler and B.M. Kozyrev, "Electron Paramagnetic Resonance", English Translation edited by C.P. Poole, Jr., 1964, Acad.Press, New York.
5. B.M. Kozyrev, Doctoral Dissertation, Phys.Inst.Acad.Sci., Moscow, 1957.
6. D.Kivelson, J.Chem.Phys., 1960, 33, 1094.
7. R.Wilson and D. Kivelson, J.Chem.Phys., 1966, 44, 154.
8. P.W. Atkins and D.Kivelson, J.Chem.Phys., 1966, 44, 169.
9. R.Wilson and D.Kivelson, J.Chem.Phys., 1966, 44, 4440.
10. R.Wilson and D.Kivelson, J.Chem.Phys., 1966, 44, 4445.
11. R.N. Rogers and G.E. Pake, J.Chem.Phys., 1960, 33, 1107.
12. N.M. Atherton, "Electron Spin Resonance", Ellis Horwood Limited, London, 1973, 345.
13. N. Bloembergen, E.M. Purcell and R.V. Pound, Phys.Rev., 1948, 73, 679.
14. F. Bloch, Phys.Rev., 1956, 102, 104.
15. F. Bloch, Phys.Rev., 1957, 105, 1206.
16. A.G. Redfield, I.B.M. J.Res.Dev., 1957, 1, 19.
17. A.G. Redfield, "Advance Magnetic Resonance", 1965, 1, 1.
18. J.H. Freed and G.K. Fraenkel, J.Chem. Phys., 1963, 39, 326.
19. C.P. Slichter, "Principles of Magnetic Resonance", Harper and Row, New York, 1963, 127.
20. A. Hudson and G.R. Luckhurst, Chem.Rev., 1969, 69, 191.

21. W.B. Lewis and R.O. Morgan, "Transition Metal Chemistry", R.L. Carlin ed., Edward Arnold, London, 1966, 4, 33.
22. P. Debye, "Polar Molecules" Dover Publications Inc., New York, 1945, Chapter 5.
23. A. Carrington and A.D. McLachlan, "Introduction to Magnetic Resonance", Harper and Row, New York, 1967, 187.
24. International Critical Tables, McGraw-Hill Book Company, Inc., New York, 1930, 7, 218.
25. G.F. Kokoszka, H.C. Allen and G. Gordon, J.Chem.Phys., 1967, 46, 3013, 3020.
26. H. Kon and N.E. Sharpless, J.Chem.Phys., 1965, 42, 906.
27. H. Kon and N.E. Sharpless, J.Chem.Phys., 1965, 43, 1081.
28. J. Sierro, Phys.Chem.Solids, 1967, 28, 417.
29. J.H. Thornley, B.W. Magnum, J.H.E. Phillips and J.Owen, J.Proc.Phys. Soc. (London), 1961, 78, 1263.

PART IV

THE ELECTRONIC GROUND STATES OF THE TRIGONAL-PRISMATIC RHENIUM COMPLEXES, TRIS(CIS-1,2-DIPHENYLETHENE-1,2-DITHIOLATO) RHENIUM, $\text{Re}(\text{C}_2\text{S}_2\text{Ph}_2)_3$, AND TRIS(TOLUENE-3,4-DITHIOLATO) RHENIUM, $\text{Re}(\text{S}_2\text{C}_6\text{H}_3\text{CH}_3)_3$.

4.1 Introduction

The electronic structures of six-coordinated complexes of bidentate, unsaturated sulphur donor ligands in which the central metal ions are V, Cr, Mo, W and Re have been the subject of several investigations ¹. The structure of $\text{Re}(\text{S}_2\text{C}_2\text{Ph}_2)_3$ ^{2,3} and $\text{Mo}(\text{S}_2\text{C}_2\text{H}_2)_3$ ⁴ have been solved by single crystal X-ray diffraction analyses, and it has been found that the central metal ions are surrounded by an almost perfect trigonal prism of six sulphur atoms. The coordination geometry of the rhenium and molybdenum complexes are D_{3h} and the over-all molecular symmetry belongs very nearly the point group C_{3h} . Spectroscopic and powder X-ray measurements ⁵ strongly indicate that this geometry is also encountered in the $\text{M}(\text{S}_2\text{C}_2\text{Ph}_2)_3$, $\text{M}(\text{S}_2\text{C}_6\text{H}_3\text{CH}_3)_3$ and $\text{M}(\text{S}_2\text{C}_6\text{H}_4)_3$ systems with M = Re, W or Mo.

Schrauzer and Mayweg ^{6,7} carried out an extended Hückel L.C.A.O. molecular orbital calculation on the tris(dithioglyoxalates), $\text{M}(\text{S}_2\text{C}_2\text{H}_2)_3$, with M = Cr, Mo

or W, from which they were able to predict the relative energies of the molecular orbitals in the complexes. They found that there is extensive delocalisation of electrons in the ground states of these complexes.

Gray, et al. ^{8,9} carried out similar calculations on $\text{Re}(\text{S}_2\text{C}_2\text{Ph}_2)_3$ but reached a different conclusion about the relative ordering of the most important levels. The energy level scheme obtained in this calculation predicts that the unpaired electron is in a molecular orbital which is essentially metal ion in character.

Conductivity measurements ⁷ were made on $\text{M}(\text{S}_2\text{C}_2\text{R}_2)_3$ with $\text{M} = \text{V}, \text{Cr}, \text{Mo}, \text{W}$ or Re and $\text{R} = \text{H}, \text{CH}_3$ or Ph by Rosa and Schrauzer. Their results show that the rhenium complexes are the best conductors of all, and they indicate that the unpaired electron must be in a molecular orbital which is delocalised over the whole molecular complex.

Several dithiolate complexes of vanadium, chromium, molybdenum, tungsten and rhenium have been investigated polarographically ^{5,9} and it has been found that only, the rhenium complexes $\text{Re}(\text{S}_2\text{C}_2\text{Ph}_2)_3$ and $\text{Re}(\text{S}_2\text{C}_6\text{H}_3\text{CH}_3)_3$ exhibit oxidation waves corresponding to the formation of monocations.

The magnetic data obtained from the tris(dithiolato) complexes are relatively sparse. McCleverty and coworkers ¹⁰ have been unable to reconcile magnetic

moment measurements for the complexes $[M(S_2C_2R_2)_3]^{2-}$ with $M = V, Cr, Mo$ or W and $R = CN$ or CF_3 in the temperature range $90 K \leq T \leq 300 K$ with the molecular orbital scheme constructed by Schrauzer and Mayweg on the one hand and by Gray et al., on the other.

Initial e.p.r. studies of the tris(dithiolato) complexes were carried out by Davison et al., ^{11,12} on various complexes of vanadium and molybdenum and it was concluded that the values of g and of hyperfine interactions obtained from these complexes could not be accommodated by placing the unpaired electron in a molecular orbital which had a large amount of metal ion character:

Davison, et al. were forced to conclude that the unpaired electron was localised in ^a molecular orbital which is principally ligand in character. The interpretation of e.p.r. spectra of vanadium tris(malonitriledithiolene), $V(mnt)_3^{2-}$ has given rise to some controversy. Atherton and Winscom ¹³ state that the spectrum is consistent with a d^1 configuration in a distorted D_{3h} crystal field and that the unpaired electron lies in a molecular orbital which is derived principally from vanadium $3d_{z^2}$ and $3d_{yz}$ orbitals, while Whei-Lu Kwick and Stiefel ¹⁴ state that the spectrum is consistent with the assumption that the unpaired electron is in a non-degenerate molecular orbital compounded substantially from $3d_{z^2}$ orbital in D_3 symmetry and it is strongly delocalised on to the sulphur ligand orbitals.

The e.p.r. spectra of rhenium tris(dithiolato) complexes in solution at room temperature and in magnetically concentrated samples have been reported ⁹. In an attempt to more definitely identify the nature of the ground states in these species, it was decided to study their e.p.r. spectra in magnetically dilute solutions at room temperature and at 77 K.

4.2 Experimental

Tris(dithiolato) complexes of rhenium were prepared by the following methods ⁹.

1: $\text{Re}(\text{S}_2\text{C}_2\text{Ph}_2)_3$ was prepared by mixing benzoin with P_4S_{10} in xylene solution, and the reaction mixture was refluxed for 3 hours and then cooled and filtered. Rhenium pentachloride, ReCl_5 , in ethanol was added to the xylene solution and the resulting mixture was heated for 4 hours. The volume of the green solution was reduced by evaporating it in vacuum. The solution was then allowed to stand overnight after addition of hexane solution. The resulting mixture was filtered and the filtrate was concentrated to give black-green crystals. These crystals were collected, washed with pentane and dried under vacuum for 14 hours.

2: $\text{Re}(\text{S}_2\text{C}_6\text{H}_3\text{CH}_3)_3$ was prepared by addition of ReCl_5 in CCl_4 to a solution of toluene-3,4-dithiol in the same solvent. The green mixture was then refluxed for 3 hours and the solution was cooled, filtered and

reduced to small volume. After addition of hexane solution the mixture was allowed to stand overnight and the resulting precipitate was filtered and redissolved in CH_2Cl_2 . The CH_2Cl_2 solution was filtered, and the complex was precipitated by addition of pentane. The resultant green precipitate was washed with pentane and dried under vacuum for 4 hours.

These two complexes are soluble and stable in nonpolar organic solvents such as CCl_4 , CHCl_3 , CH_2Cl_2 and benzene, giving intensely green solutions. The purity of these complexes was checked by infra red measurements in Nujol mull and in solutions and the observed IR frequencies are in good agreement with published data ⁹.

The e.p.r. spectra were recorded using 10^{-3}M solutions for the measurements at room temperature and 10^{-4}M for the measurements at 77 K.

The electronic spectra of these complexes were recorded on Unicam SP700 and 800 spectrophotometers.

4.3 Analysis of the e.p.r. spectra

The e.p.r. spectra of the complexes $\text{Re}(\text{S}_2\text{C}_2\text{Ph}_2)_3$ and $\text{Re}(\text{S}_2\text{C}_6\text{H}_3\text{CH}_3)_3$ each show a single line in chloroform solution at room temperature and in magnetically concentrated samples. The extracted g values of 2.0151 for $\text{Re}(\text{S}_2\text{C}_2\text{Ph}_2)_3$ and 2.0138 for $\text{Re}(\text{S}_2\text{C}_6\text{H}_3\text{CH}_3)_3$ are close to the spin-only value. Very hard dilution of

these complexes in different thoroughly outgassed solvents was tried in order to resolve the hyperfine splitting if there is any, but all the spectra show only one line. The lack of hyperfine splitting in the spectra indicates that the electron is in an orbital which has no rhenium metal orbital character as will be explained fully later. The observed spectra of these complexes in chloroform at room temperature are shown in Figure 4.1. The e.p.r. spectra obtained from magnetically dilute glasses at 77 K of these complexes in different solvents are characteristic of one unpaired electron moving in an orbital which has rhombic symmetry, so that the spectra can be interpreted in terms of a spin-Hamiltonian of the form ¹⁵

$$\mathcal{H} = \beta_e \underline{H} \cdot \underline{g} \cdot \underline{S} + \underline{S} \cdot \underline{A} \cdot \underline{I}$$

Where, once again, g and A are the anisotropic g and hyperfine tensors, and it is assumed that the two tensors can be simultaneously diagonalised. The glassy spectra of the complexes were analysed in terms of a superposition of six Kneubühl curves of the type described in detail in Appendix C and the principal components of the g tensor and the hyperfine tensor, A , can be obtained from it with the help of computer programme, whereby it was possible to simulate the spectrum by the methods described for ReOCl_4 and its adducts. The observed and calculated spectra of

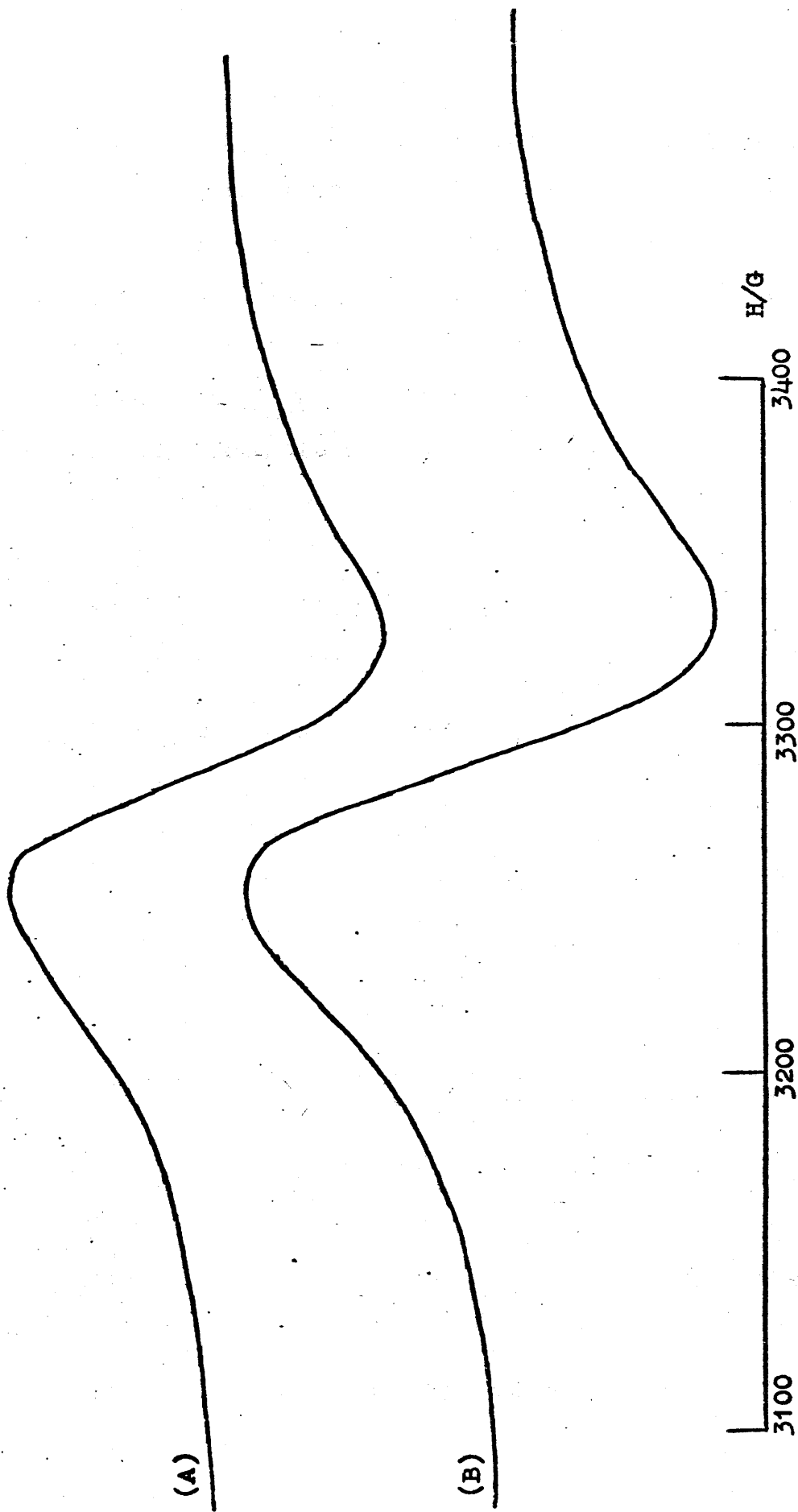


Figure 4.1 I.r. spectra of 10^{-3} M solutions of $\text{Re}(\text{S}_2\text{C}_2\text{Ph}_2)_3$, A, and $\text{Re}(\text{S}_2\text{C}_6\text{H}_3\text{CH}_3)_3$, B, in chloroform at 298 K.

$\text{Re}(\text{S}_2\text{C}_2\text{Ph}_2)_3$ and $\text{Re}(\text{S}_2\text{C}_6\text{H}_3\text{CH}_3)_3$ in chloroform together with ReOCl_4 at 77 K are shown in Figure 4.2 and the spin-Hamiltonian parameters obtained from these spectra at room temperature and at 77 K are listed in Table 4.1. The spectra of the tris(dithiolato)-rhenium complexes in solutions at room temperature and at 77 K are quite different from the spectra of ReOCl_4 . The principal components of the g-tensor in ReOCl_4 differ very markedly from the spin-only value of 2.00232 while in the tris(dithiolato)rhenium complexes the g-tensor components are close to this value. In addition, the hyperfine interactions in ReOCl_4 are very large while in tris(dithiolato) complexes they are very small.

All these results indicate that the unpaired electron in the complex must be localised in an orbital which has no metal orbital character and in fact all the observed spectra of tris(dithiolato)-rhenium complexes are very characteristic of sulphur-containing organic radicals ^{16,17}.

4.4 The electronic spectra of $\text{Re}(\text{S}_2\text{C}_2\text{Ph}_2)_3$ and $\text{Re}(\text{S}_2\text{C}_6\text{H}_3\text{CH}_3)_3$

The frequencies of the band maxima ⁹ observed in the spectra of these complexes in CHCl_3 are given in Table 4.2. An example of the spectrum for $\text{Re}(\text{S}_2\text{C}_2\text{Ph}_2)_3$ in CHCl_3 below $30,000 \text{ cm}^{-1}$ is shown in Figure 4.3.

The bands observed in the complexes spectra in CHCl_3 solution below $30,000 \text{ cm}^{-1}$ can be summarised in the

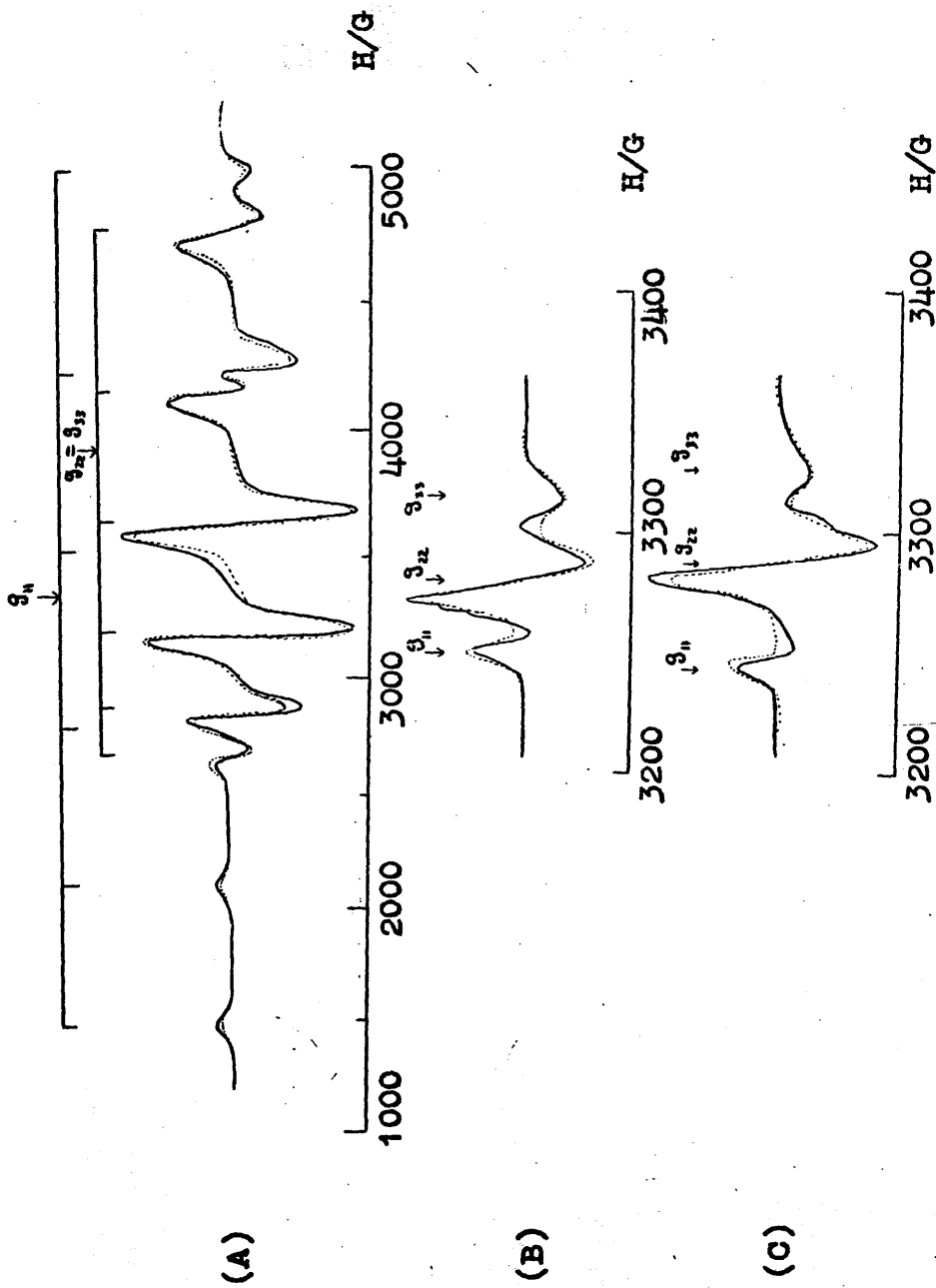


Figure 4.2. Observed (full line) and calculated (dotted line) e.p.r. spectra of 10^{-3} M solution of ReOCl_4 in CCl_4 , A, and 10^{-4} M solutions of $\text{Re}(\text{S}_2\text{C}_6\text{H}_3\text{CH}_3)_3$, B, and $\text{Re}(\text{S}_2\text{C}_6\text{H}_3\text{CH}_3)_3$, C, in CHCl_3 at 77K.

Table 4.1

Spin Hamiltonian parameters for ReOCl_4 , $\text{Re}(\text{S}_2\text{C}_2\text{Ph}_2)_3$ and $\text{Re}(\text{S}_2\text{C}_6\text{H}_3\text{CH}_3)_3$

at 77 K. All hyperfine tensors components are in units of cm^{-1}

<u>Compound</u>	<u>Solvent</u>	<u>g_{11}</u>	<u>g_{22}</u>	<u>g_{33}</u>	<u>A_{11}</u>	<u>A_{22}</u>	<u>A_{33}</u>	<u>Q'</u>
ReOCl_4	CCl_4	1.974	1.708	1.708	-0.0636	-0.0323	-0.0323	± 0.0020
$\text{Re}(\text{S}_2\text{C}_2\text{Ph}_2)_3$	CHCl_3	2.0376	2.0182	1.9963	-0.0001	+0.0003	-0.0002	-
$\text{Re}(\text{S}_2\text{C}_6\text{H}_3\text{CH}_3)_3$	CHCl_3	2.0408	2.0132	1.9892	-0.0001	+0.0003	-0.0002	-

following way:

1. A weak absorption band is observed at 8230 cm^{-1} in the spectra of $\text{Re}(\text{S}_2\text{C}_2\text{Ph}_2)_3$, and as shown later this band may be assignable to a transition in which an electron is transferred from a filled bonding orbital to the orbital containing the unpaired electron. This band is shifted to lower energy in the spectrum of $\text{Re}(\text{S}_2\text{C}_6\text{H}_3\text{CH}_3)_3$.
2. A strong absorption band is observed at 14200 cm^{-1} , which may be due to the transfer of the unpaired electron in the complex into empty antibonding molecular orbitals. This band is shifted slightly to a higher energy in the spectrum of $\text{Re}(\text{S}_2\text{C}_6\text{H}_3\text{CH}_3)_3$.
3. Another strong absorption band is observed at 23400 cm^{-1} which again may be due to the transfer of the unpaired electron into empty antibonding molecular orbitals. The intensity of this band is less than the second band observed at 14200 cm^{-1} . In $\text{Re}(\text{S}_2\text{C}_6\text{H}_3\text{CH}_3)_3$ this band is observed at slightly higher energy.

The similarity of the electronic spectra of $\text{Re}(\text{S}_2\text{C}_2\text{Ph}_2)_3$ and $\text{Re}(\text{S}_2\text{C}_6\text{H}_3\text{CH}_3)_3$ in solutions indicates that the electronic structures are very similar for these two complexes. In addition, the solid state spectra⁹ of these complexes do not differ significantly from the solution spectra. This indicates that the electronic structures of these complexes are very similar in the solid state and in solution.

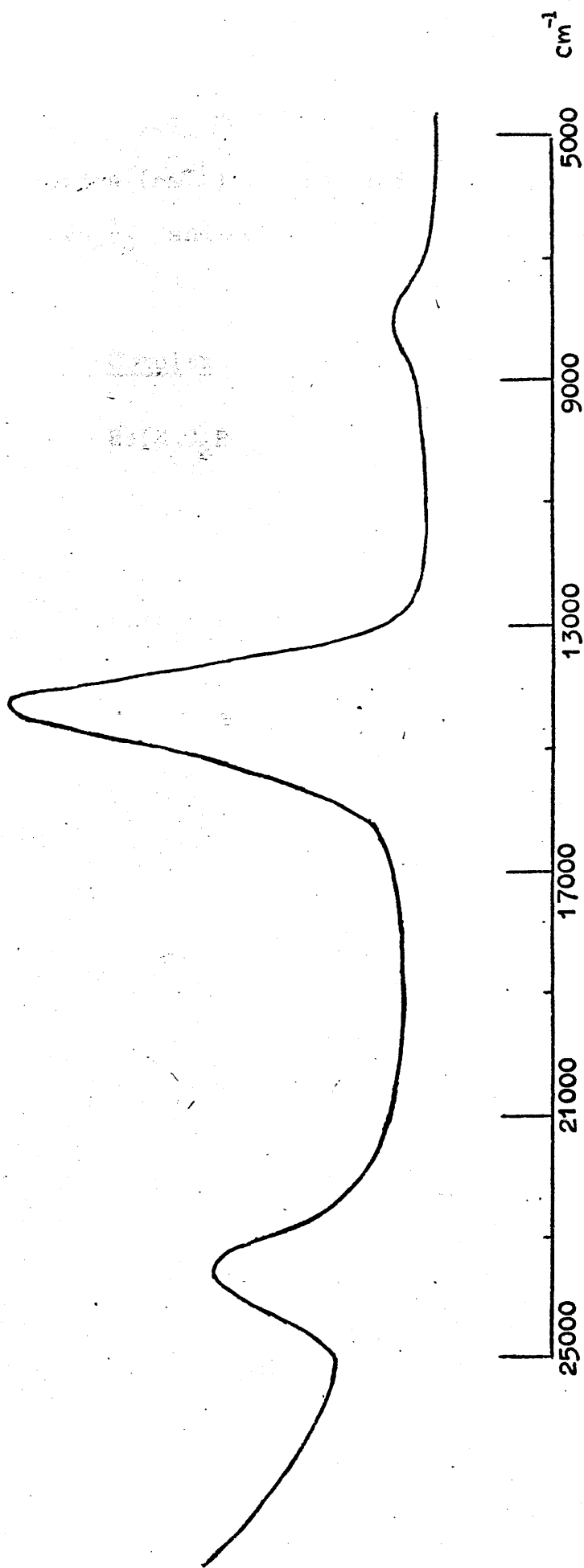


Figure 4.3. Electronic spectrum of $\text{Re}(\text{S}_2\text{C}_2\text{Ph}_2)_3$ in CHCl_3 at 298K.

Table 4.2

Band maxima (cm^{-1}) in the electronic spectra of
 $\text{Re}(\text{S}_2\text{C}_2\text{Ph}_2)_3$ and $\text{Re}(\text{S}_2\text{C}_6\text{H}_3\text{CH}_3)_3$ in chloroform.

<u>Complex</u>	<u>Band maxima</u>
$\text{Re}(\text{S}_2\text{C}_2\text{Ph}_2)_3$	8,230
	14,200
	23,400
$\text{Re}(\text{S}_2\text{C}_6\text{H}_3\text{CH}_3)_3$	7,920
	14,380
	24,950

4.5 Molecular orbitals in tris(dithiolato)-rhenium complexes

Crystallographic analysis ^{2,3}, shows that in tris (cis-1,2-diphenylethene-1,2-dithiolato)-rhenium, $\text{Re}(\text{S}_2\text{C}_2\text{Ph}_2)_3$, the central rhenium atom is surrounded by an almost perfect trigonal prism of six sulphur atoms. The average Re-S distance is 2.325 \AA , and the average S-Re-S angle is 81.4° . A perspective drawing of the coordination geometry is shown in Figure 4.4. The coordination geometry of the complex is D_{3h} and the over-all molecular symmetry belongs very nearly to the point group C_{3h} . The phenyl rings are twisted out of the planes of the chelate rings and do not appear to conjugate with the rest of the structure. Molecular orbitals for this complex can be constructed from a basis obtained from the 5d, 6s and 6p rhenium orbitals and twenty-four ligand orbitals. These ligand orbitals fall into the following categories.

- 1) Six σ -orbitals are derived from the sulphur sp^2 hybrids which point in towards the central rhenium atoms.
- 2) Six π_h -orbitals are derived from the sulphur sp^2 hybrids oriented at 120° to the σ -orbitals.
- 3) Twelve π_v orbitals are derived from the three sets of four ligand π -orbitals which lie at right angles to the planes of each of the three chelate rings. These are delocalised over the S-C-C-S frameworks and are designated in order of increasing energy as $1\pi_v$, $2\pi_v$, $3\pi_v$ and $4\pi_v$, respectively. The $3\pi_v$ orbital derived from the dithiolate residue involving,

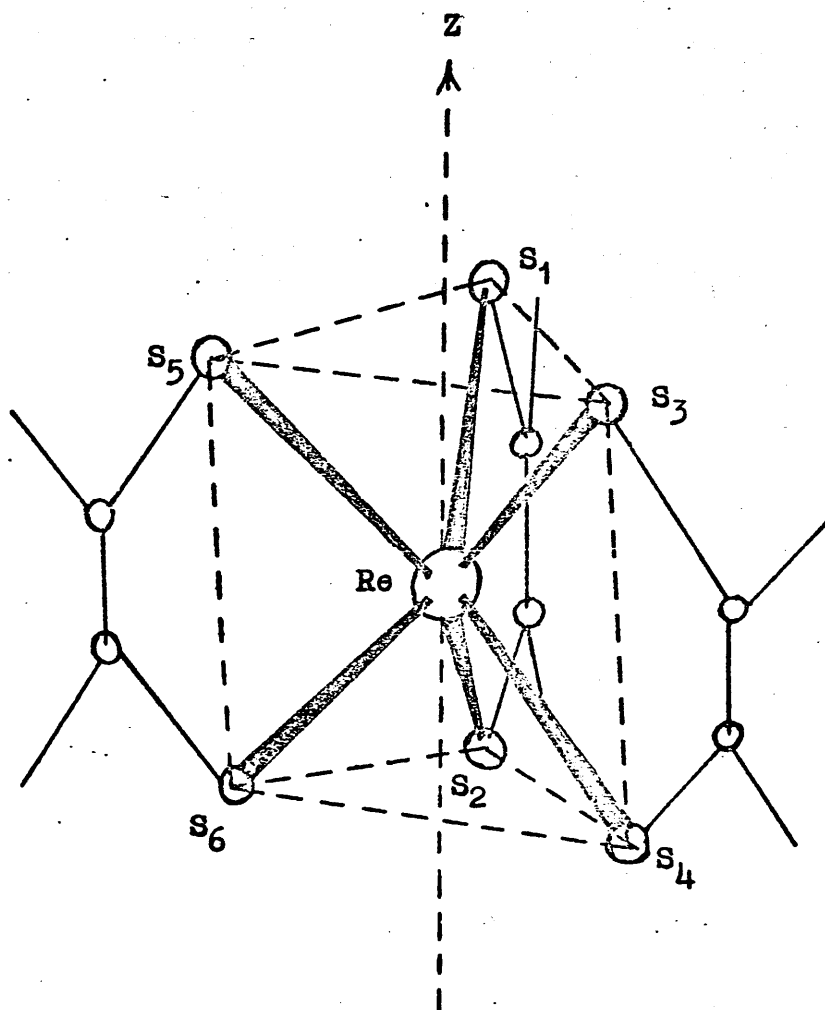


Figure 4.4. Coordination system for trigonal-prismatic rhenium complexes.

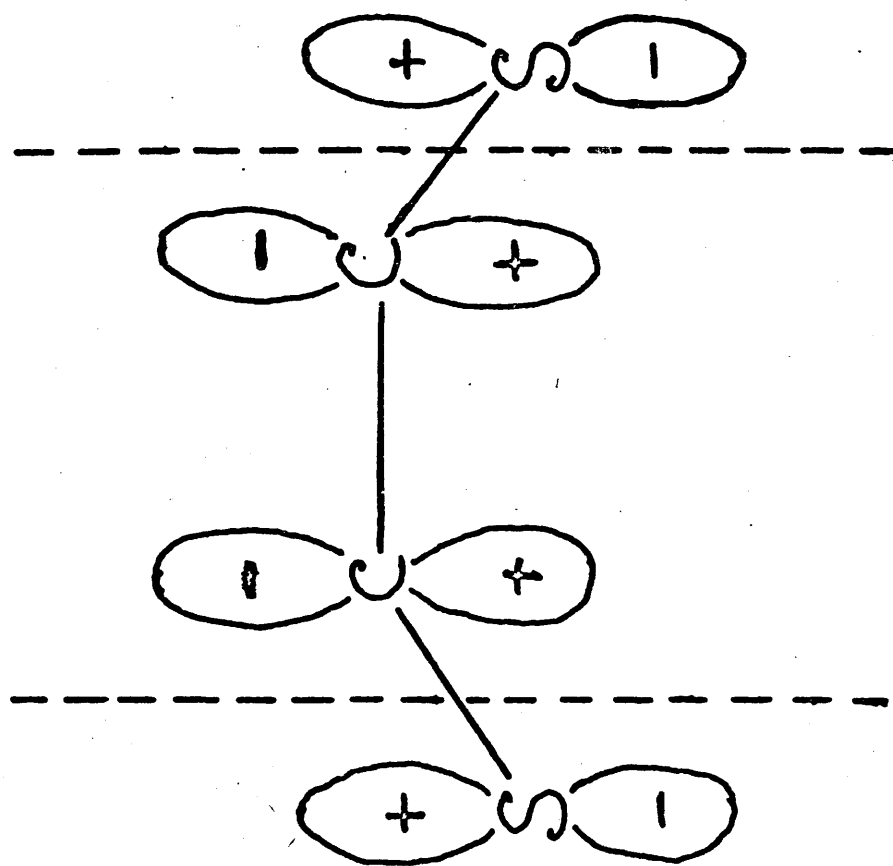


Figure 4.5. $3\pi_v$ molecular orbital in dithioglyoxal complexes.

for example, S_1 and S_2 is designated $3\pi_v(1,2)$, and is shown schematically in Figure 4.5. The ligand $3\pi_v$ and the $5d$ orbitals of rhenium have comparable energies.

In the D_{3h} group these thirty-three basis orbitals fall into the symmetry classes as shown below⁹

<u>Representation</u>	<u>Metal-ion orbitals</u>	<u>Ligand orbitals</u>
A'_1	$5d_{z^2}; 6s$	$\frac{1}{\sqrt{6}}(\sigma'_1 + \sigma'_2 + \sigma'_3 + \sigma'_4 + \sigma'_5 + \sigma'_6)$ $\frac{1}{\sqrt{6}}(\pi_{h1} + \pi_{h2} + \pi_{h3} + \pi_{h4} + \pi_{h5} + \pi_{h6})$
A''_1	-	$\frac{1}{\sqrt{3}}[2\pi_v(1,2) + 2\pi_v(3,4) + 2\pi_v(5,6)]$ $\frac{1}{\sqrt{3}}[4\pi_v(1,2) + 4\pi_v(3,4) + 4\pi_v(5,6)]$
A'_2	-	$\frac{1}{\sqrt{3}}[1\pi_v(1,2) + 1\pi_v(3,4) + 1\pi_v(5,6)]$ $\frac{1}{\sqrt{3}}[3\pi_v(1,2) + 3\pi_v(3,4) + 3\pi_v(5,6)]$
A''_2	$6p_z$	$\frac{1}{\sqrt{6}}(\sigma'_1 + \sigma'_3 + \sigma'_5 - \sigma'_2 - \sigma'_4 - \sigma'_6)$ $\frac{1}{\sqrt{6}}(\pi_{h1} + \pi_{h3} + \pi_{h5} - \pi_{h2} - \pi_{h4} - \pi_{h6})$
E'	$5d_{xy}; 5d_{x^2-y^2};$ $6p_x; 6p_y$	$\frac{1}{2\sqrt{3}}(2\sigma'_1 - \sigma'_3 - \sigma'_5 + 2\sigma'_2 - \sigma'_4 - \sigma'_6)$ $\frac{1}{2}(\sigma'_3 - \sigma'_5 + \sigma'_4 - \sigma'_6)$ $\frac{1}{2\sqrt{3}}(2\pi_{h1} - \pi_{h3} - \pi_{h5} + 2\pi_{h2} - \pi_{h4} - \pi_{h6})$ $\frac{1}{2}(\pi_{h3} - \pi_{h5} + \pi_{h4} - \pi_{h6})$

$$\frac{1}{\sqrt{2}} [1 \pi_v(3,4) - 1 \pi_v(5,6)]$$

$$\frac{1}{\sqrt{6}} \{ 2 [1 \pi_v(1,2)] - 1 \pi_v(3,4) - 1 \pi_v(5,6) \}$$

$$\frac{1}{\sqrt{2}} [3 \pi_v(3,4) - 3 \pi_v(5,6)]$$

$$\frac{1}{\sqrt{6}} \{ 2 [3 \pi_v(1,2)] - 3 \pi_v(3,4) - 3 \pi_v(5,6) \}$$

E''

5d_{xz}; 5d_{yz}

$$\frac{1}{2\sqrt{3}} (2\sigma_1 - \sigma_3 - \sigma_5 - 2\sigma_2 + \sigma_4 + \sigma_6)$$

$$\frac{1}{2} (\sigma_3 - \sigma_4 - \sigma_5 + \sigma_6)$$

$$\frac{1}{2\sqrt{3}} (2\pi_{h1} - \pi_{h3} - \pi_{h5} - 2\pi_{h2} + \pi_{h4} + \pi_{h6})$$

$$\frac{1}{2} (\pi_{h3} - \pi_{h4} - \pi_{h5} + \pi_{h6})$$

$$\frac{1}{\sqrt{2}} [2 \pi_v(3,4) - 2 \pi_v(5,6)]$$

$$\frac{1}{\sqrt{6}} \{ 2 [2 \pi_v(1,2)] - 2 \pi_v(3,4) - 2 \pi_v(5,6) \}$$

$$\frac{1}{\sqrt{2}} [4 \pi_v(3,4) - 4 \pi_v(5,6)]$$

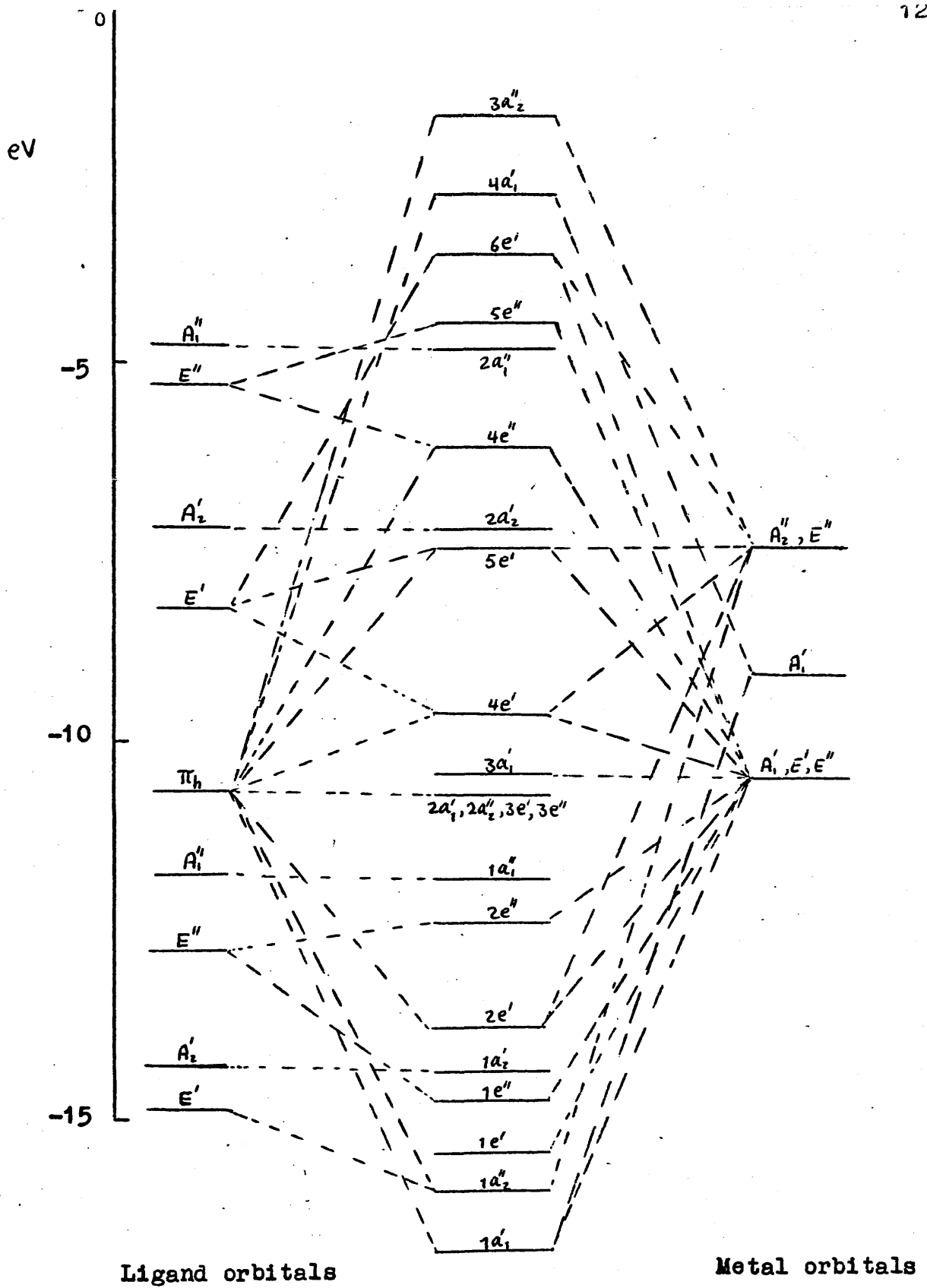
$$\frac{1}{\sqrt{6}} \{ 2 [4 \pi_v(1,2)] - 4 \pi_v(3,4) - 4 \pi_v(5,6) \}$$

Standard Hückel calculations lead to the energy levels and molecular orbitals available to the complex, and the electronic configuration for its ground state can be obtained by feeding forty-three electrons into these levels. Two groups of workers have, separately, carried out such calculations and have reached rather different

conclusions regarding the location of the unpaired electron in the rhenium tris(dithiolates).

Schrauzer and Mayweg have derived ⁶ the energy level diagram shown in Figure 4.6 and they conclude that the electronic configuration for the ground states of the neutral complexes $M(S_2C_2R_2)_3$, $M = Cr, Mo$ or W is $(3a_1^t)^2(4e^t)^4$. In these, the $4e^t$ molecular orbital is formed from a linear combination of the lowest antibonding (E^t) ligand π -orbital (41%), the sulphur sp^2 (17%), and the metal d and p orbitals of (E^t) symmetry (25% and 17% respectively). The next lowest unoccupied molecular orbitals are the $5e^t$ and $2a_2^t$ orbitals. The $5e^t$ orbitals are, "composed similarly as $4e^t$, but over a relatively broad range of metal input Coulomb terms always have somewhat greater metal character than $4e^t$ ". $2a_2^t$ is a pure ligand π -molecular orbital, and the relative energies of the $5e^t$ and $2a_2^t$ orbitals depend critically on the input parameters employed in the Hückel calculation. Paramagnetic resonance measurements on the monoanions $M(S_2C_2R_2)_3^-$, $M = Cr, Mo$ or W indicate significant metal character and are consistent with the ground state configuration $(3a_1^t)^2 (4e^t)^4 (5e^t)^1$, and, furthermore, they definitely rule out the configuration $(3a_1^t)^2 (4e^t)^4 (2a_2^t)^1$ in these ions.

Stiefel, Eisenberg, Rosenberg and Gray ^{8,9}, independently and almost simultaneously, carried out similar calculations on $Re(S_2C_2Ph_2)_3$. Their ordering



Ligand orbitals

Metal orbitals

Figure 4.6. Schrauzer and Mayweg molecular orbital correlation diagram for a prismatic complex of the type $M(S_2C_2H_3)_3$.

of the molecular orbitals differs from that of Schrauzer and Mayweg and they conclude that the ground state electronic configuration is $(4e^i)^4 (2a_2^i)^2 (3a_1^i)^1$: part of their energy level diagram is shown in Figure 4.7. Their $(3a_1^i)$ orbital is largely metal ion $5d_{z^2}$ in character. Their $(4e^i)$ orbital contains considerable $5d$ and $3\pi_v$ character, and it is thoroughly delocalised over $5d_{xy}$, $5d_{x^2-y^2}$ and $3\pi_v$ basis orbitals. $(2a_2^i)$ is a non-bonding linear combination of the ligand $3\pi_v$ orbitals.

The electron paramagnetic resonance spectra of $\text{Re}(\text{S}_2\text{C}_2\text{Ph}_2)_3$ and $\text{Re}(\text{S}_2\text{C}_6\text{H}_3\text{CH}_3)_3$ are not consistent with either of the ground state configurations $(3a_1^i)^2 (4e^i)^4 (5e^i)^1$ or $(4e^i)^4 (2a_2^i)^2 (3a_1^i)^1$ proposed by these two groups of workers, but are consistent with configuration $(3a_1^i)^2 (4e^i)^4 (2a_2^i)^1$ rejected by the first group.

4.6 Results and discussion

The ground states of the tris(dithiolato)-rhenium complexes as predicted by Schrauzer and Mayweg and by Gray, et al., are not consistent with the electron paramagnetic resonance spectra or with the semiconductor properties of these complexes. The ground state configurations must be $(3a_1^i)^2 (4e^i)^4 (2a_2^i)^1$. The results obtained from e.p.r. spectra and the

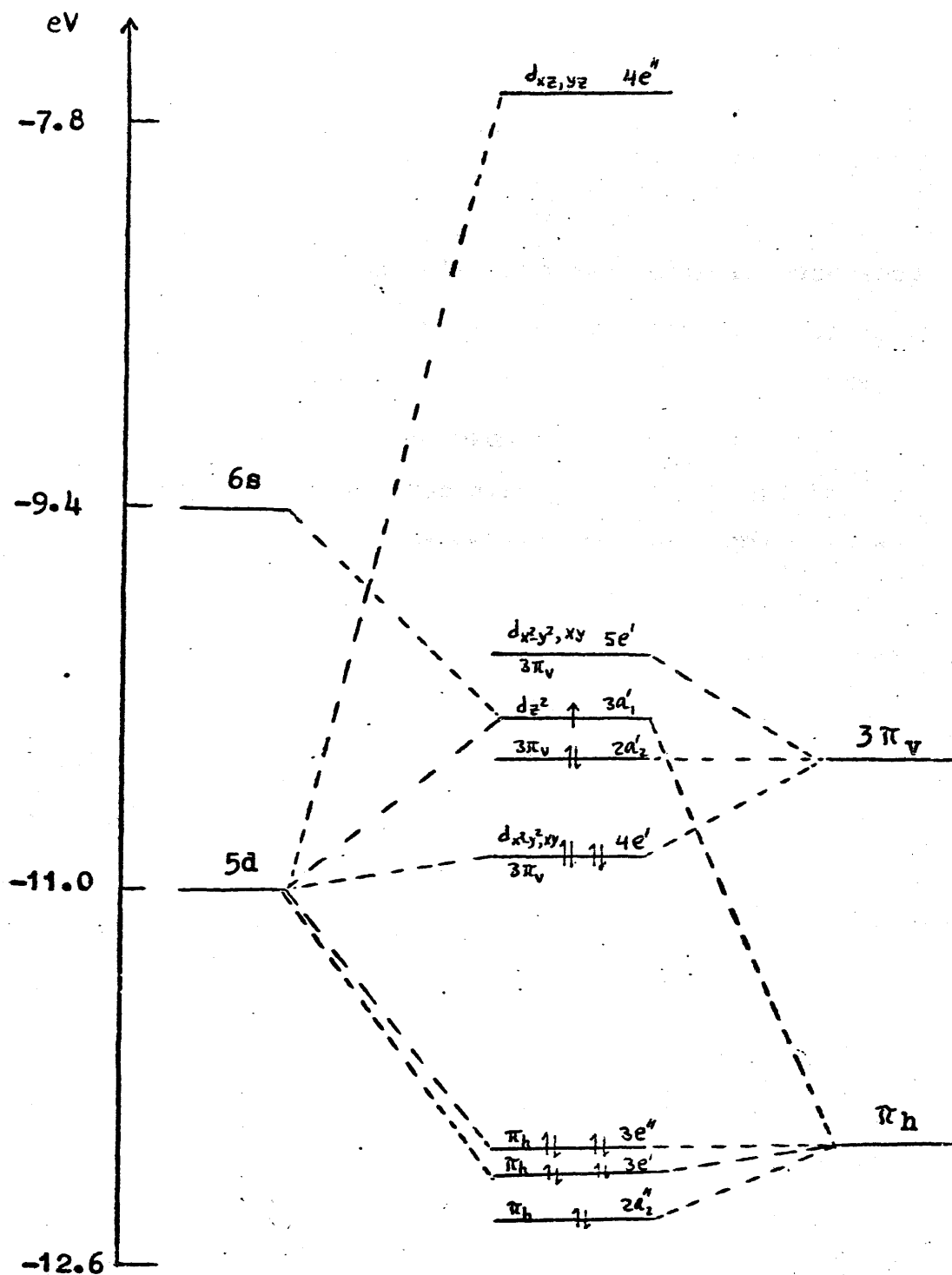


Figure 4.7 Gray, et al. molecular orbital correlation diagram for a prismatic complex $\text{Re}(\text{S}_2\text{C}_2\text{Ph}_2)_3$.

semiconductor ⁷ and Voltammetric Properties ⁹ which confirm this configuration can be summarized as follows:

1. The analysis of the electron paramagnetic resonance spectra of ReOCl_4 shows that the unpaired electron is in a molecular orbital which is a linear combination of the $5d_{xy}$ orbital of rhenium (67%) and a group orbital (33%) derived from chloride ion $3p_x$ and $3p_y$ orbitals. Strong spin-orbit coupling in ReOCl_4 causes the principal components of the g-tensor to differ very markedly from 2.00232 and hyperfine interactions in this compound are very large. If the unpaired electron in the tris(dithiolato)-rhenium complexes is located in the molecular orbitals predicted by either of the above mentioned two groups of workers, then the e.p.r. spectra of these complexes would show very large hyperfine coupling and considerable anisotropy in the g-tensor as was found in ReOCl_4 and its adducts. The electron paramagnetic resonance spectra of the tris(dithiolato)-rhenium complexes are quite different from the spectra of ReOCl_4 . The small g-tensor anisotropy is very characteristic of sulphur-containing organic radicals ^{16,17}. The vanishingly small rhenium hyperfine coupling, almost certainly a direct dipolar coupling, sets an upper limit of the order of 0.1% to the rhenium contribution to the molecular orbital containing the unpaired electron in these dithiolates. Thus the e.p.r. spectra show that the unpaired electron in the tris(dithiolato)-rhenium complexes is in the non-bonding ($2a_2'$) molecular orbital derived from the

ligand $3\pi_v$ orbitals.

2. Conductivity measurements ⁷ of tris(dithiolato) complexes of V, Mo, W and Re show that the rhenium complexes are much better conductors than the, essentially iso-structural, vanadium, molybdenum and tungsten compounds. The specific resistances of the solid complexes $\text{Re}(\text{S}_2\text{C}_2\text{R}_2)_3$ fall in the range $10^3 < \rho < 10^8$ ohm cm., whereas the corresponding properties of the molybdenum and tungsten analogues fall in the range $10^{12} < \rho < 10^{15}$ ohm cm. The lower specific resistance of rhenium complexes definitely rule out the ground state configurations of Schrauzer and Mayweg and of Gray, et al. for these complexes, and become natural consequences of the proposed ground state in which the unpaired electron is in the non-bonding ($2a_2'$) molecular orbital.

The Voltammetric properties of the rhenium tris(dithiolates) are not inconsistent with the proposed ground state configuration $(3a_1')$ ² $(4e')$ ⁴ $(2a_2')$ ¹. In this configuration the most loosely bound electron is placed right out on the outside of these complexes, i.e. in that region where it can most readily exchange and take part in redox reactions with neighbouring molecules.

The specific resistances of the solid complexes of V, Mo, W and Re together with the polarographic data are listed in Tables 4.3 and 4.4 respectively.

Table 4.3

Resistivities of tris(dithiolato) complexes of tungsten, molybdenum and rhenium.

<u>Complex</u>	<u>R</u>	<u>ρ ohms cm</u>
$WS_6C_6R_6$	Ph	4×10^{13}
	PhCH ₃	3×10^{14}
$MoS_6C_6R_6$	H	1.4×10^{12}
	CH ₃	3×10^{14}
$ReS_6C_6R_6$	H	10^3
	CH ₃	4×10^5
	Ph	6×10^7

Table 4.4

Polarographic data for tris(dithiolato) complexes of tungsten, molybdenum and rhenium.

<u>Complex</u>	<u>$E_{1/2}$ (v)</u>			
	<u>$n=1 \rightarrow n=0$</u>	<u>$n=0 \rightarrow n=-1$</u>	<u>$n=-1 \rightarrow n=-2$</u>	<u>$n=-2 \rightarrow n=-3$</u>
$Re(S_2C_2Ph_2)_3^n$	+0.163	-0.340	-1.812	-2.591
$Re(S_2C_6H_3CH_3)_3^n$	+0.387	-0.065	-1.577	-2.375
$W(S_2C_2Ph_2)_3^n$		-0.542	-1.135	
$W(S_2C_6H_3CH_3)_3^n$		-0.247	-1.075	
$Mo(S_2C_2Ph_2)_3^n$		-0.489	-1.095	-2.92
$Mo(S_2C_6H_3CH_3)_3^n$		-0.219	-0.895	-2.62

The two sets of molecular orbital calculations and these deductions from e.p.r. spectroscopy can be made self-consistent (i) by slightly altering Schrauzer and Mayweg's input parameters, and thereby lowering the energy of their ($2a_2^i$) orbital below their ($5e^i$) levels, and (ii) by raising the energy of Gray and coworkers $3\pi_v$ orbitals. This produces the energy level diagram shown in Figure 4.8 and leads to a ground state electronic configuration $(3a_1^i)^2 (4e^i)^4 (2a_2^i)^1$ for $\text{Re}(\text{S}_2\text{C}_2\text{R}_2)_3$ complexes.

The band maxima of the electronic spectra listed in Table 4.2 can now be assigned by using the resulting molecular orbital levels as follows.

<u>Band maxima (cm^{-1})</u>	<u>Transition</u>
8,230	$4e^i \longrightarrow 2a_2^i$
14,200	$2a_2^i \longrightarrow 5e^i$
23,400	$2a_2^i \longrightarrow 4e^{ii}$

The large intensities of the observed bands are consistent with transitions between levels which have sulphur orbital components and are expected to be strongly allowed for electric-dipole radiation.

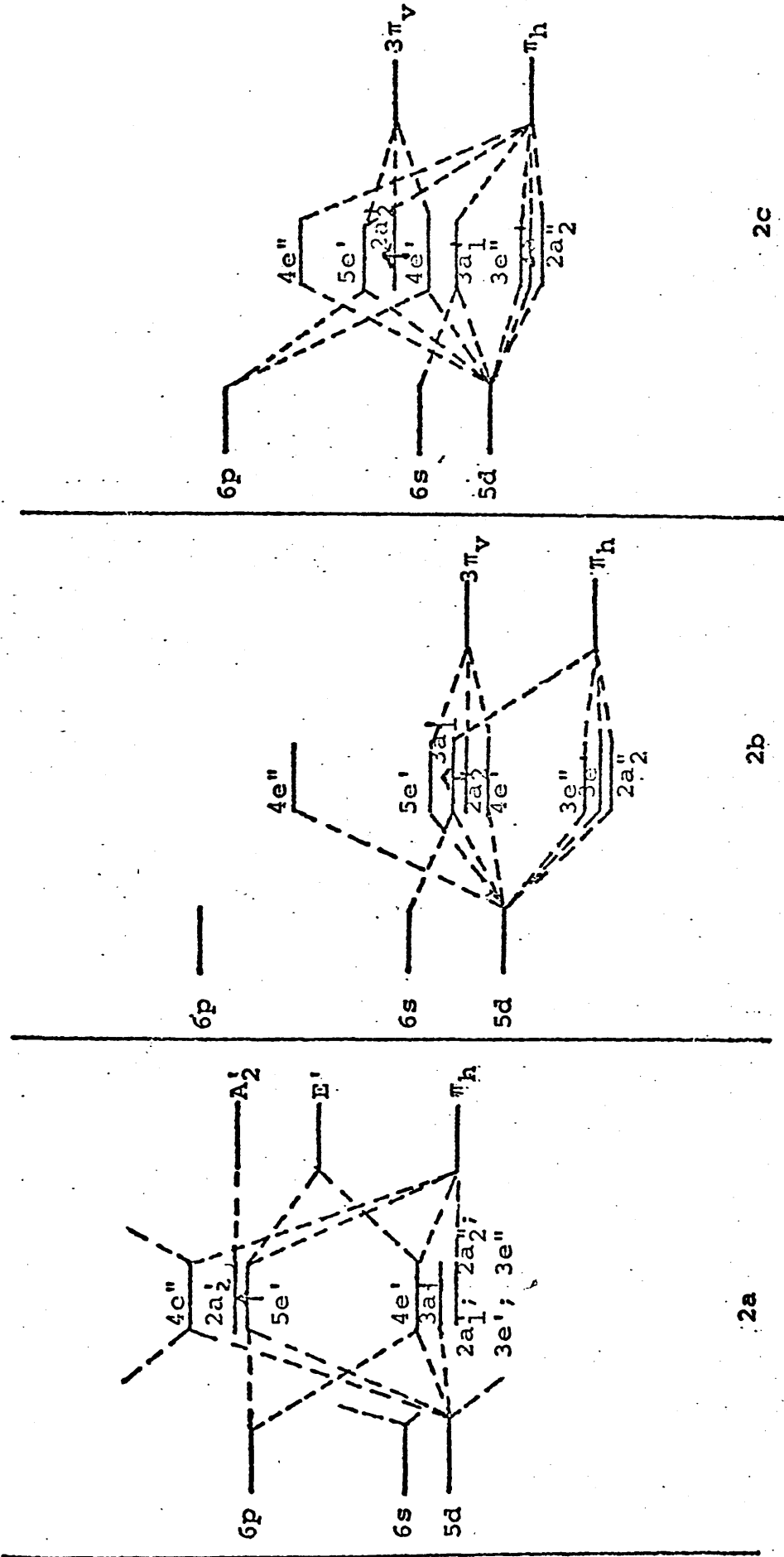


Figure 4.8. The resulting molecular orbitals, (2C), from altering Schrauzer and Mayweg's input parameters, (2a), and raising the energy of Gray, et al. 3π_v orbitals, (2b).

2a

2b

2c

4.7 Summary of Part IV

In this study the electron paramagnetic resonance spectra of the six-coordinated prismatic complexes, $\text{Re}(\text{S}_2\text{C}_2\text{Ph}_2)_3$ and $\text{Re}(\text{S}_2\text{C}_6\text{H}_3\text{CH}_3)_3$, have been recorded in solution at 298 K and in magnetically dilute glasses at 77 K. These e.p.r. spectra are quite different from those that have been obtained from the other rhenium complexes that have been studied in Part II. Each trigonal pyramidal rhenium complex shows a single electron resonance signal in both magnetically concentrated solid and in solution at room temperature. The spectra of magnetically dilute glasses at 77 K of the tris(dithiolato)-rhenium complexes show small g-tensor anisotropy and vanishingly small rhenium nuclear hyperfine coupling. The small g-tensor anisotropy is very characteristic of sulphur-containing organic radicals and the vanishing small rhenium nuclear hyperfine coupling, almost certainly a direct dipolar coupling, sets an upper limit of the order of 0.1% to the rhenium contribution to the molecular orbital containing the unpaired electron in these complexes. The e.p.r. spectra show that the unpaired electron in these complexes is in a non-bonding molecular orbital derived from the ligand π -orbitals.

E.P.R. properties, electronic absorption spectra, Voltammetric properties, the magnetic properties of ions derived from $\text{Re}(\text{S}_2\text{C}_2\text{R}_2)_3$, and the unusually high electrical conductivities exhibited by the solids, are

all consistent with an electronic ground state configuration $(3a'_1)^2 (4e'_1)^4 (2a'_2)^1$ for these complexes.

The electron paramagnetic resonance spectra and the optical spectra of rhenium (VI) in the square antiprism and in the dodecahedron will be illustrated with reference to the octacyano-rhenium complexes in the following section of this thesis.

References to Part IV

1. J.A. McCleverty "Progress in Inorganic Chemistry," Interscience, London, 1968, 10, 143.
2. R.Eisenberg and J.A. Ibers, J.Am.Chem.Soc., 1965, 87, 3776.
3. R.Eisenberg and J.A.Ibers, Inorg.Chem., 1966, 5, 411.
4. A.E.Smith, G.N. Schrauzer, U.P.Mayweg and W.Heinrich, J.Am.Chem.Soc., 1965, 87, 5798.
5. E.I.Stiefel and H.B.Gray, J.Am.Chem.Soc., 1965, 87, 4012.
6. G.N. Schrauzer and U.P.Mayweg J.Am.Chem.Soc., 1966, 88, 3235.
7. E.J.Rosa and G.N.Schrauzer, J.Phys.Chem., 1969, 73, 3132.
8. H.B.Gray, Trans.N.Y.Acad.Sci., 1966 (2), 28, 898.
9. E.I.Stiefel, R.Eisenberg, R.C. Rosenberg and H.B.Gray. J.Am.Chem.Soc., 1966, 88, 2956.
10. J.A.McCleverty, J.Locke and E.J.Wharton, J.Chem.Soc.(A), 1968, 816.
11. A.Davison, N.Edelstien, R.H.Holm and A.H.Maki, J.Am. Chem. Soc., 1964, 86, 2799.
12. A.Davison, N.Edelstien, R.H.Holm and A.H.Maki, Inorg. Chem., 1965, 4, 55.
13. N.M.Atherton and C.J.Winscom, Inorg.Chem., 1973, 12, 383.
14. Whei-Lu Kwik and E.I. Stiefel, Inorg.Chem., 1973, 12, 2337.
15. A.Abragam and M.H.L.Pryce, Proc.Roy.Soc.(A), 1951, 205, 135.
16. R.D.Schmitt and A.H. Maki, J.Am.Chem.Soc., 1968, 90, 2288.
17. P.B.Ayscough, "Electron Spin Resonance in Chemistry", Methuen and Co.Ltd., London, 1967, 349 and references therein.

PART VELECTRON PARAMAGNETIC RESONANCE AND OPTICAL SPECTRA
OF THE OCTACYANORHENIUM COMPLEXES5.1 Introduction

Although the structure of the octacyano complexes of molybdenum, tungsten and rhenium is a topic which has received a great deal of attention ^{1,2}, it is still not certain whether these compounds are dodecahedra or are square antiprisms. Energetically, there appears to be little difference between these two structures ³. The factors which should control the geometry of a complex, of which the most important are the metal-ligand bond energies and the mutual repulsions of the ligands, differ very little for the square antiprism and the dodecahedron ^{1,2,3}. The closed-shell ligand-ligand repulsions are generally smaller for the antiprism by about 1Kcal/mole, but this effect could be offset in highly polar complexes by the coulombic repulsions which, if account is taken of the shielding effect of the metal atom, may favour the dodecahedron ⁴.

On the basis of X-ray diffraction analysis of octacyanomolybdate $\text{Mo}(\text{CN})_8^{4-}$, Hoard and Nordsieck ⁵ found the structure of $\text{K}_4\text{Mo}(\text{CN})_8 \cdot 2\text{H}_2\text{O}$ to be dodecahedral.

Weissmand and Cohn ⁶ found, however, that in solution the isotropic coupling interaction with C^{13} in $\text{K}_4\text{Mo}(\text{CN})_8$ was nearly the same for all eight CN ligands,

thus supporting the square antiprism structure where all the CN groups are equivalent.

Stammreich and Sala ⁷ found that the Raman spectrum of an aqueous solution of the potassium salt of the octacyanomolybdenum complex contains three lines in the $C\equiv N$ stretching region. This observation, coupled with Hildago and Matthieu's report ⁸ of two bands in the infra-red spectrum of the solid, led them to propose that the anion had a square antiprismatic structure in both solid and solution.

McGarvey ⁹ carried out electron paramagnetic resonance studies on $K_4Mo(CN)_8$ and on $K_4W(CN)_8$ in magnetically dilute glasses and in polycrystalline samples. He found that the e.p.r. spectra of these ions in solution are consistent with the square antiprism structure, but in the crystalline state, the e.p.r. spectra however, are consistent with the dodecahedron structure. Thus dodecahedron symmetry has been forced upon the ion in the host lattice, but the crystal field is relaxed in solution and the square antiprism structure becomes more stable.

Support for the assignment of solid $Mo(CN)_8^{4-}$ being dodecahedral (D_{2d}) and its aqueous solution being square antiprismatic (D_{4d}) have since come from the infra-red and Raman studies of this compound which have been carried out by Parish and his coworkers ^{10,11}.

The same authors conclude that the corresponding tungsten compound has similar structure.

Hayes¹² carried out similar e.p.r. studies on the same complexes in magnetically dilute glasses and he concludes, that the electron paramagnetic resonance data favour a square antiprism structure for the free $\text{Mo}(\text{CN})_8^{3-}$ and $\text{W}(\text{CN})_8^{3-}$ ions.

The bonding in the octacyano complexes is described from a valence-bond approach in term of d^4sp^3 hybrids. The crystal-field and ligand-field descriptions show that one of the d-orbitals is strongly stabilised, $d_{x^2-y^2}$ for a dodecahedron and d_{z^2} for a square antiprism¹³⁻²⁰. Neither of these orbitals has the correct symmetry for σ -bonding.

No e.p.r. studies at all have been carried out on the octacyanorhenium complexes and only meagre I.R. data is available²¹. It was therefore decided to study in detail the e.p.r., I.R. and u.v. spectra of these complexes and to see whether these species favour the dodecahedron or square antiprism structure in the solid state.

5.2 Experimental

The pentavalent octacyano rhenium complex, $\text{K}_3\text{Re}(\text{CN})_8$, and the hexavalent, $[\text{Ph}_4\text{As}]_2[\text{Re}(\text{CN})_8]$, were prepared by the following methods^{21, 22}.

I) Potassium octacyanorhenate (V), $K_3Re(CN)_8$, was prepared by dissolving potassium hexaiodorhenate (IV), K_2ReI_6 , in dry methanol and the mixture was run into a refluxing solution of KCN in dry methanol. The colour changed immediately from deep red to light yellow-brown. The solution was refluxed for 10 minutes more, and the brown solid which separated was then filtered off, suspended in more dry methanol and refluxed for 10 minutes. The brown product was filtered off, washed several times with hot methanol, and dried. The complex is insoluble in all organic solvents but it is very soluble in water to give a brown solution.

II) Tetraphenylarsonium octacyanorhenate (VI), $[Ph_4As]_2[Re(CN)_8]$, was made by oxidation of the octacyanorhenate, $K_3Re(CN)_8$, in solution. $K_3Re(CN)_8$ was dissolved in oxygenated cold water, and the solution acidified with concentrated HCl. Immediate addition of saturated tetraphenylarsonium chloride solution gave a purple precipitate of $[Ph_4As]_2[Re(CN)_8]$, which was centrifuged, washed thoroughly with water and acetone and dried. The behaviour of the octacyanorhenate (VI) ion in solution is most unusual²¹. When aqueous $K_3Re(CN)_8$ in air is acidified, the purple solution formed is at first paramagnetic as expected, but it becomes diamagnetic without further colour change and the change in susceptibility is exponential with a half life of 5 ± 2 seconds. The paramagnetic complex

$[\text{Ph}_4\text{As}]_2[\text{Re}(\text{CN})_8]$ is insoluble in all organic solvents but it is very slightly soluble in water to give a purple solution.

Infra-red spectra of these complexes were obtained on KBr discs with a Perkin-Elmer 257 spectrophotometer. Visible-u.v. absorption spectra of aqueous solutions of each compound were recorded on Unicam SP700C and 800 spectrophotometers, using matched 1-cm quartz cells. The e.p.r. spectra of the paramagnetic species $[\text{Ph}_4\text{As}]_2[\text{Re}(\text{CN})_8]$ were recorded on polycrystalline samples at 290K and at 77K.

5.3 Analysis of the e.p.r. spectra of $[\text{Ph}_4\text{As}]_2[\text{Re}(\text{CN})_8]$

The hyperfine structure in the electron paramagnetic resonance spectra of $[\text{Ph}_4\text{As}]_2[\text{Re}(\text{CN})_8]$ was well resolved in undiluted polycrystalline samples. This unusual observation seems to be due to the reduction of the dipole-dipole interaction of neighbouring unpaired electrons. The electronic dipole-dipole interaction between neighbouring rhenium atoms in this large molecule is so reduced, even in the concentrated crystals, that the separate hyperfine components of the spectra can be clearly resolved without resorting to dilution with an isomorphous diamagnetic compound. Due to solubility difficulties encountered with this complex the spectra were only recorded in undiluted polycrystalline samples and the observed spectra

obtained at room temperature is shown in Figure 5.1. The spectra at room temperature and at 77 K are similar and are characteristic of one unpaired electron moving in an axially symmetric orbital. Thus as shown in the Appendix A, the spin Hamiltonian for this system has the form ²³

$$\mathcal{H} = g_{11}\beta_e H_z S_z + g_1\beta_e (H_x S_x + H_y S_y) + A S_z I_z + B(S_x I_x + S_y I_y) + Q' \left[I_z^2 - \frac{1}{3}I(I+1) \right]$$

..... 5.1

The quadrupole interaction in this complex is very small so it can be ignored. The spin-Hamiltonian parameters derived from the spectra are given in Table 5.1. All the spectra are characteristic in which $A > B$, with little anisotropy in the g tensor components. The value of A was obtained by measuring the separation of the two sharp lines of the low and high field side of the spectrum.

5.4 Visible-u.v. spectra of $[\text{Ph}_4\text{As}]_2[\text{Re}(\text{CN})_8]$ and $\underline{\text{K}_3\text{Re}(\text{CN})_8}$

The band-maxima observed in the spectra of $[\text{Ph}_4\text{As}]_2[\text{Re}(\text{CN})_8]$ and $\text{K}_3\text{Re}(\text{CN})_8$ in aqueous solution can be summarized as follows:

- a) $[\text{Ph}_4\text{As}]_2[\text{Re}(\text{CN})_8]$ shows a weak absorption band at $18,870 \text{ cm}^{-1}$ which, from its position and intensity, is almost certainly a d-d transition, involving the transfer

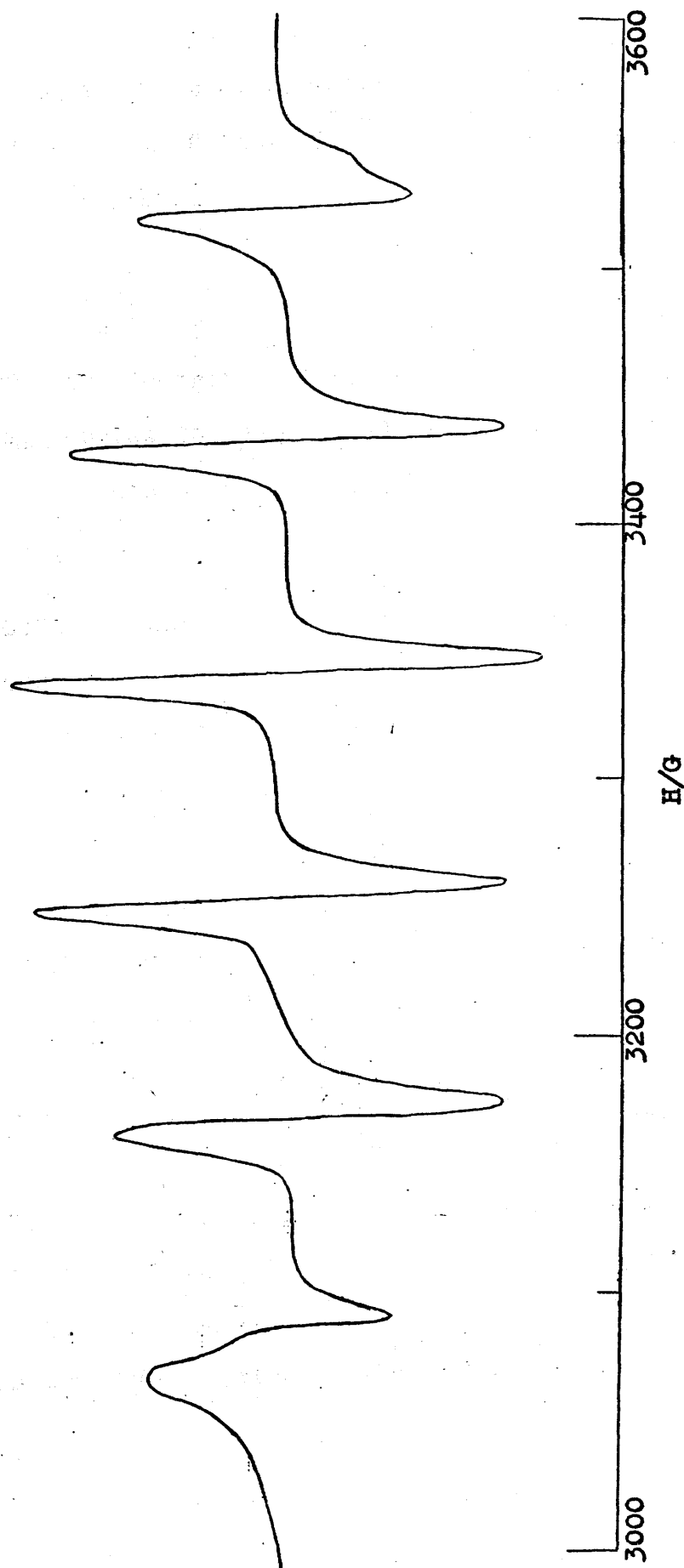


Figure 5.1. E.p.r. spectrum of polycrystalline sample of $[\text{Ph}_4\text{As}]_2 [\text{Re}(\text{CN})_8]$ at 290K.

of the unpaired electron to an empty antibonding orbital. This band is shifted to higher energy in the case of the diamagnetic complex, $K_3Re(CN)_8$, which involves a transfer of one of the paired electrons to an empty antibonding orbital.

b) $[Ph_4As]_2[Re(CN)_8]$ shows a strong absorption band at $33,330\text{ cm}^{-1}$. This is assignable to a transition in which an electron is transferred from a filled bonding orbital to the orbital containing the unpaired electron. This band is shifted to lower energy in $K_3Re(CN)_8$.

c) Other strong absorption bands at $39,200$ and $36,360\text{ cm}^{-1}$ have been observed for $[Ph_4As]_2[Re(CN)_8]$ and $K_3Re(CN)_8$ respectively, which may be assigned to charge transfer bands.

The u.v.-visible spectra of $[Ph_4As]_2[Re(CN)_8]$ and $K_3Re(CN)_8$ in aqueous solution are shown in Figures 5.2 and 5.3 respectively and the frequencies of the band maxima of the two complexes are listed in Table 5.2.

5.5 Infra-red spectra of $K_3Re(CN)_8$ and $[Ph_4As]_2[Re(CN)_8]$

The infra-red spectra of $K_3Re(CN)_8$ and $[Ph_4As]_2[Re(CN)_8]$ in the solid phase (KBr disc) have been measured in the range $1900-2200\text{ cm}^{-1}$, since this region of the spectrum covers the $C\equiv N$ stretching frequencies and is very important for structural determination of the complexes.

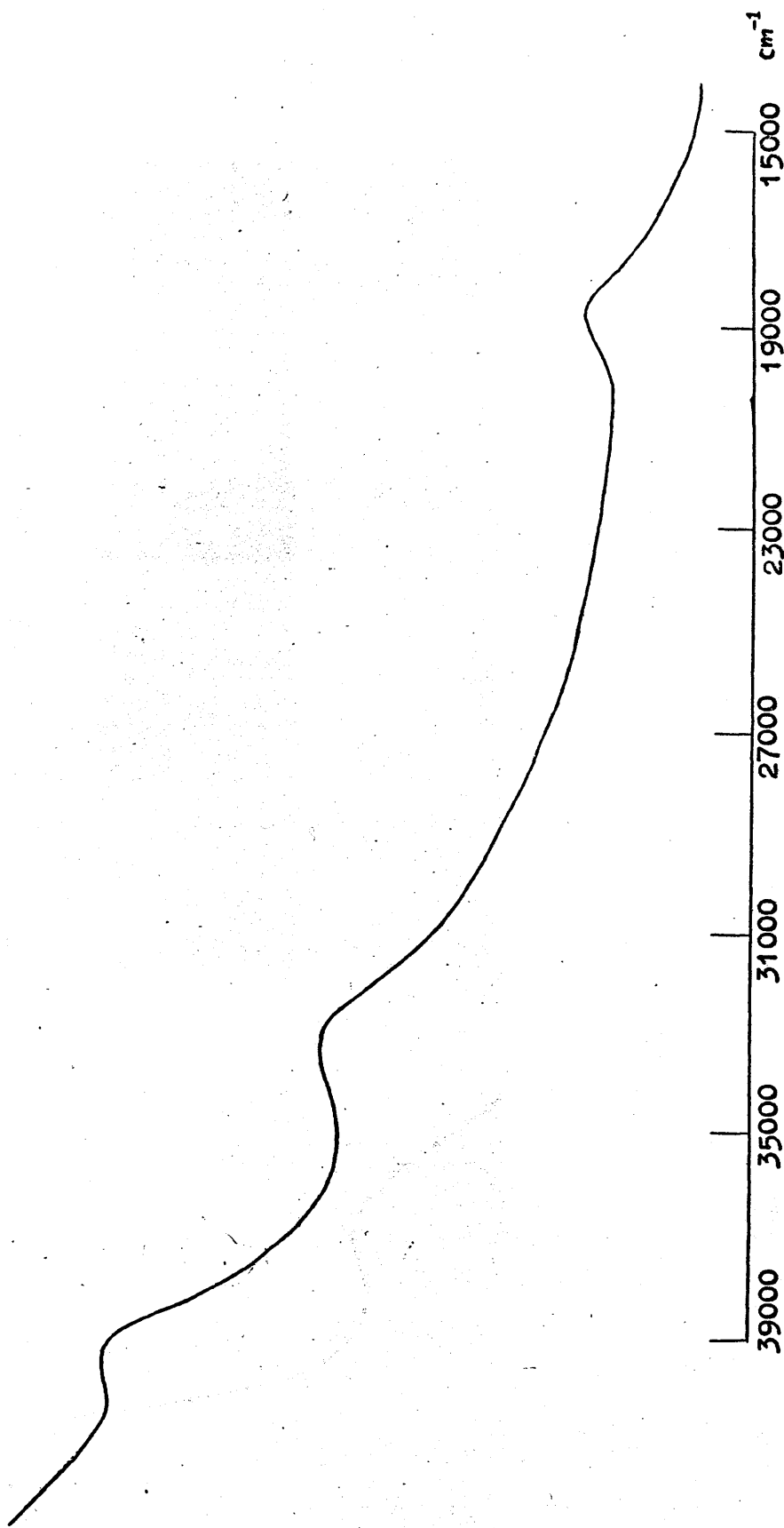


Figure 5.2. U.v.-visible spectrum of an aqueous solution of $[\text{Ph}_4\text{As}]_2 [\text{Re}(\text{CN})_8]$ at 290K.

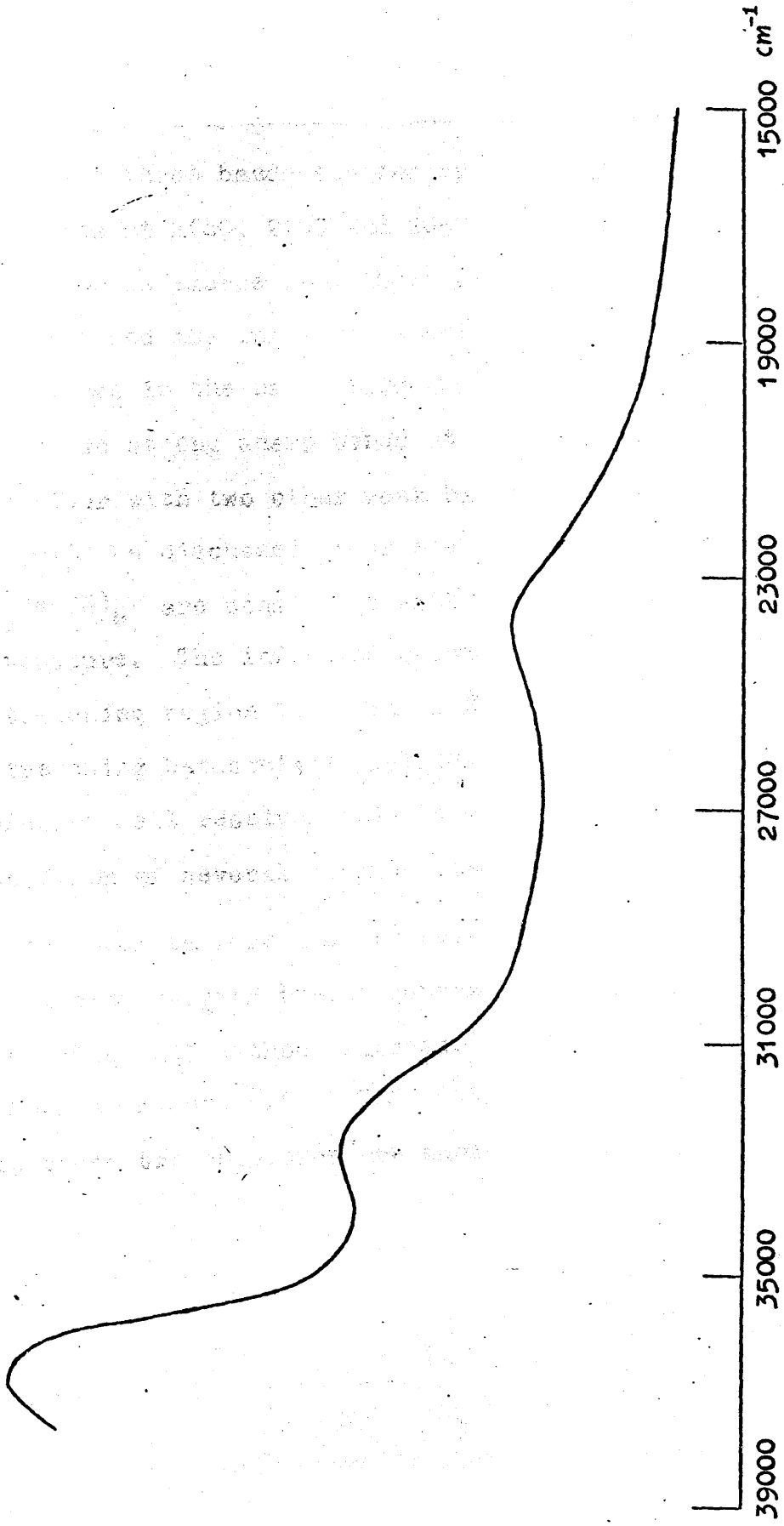


Figure 5.3. U.v.-visible spectrum of an aqueous solution of $K_3Re(CN)_8$ at 290K.

The infra-red spectra of $K_3Re(CN)_8$ in Nujolmulls have been reported by Wilkinson and his coworkers²¹. They observed three bands for the cyanide stretching frequencies at 2140, 2100 and 2050 cm^{-1} , but no definite conclusions emerge from their work. We have, therefore, re-examined the infra-red spectra of $K_3Re(CN)_8$ in KBr discs in the range 1900-2200 cm^{-1} . These spectra show two strong sharp bands at 2130 and 2050 cm^{-1} together with two other weak bands at 2095 and 2080 cm^{-1} . As will be discussed later the infra-red spectra of $K_3Re(CN)_3$ are consistent with the dodecahedron structure. The infra-red spectrum for the $C\equiv N$ stretching region is shown in Figure 5.4. The $C\equiv N$ stretching bands of $[Ph_4As]_2[Re(CN)_8]$ in a KBr disc are not well resolved and the spectrum shows a superposition of several peaks centred at 2070 cm^{-1} . Many attempts were made to resolve this spectrum, including varying the concentration of the sample in the disc, all without success. This spectrum is shown in Figure 5.5. $C\equiv N$ stretching frequencies in these two complexes are shown in Table 5.3.

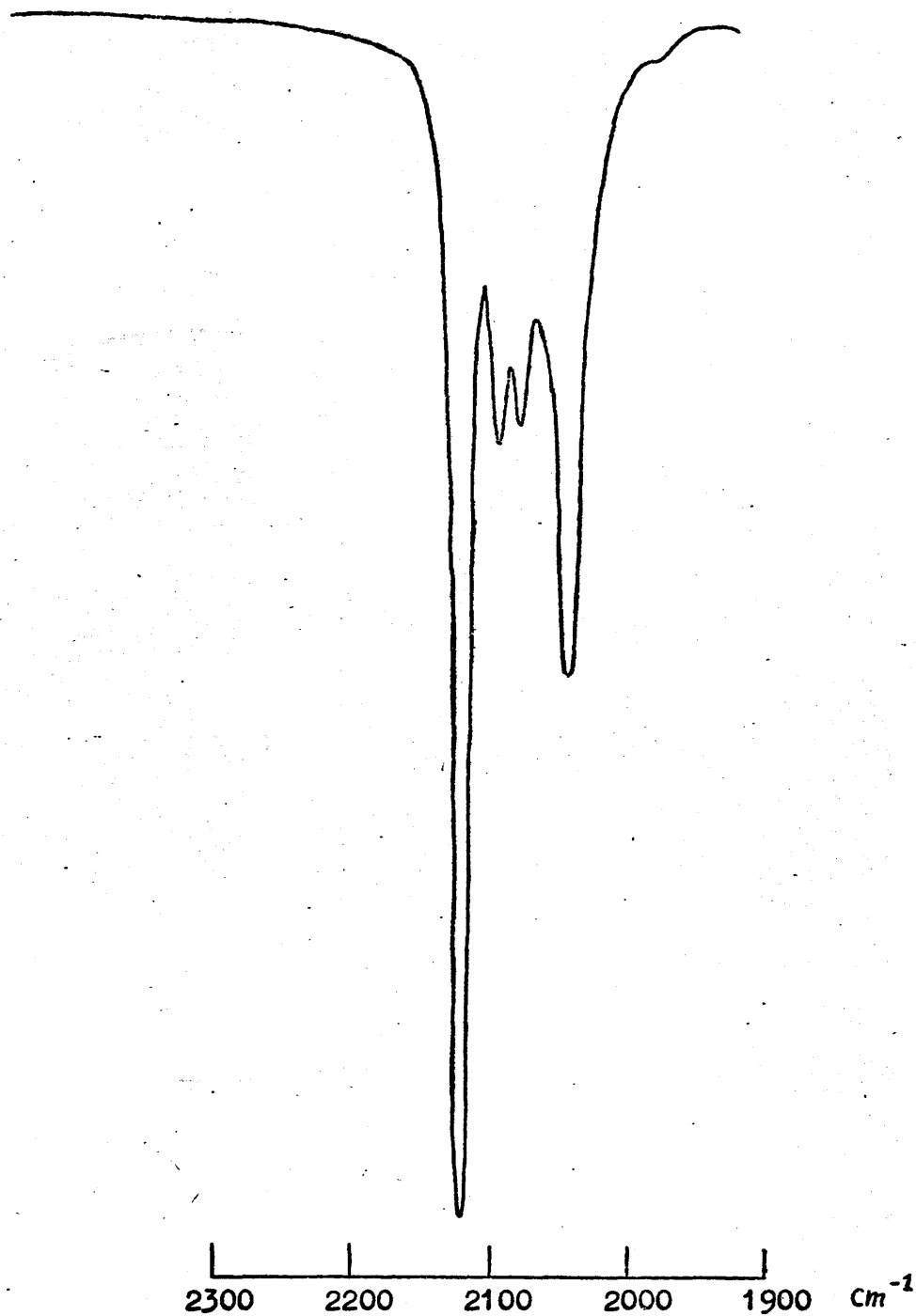


Figure 5.4. Infra-red spectrum of $\text{K}_3\text{Re}(\text{CN})_8$ in the $\text{C}\equiv\text{N}$ stretching frequencies region at 290K.

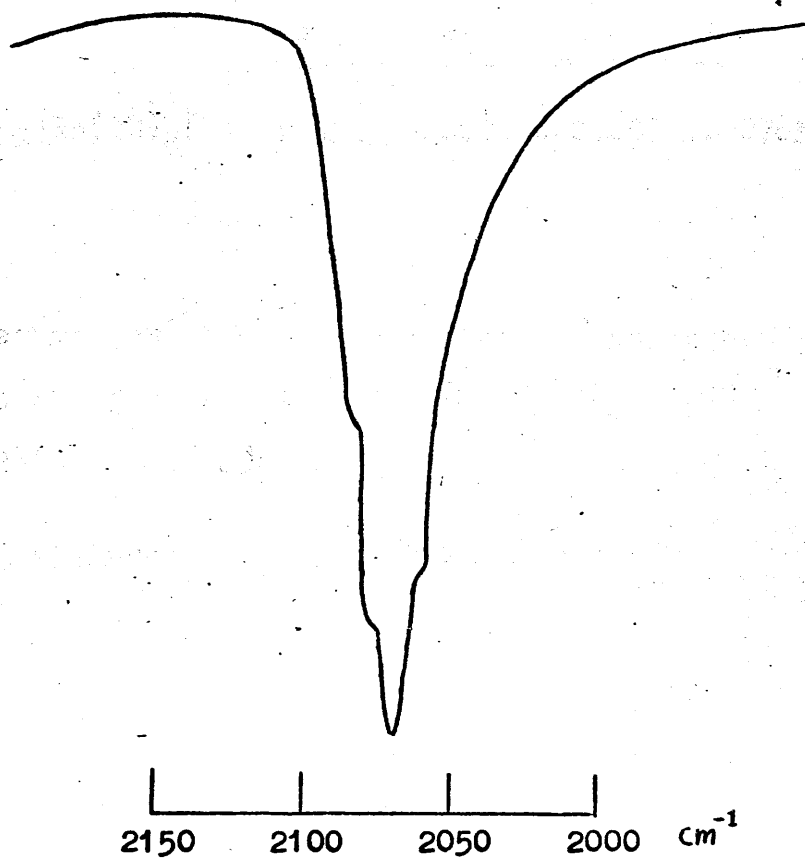


Figure 5.5 Infra-red spectrum of $[\text{Ph}_4\text{As}]_2[\text{Re}(\text{CN})_8]$ in the $\text{C}\equiv\text{N}$ stretching frequencies region at 290K.

Table 5.1

Spin Hamiltonian parameters for a polycrystalline sample of $[\text{Ph}_4\text{As}]_2[\text{Re}(\text{CN})_8]$ at 290 K. The hyperfine coupling tensor components are in units of cm^{-1} . Limits of error are g_{11} and $g_1 \pm 0.0003$, A and B $\pm 0.00002 \text{ cm}^{-1}$.

	<u>g_{11}</u>	<u>g_1</u>	<u>A</u>	<u>B</u>
$[\text{Ph}_4\text{As}]_2[\text{Re}(\text{CN})_8]$	1.9925	2.0005	0.00893	0.00765

Table 5.2

Band maxima (cm^{-1}) in the visible-u.v. absorption spectra of aqueous solutions of $[\text{Ph}_4\text{As}]_2[\text{Re}(\text{CN})_8]$ and $\text{K}_3\text{Re}(\text{CN})_8$ at 290 K.

<u>Compound</u>	<u>Absorption band</u>
$[\text{Ph}_4\text{As}]_2[\text{Re}(\text{CN})_8]$	18,870; 33,330; 39,200
$\text{K}_3\text{Re}(\text{CN})_8$	23,800; 32,780; 36,360

Table 5.3

Infra-red absorption frequencies (cm^{-1}) in the $\text{C}\equiv\text{N}$ stretching region of solid samples of $[\text{Ph}_4\text{As}]_2[\text{Re}(\text{CN})_8]$ and $\text{K}_3\text{Re}(\text{CN})_8$ at 290 K.

<u>Compound</u>	<u>Cyanide stretching frequency</u>
$[\text{Ph}_4\text{As}]_2[\text{Re}(\text{CN})_8]$	2070
$\text{K}_3\text{Re}(\text{CN})_8$	2130; 2095; 2080; 2050

5.6 Theory

The eight cyanide ligands around the central rhenium atom could possibly be arranged ⁹ in one or other of five different ways as follows:

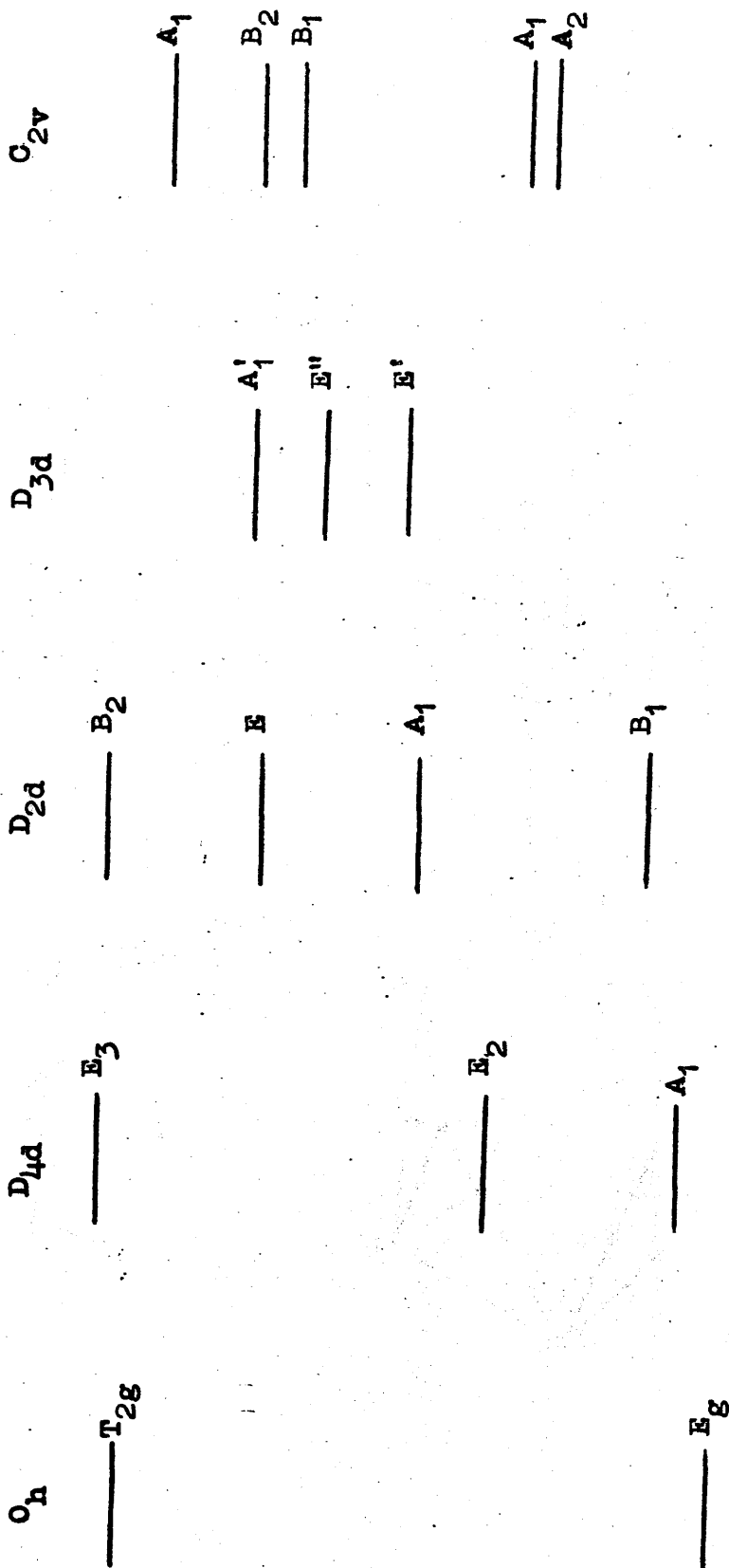
1. A cube which belongs to O_h symmetry with degenerate d_{z^2} and $d_{x^2-y^2}$ orbitals as the highest occupied orbitals.
2. A square antiprism which belongs to D_{4d} symmetry with d_{z^2} as the highest occupied orbital.
3. A dodecahedron of D_{2d} symmetry in which the d_{xy} orbital is the highest occupied orbital.
4. A trigonal prism with ligands in the centres of the two end faces, belonging to D_{3d} with degenerate d_{xy} and $d_{x^2-y^2}$ orbitals as the highest occupied orbitals.
5. A trigonal prism with ligands centred on two side faces, belonging to C_{2v} symmetry, with $d_{x^2-y^2}$ orbital as the highest occupied orbital.

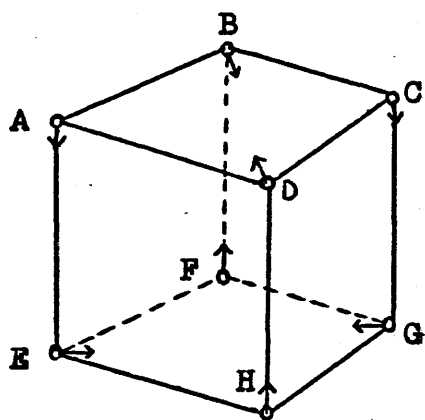
The energy level spacings for each above symmetry have been calculated ⁹ from crystal field theory and are shown in Figure 5.6.

The dodecahedron and square antiprism structures are both obtained by distortion of a cube ² as shown in Figure 5.7. By rotating a pair of opposite faces in the cube until they are mutually at 45° , the square antiprism structure is obtained and the final symmetry

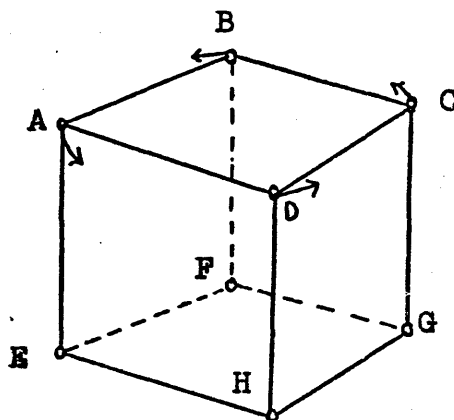
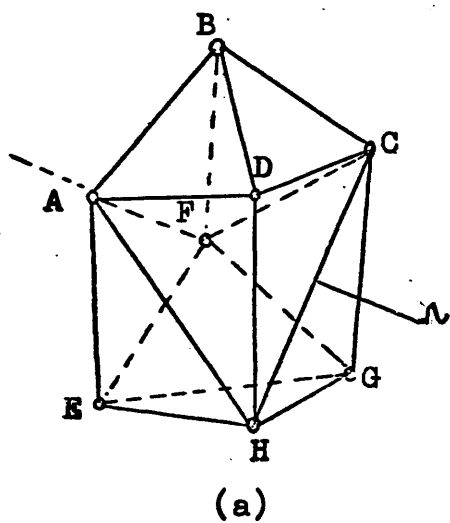
Figure 5.6

Crystal-field splitting for d-orbitals in five possible arrangements of eight equivalent charges about a central metal atom.

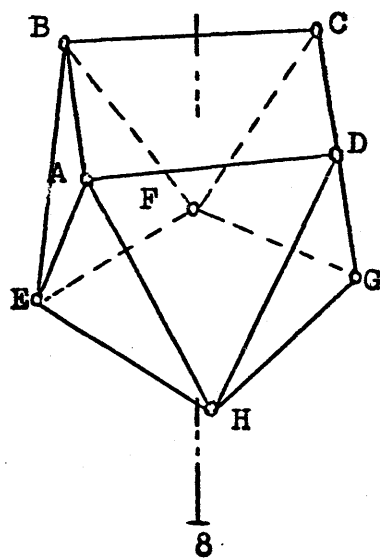




O_h
↓
 D_{2d}



O_h
↓
 D_{4d}



(b)

Figure 5.7. Distortion of the cube to form (a) the dodecahedron (b) the square antiprism.

is D_{4d} . In the resultant structure all ligands around the central metal ion are in equivalent positions. To obtain a dodecahedron from the cube, the latter is divided into its positive and negative tetrahedra, one of which is elongated and the other flattened along the same axis. Thus the ligands in this case form two non-equivalent sets and the final symmetry is D_{2d} . When the antiprism is viewed along one of the minor two-fold axes, the corresponding angles are very close to the angles of the dodecahedron, but the two polyhedra differ fundamentally in the twisting about the major axis. When the polyhedra are distorted the differences between them becomes less marked. Energetically, there is very little difference between the dodecahedron and the square antiprism structures.

The valence bond approach was used to obtain qualitative results about the bonding in eight-coordinated complexes¹³⁻²⁰. The orbital not involved in σ -bonding in both the square antiprism and in the dodecahedron is of the proper symmetry to form π -bonds with ligands. In the square antiprism this orbital is a d_z^2 orbital directed along the \bar{z} -axis and is therefore equally suitable for π -bonding to any or all of the ligand atoms as shown in Figure 5.8. In the dodecahedron structure, however, it is the $d_{x^2-y^2}$ orbital which has the proper symmetry to form π -bonds with the ligands and since this orbital lies in the XY plane, it can form a π -bond only to ligands atoms of type B as shown in Figure 5.9.

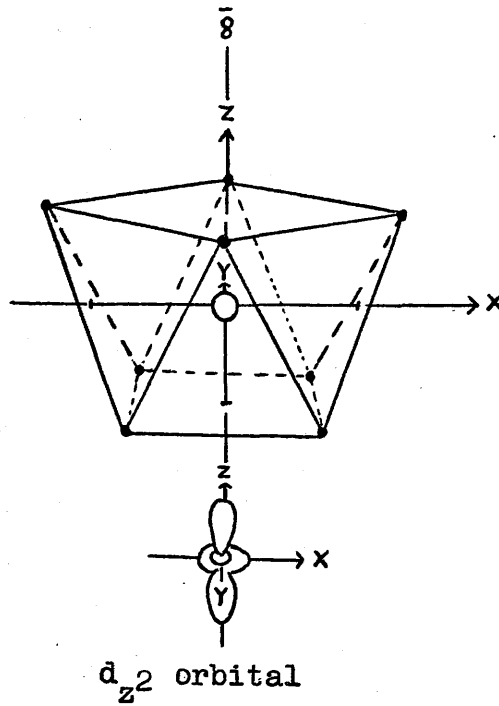


Figure 5.8 View of the square antiprism and the d_{z^2} metal atom orbital available for π -bonding with the ligand atoms.

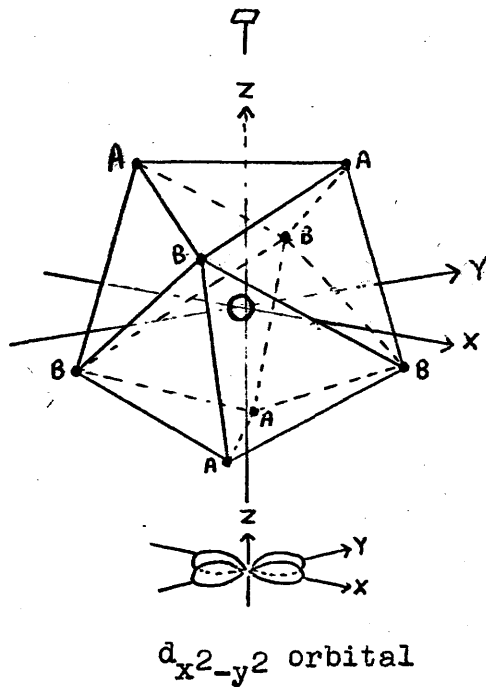


Figure 5.9 View of the dodecahedron and the $d_{x^2-y^2}$ metal atom orbital available for π -bonding with the ligand atoms.

In axial symmetry the d_{xz} and d_{yz} orbitals are degenerate so that the electron paramagnetic resonance spectrum of the octacyano complex shows that the unpaired electron must be in the $d_{x^2-y^2}$, or in the d_{xy} or in the d_z^2 orbitals. Assuming the electron to be in a pure d-atomic orbital and by using second-order perturbation theory⁹, we can readily see that if the $d_{x^2-y^2}$ orbital is the highest occupied orbital, then the parameters of the spin Hamiltonian are given by the following equations

$$g_{11} = 2.0023 - \frac{8 \xi}{E(d_{xy}) - E(d_{x^2-y^2})}$$

$$g_1 = 2.0023 - \frac{2 \xi}{E(d_{xz}, d_{yz}) - E(d_{x^2-y^2})}$$

.... 5.2

$$A = P \left[-K - \frac{4}{7} + (g_{11} - 2.0023) + \frac{3}{7} (g_1 - 2.0023) \right]$$

$$B = P \left[-K + \frac{2}{7} + \frac{11}{14} (g_1 - 2.0023) \right]$$

where ξ is the spin-orbit coupling constant, $P = 2.0023 g_N \beta_N \beta_e \langle r^{-3} \rangle_{av}$, and K is the isotropic contribution to the hyperfine constant due to polarization of the inner electron spin density by the unpaired d-electron. The same equations are also obtained when the d_{xy} orbital is the highest occupied orbital except that x^2-y^2 and xy are interchanged.

On the other hand, if the orbital d_{z^2} is the highest occupied orbital, the above parameters are given by the following equations

$$g_{11} = 2.0023$$

$$g_1 = 2.0023 - \frac{6\xi}{E(d_{xz}, d_{yz}) - E(d_{z^2})}$$

..... 5.3

$$A = P \left[-K + \frac{4}{7} - \frac{1}{7} (g_1 - 2.0023) \right]$$

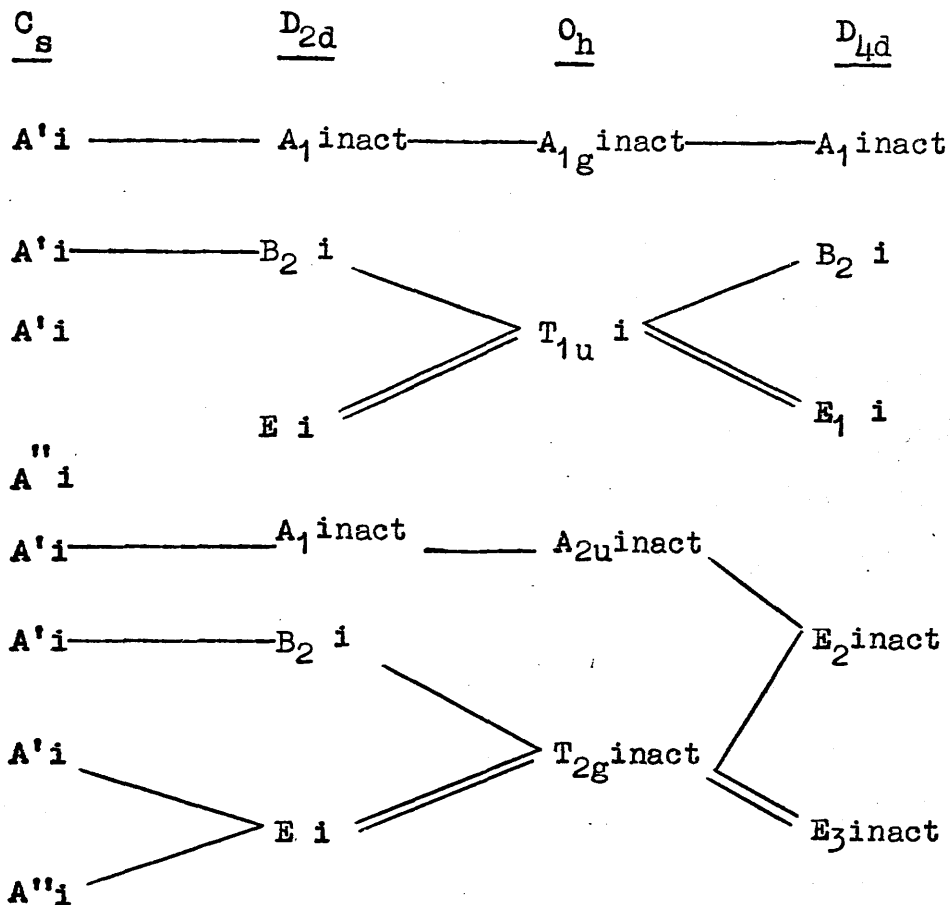
$$B = P \left[-K - \frac{2}{7} + \frac{15}{14} (g_1 - 2.0023) \right]$$

5.7 Results and discussion

The infra-red spectrum of the diamagnetic complex, $K_3\text{Re}(\text{CN})_8$, and the electron paramagnetic resonance spectrum of the paramagnetic complex, $[\text{Ph}_4\text{As}]_2[\text{Re}(\text{CN})_8]$ are characteristic of dodecahedral structures. The results obtained can be summarized as follows.

I. It is possible to distinguish between the antiprism and dodecahedron structures from the number and intensity of the peaks observed in the I.R. spectra for $\text{C}\equiv\text{N}$ stretching. The activities and symmetries of the $\text{C}\equiv\text{N}$ stretching modes expected for various possible configurations¹¹ are shown in Table 5.4. This table shows that the D_{4d} and D_{2d} configurations have two and four infra-red active $\text{C}\equiv\text{N}$ stretching modes respectively.

Table 5.4

Correlation of $C\equiv N$ stretching modes for various symmetries.

i = infra-red active, inact = inactive

Thus the D_{4d} symmetry requires two bands in the infra-red spectra of the $C\equiv N$ stretching region while D_{2d} symmetry requires four bands. Further distortion of the dodecahedron may occur as a result of crystal packing and the symmetry in this case is lowered to C_s such that the two E modes in the D_{2d} symmetry will split to give two bands of comparable, but probably not identical intensity.

It has already been noted that the infra-red spectrum of $K_3Re(CN)_8$ in the solid state contains two strong sharp bands and two weak bands in the $C\equiv N$ stretching frequency region. This observation immediately excludes O_h , D_{4d} and C_s symmetries and it is consistent with D_{2d} symmetry. By regarding the dodecahedron as a distorted cube, the T_{1u} modes will always be strongly infra-red active, while the intensity of the T_{2g} group will be strongly dependent on the distortion. Hence, the bands observed at 2130 and 2050 cm^{-1} may be assigned to T_{1u} modes and the weak bands observed at 2095 and 2080 cm^{-1} assigned to T_{2g} modes. Thus the I.R. spectrum of $K_3Re(CN)_8$ in the solid state is consistent with the dodecahedron structure.

The I.R. spectrum of the paramagnetic complex $[Ph_4As]_2[Re(CN)_8]$ in the solid state is not well resolved and shows a superposition of several bands so that it is impossible to use these spectra to determine the structure of this complex.

2. The e.p.r. spectra of $[\text{Ph}_4\text{As}]_2[\text{Re}(\text{CN})_8]$ in polycrystalline samples are characteristic of an axially symmetric system in which A is greater than B and with little difference in g-tensor components. As can be seen from equations 5.2 and 5.3, if the unpaired electron available for the complex is located in the d_{z^2} orbital, belonging to the highest occupied orbital of the square antiprism structure, then the hyperfine coupling A must be less than B and g_1 must be less than g_{11} . On the other hand, if the unpaired electron is located in the $d_{x^2-y^2}$ orbital belonging to the dodecahedron structure, then the hyperfine coupling A must be greater than B and g_1 must be greater than g_{11} . Thus the e.p.r. spectrum of $[\text{Ph}_4\text{As}]_2[\text{Re}(\text{CN})_8]$ can only be explained by assuming that in the polycrystalline solid, the structure of this complex is a dodecahedron.

The small size of rhenium hyperfine coupling and the small anisotropy in the g and hyperfine tensor components of this complex indicates that the rhenium d-orbitals must be very mixed with the cyanide orbitals in the formation of the complex.

5.8 Summary of Part V

The electron paramagnetic resonance spectra of magnetically undiluted polycrystalline $[\text{Ph}_4\text{As}]_2[\text{Re}(\text{CN})_8]$ has been recorded at room temperature and at 77 K. The spectra are characteristic of an unpaired electron moving in an axially symmetric orbital in which the hyperfine coupling A is greater than B, and the g-tensor components are almost identical. Five different arrangements of the cyanide ligands around the rhenium atom have been considered. They are: a cube, a square antiprism, a dodecahedron, a trigonal prism with ligands in the centres of the two end faces and a trigonal prism with ligands centred on two side faces. Only the dodecahedron structure is consistent with the e.p.r. results for the paramagnetic complex $[\text{Ph}_4\text{As}]_2[\text{Re}(\text{CN})_8]$. The small size of the rhenium hyperfine coupling and the small anisotropy in the g-tensor components of this complex indicate that the rhenium d-orbitals must be very mixed with the cyanide orbitals in the formation of the complex.

The infra-red spectra of the complexes, $\text{K}_3\text{Re}(\text{CN})_8$, and $[\text{Ph}_4\text{As}]_2[\text{Re}(\text{CN})_8]$ have been recorded in solid phase at room temperature. The infra-red spectrum of $\text{K}_3\text{Re}(\text{CN})_8$ contains two strong sharp bands and two weak bands in $\text{C}\equiv\text{N}$ stretching region. Since the dodecahedron with D_{2d} symmetry has two strong infra-red active $\text{C}\equiv\text{N}$

stretching modes and two weak modes, therefore, the infra-red spectrum of $K_3Re(CN)_8$ is consistent with this structure. The infra-red spectrum of $[Ph_4As]_2[Re(CN)_8]$ is not well resolved and shows superposition of several bands, so that it is not possible to get information from this spectrum about the actual structure of this complex.

So far we have discussed the e.p.r. spectra and the electronic structures of the rhenium ion in different environments; in the square pyramid, in the axially distorted octahedron; in the trigonal-prism and in the dodecahedron.

Manganese (VI) in a distorted tetrahedron will now be discussed in the last part of this thesis.

References to Part V

1. R.V. Parish, *Coordination Chemistry Review*, 1966, 1, 439.
2. S.J. Lippard, *Progress in Inorganic Chemistry*, 1968, 8, 109.
3. J.L. Hoard and J.V. Silverton, *Inorg. Chem.*, 1963, 2, 235.
4. R.V. Parish and P.G. Perkins, *J. Chem. Soc. (A)*, 1967, 345.
5. J.L. Hoard and H.H. Nordsieck, *J. Am. Chem. Soc.*, 1939, 61, 2853.
6. S.I. Weissman and M. Cohn, *J. Chem. Phys.*, 1957, 27, 1440.
7. H. Stammreich and O. Sala, *Z. Elektro Chem.*, 1960, 64, 741;
1961, 65, 149.
8. A. Hildago and J.P. Matthieu, *Compt. Rend.*, 1959, 249, 233.
9. B.R. McGarvey, *Inorg. Chem.*, 1966, 5, 476.
10. R.V. Parish, P.G. Simms, M.A. Wells and L.A. Woodward,
J. Chem. Soc. (A), 1968, 2882.
11. R.V. Parish, *Spectrochimica Acta*, 1966, 22, 1191.
12. R.G. Hayes, *J. Phys. Chem.*, 1966, 44, 2210.
13. J.H. Griffiths, J. Owen and I.M. Ward, *Proc. Roy. Soc. (London)*,
1953, A219, 529.
14. L.E. Orgel, *J. Inorg. Nucl. Chem.*, 1960, 14, 136.
15. R.J. Gillespie, *Can. J. Chem.*, 1961, 39, 2336.
16. M. Randic, *J. Chem. Phys.*, 1962, 36, 2094.
17. R.M. Golding and A. Carrington, *Mol. Phys.*, 1962, 5, 377.
18. G. Glieman, *Theor. Chim. Acta*, 1962, 1, 14.
19. E. König, *Theor. Chim. Acta*, 1962, 1, 23.
20. J.R. Perumareddi, A.D. Liehr and A.W. Adamson, *J. Am. Chem. Soc.*
1963, 85, 249.
21. R. Colton, R.D. Peacock and G. Wilkinson, *J. Chem. Soc.*, 1960, 1374.
22. C.J.L. Lock and G. Wilkinson, *J. Chem. Soc.*, 1964, 2281.
23. A. Abragam and M.H.L. Pryce, *Proc. Roy. Soc. (A)*, 1951, 205, 135.

PART VIAN ELECTRON PARAMAGNETIC RESONANCE STUDY OF DICHLORODIOXOMANGANESE (VI), MnO_2Cl_2 6.1 Introduction

Electron paramagnetic resonance spectroscopy has been used to study some complexes containing vanadium (IV) ¹⁻⁸, niobium (IV) ⁹⁻¹⁰, chromium (V) ¹¹, molybdenum (V) ¹² and tungsten (V) ¹² in tetrahedral or pseudotetrahedral environments. The only previously reported study of Mn (VI) in a tetrahedral system concerns MnO_4^{2-} in K_2CrO_4 ^{13,14} and in $BaSO_4$ ¹⁵.

Provided weak interactions are ignored, the ground state of a d^1 ion in a pure tetrahedral ligand field has two-fold orbital degeneracy. Small deviations from pure tetrahedral symmetry remove this degeneracy and result in excited states which are very close to the ground state. Low-lying excited states in their turn cause spin-lattice relaxation times in nearly tetrahedral d^1 complexes to be very short, so that often electron paramagnetic resonance phenomena can only be detected in these species at low temperatures, e.g., at 4 K. At these low temperatures relatively small deviations from tetrahedral symmetry can bring about large changes in the way in which the unpaired electron is distributed in these molecules, and can very markedly effect their electron paramagnetic resonance properties. At 4 K for example, in the tetrahedral MnO_4^{2-} ion doped into K_2CrO_4 ,

the unpaired electron lies ^{13,14} essentially in the $3d_{x^2-y^2}$ orbital of the Mn^{VI} ion, whereas in MnO_4^{2-} doped into $BaSO_4$ the unpaired electron lies ¹⁵ in an orbital derived from the $3d_{z^2}$ orbital of the central metal ion. In both cases considerable delocalisation on to the ligands also takes place.

Sexivalent manganese appears to be confined to the manganate ion and to the oxychloride, MnO_2Cl_2 . The magnetic properties of the latter compound have not been reported and so we have carried out a detailed analysis of its e.p.r. spectra in order to obtain information about the effects of the extra axial ligand field component on the electron distribution, and on the paramagnetic properties of this molecule.

6.2 Experimental

Dichlorodioxomanganese(VI), MnO_2Cl_2 was prepared by reducing permanganyl chloride, MnO_3Cl , with sulphur dioxide by Briggs' method.¹⁶ The permanganyl chloride was prepared by slowly adding powdered potassium permanganate to a mixture of chlorosulphonic acid (20 ml) and 97% sulphuric acid (10 ml) kept at $-60^\circ C$. SO_2 gas (3 mmol.) was then added to this mixture at $-60^\circ C$ and reduction was effected by allowing the temperature of the mixture to rise to $0^\circ C$ and then quickly cooling it to $-60^\circ C$. The MnO_2Cl_2 was purified by distillation at $-30^\circ C$ on a vacuum line which incorporated two traps, the first held at $-30^\circ C$ and the second, containing

purified carbon tetrachloride, held at -68°C . Mn_2O_7 and HSO_3Cl collect in the first trap and the MnO_2Cl_2 is distilled into the -68°C trap. Solutions of MnO_2Cl_2 in CCl_4 obtained in this way were then thoroughly out-gassed and sealed off on the vacuum line and their spectra recorded immediately.

The e.p.r. spectrum of MnO_2Cl_2 was recorded at 77 K in about 10^{-3}M CCl_4 solution. This spectrum could still be observed at 298 K for a short period. Visible -u.v spectra were recorded, in CCl_4 solution, on Unicam SP 700C and SP 800 spectrophotometers. The observed absorption maxima, $\bar{\nu}_{\text{max}}$, and approximate estimates of extinction coefficients, ξ , are

$\bar{\nu}_{\text{max}}$ (cm^{-1})	ξ
16,200	~ 100
21,500	~ 1100
32,000	~ 1200

The first of these is assigned to weak d-d transitions and to more intense charge-transfer transitions. The second and third are assigned to charge-transfer transitions.

6.3 Analysis of the e.p.r. spectra

MnO_2Cl_2 gave a broad six-lines spectrum in CCl_4 at 298 K due to the interactions of one unpaired electron with an applied magnetic field and with one manganese

nucleus; the nuclear spin-quantum number, I , for ^{55}Mn (natural abundance = 100%) is $5/2$. This spectrum could be interpreted using the usual isotropic spin Hamiltonian ¹⁷,

$$\mathcal{H} = g_0 \beta_e \underline{H} \cdot \underline{S} + A_0 \underline{S} \cdot \underline{I} \quad \dots\dots 6.1$$

The values of g_0 and A_0 obtained from the CCl_4 solution spectrum of MnO_2Cl_2 are listed in Table 6.1.

The e.p.r. spectrum obtained from magnetically dilute glasses of MnO_2Cl_2 in CCl_4 at 77 K is shown in Figure 6.1. As shown in Appendix A, expressions for the observed resonant fields can be obtained using a Hamiltonian of the form ¹⁷

$$\mathcal{H} = \beta_e \underline{H} \cdot g \cdot \underline{S} + \underline{S} \cdot \underline{A} \cdot \underline{I} + Q' \left[I_z^2 - \frac{1}{3} I(I+1) \right] \quad \dots\dots 6.2$$

It is assumed that MnO_2Cl_2 has C_{2v} symmetry, and that the principal axes of the g -tensor, the ^{55}Mn hyperfine interaction tensor, A , and the ^{55}Mn nuclear quadrupole coupling tensor, Q' , all coincide. Since the analysis showed that only the component Q'_{zz} of this last interaction is significant, the spin-Hamiltonian used was of the form ¹⁷

$$\mathcal{H} = \beta_e \left[g_{xx} H_x S_x + g_{yy} H_y S_y + g_{zz} H_z S_z \right] + A_{xx} S_x I_x + A_{yy} S_y I_y + A_{zz} S_z I_z + Q'_{zz} \left[I_z^2 - \frac{1}{3} I(I+1) \right] \quad \dots\dots 6.3$$

where, x, y , and z are the principal axes of the g , A and Q' tensors.

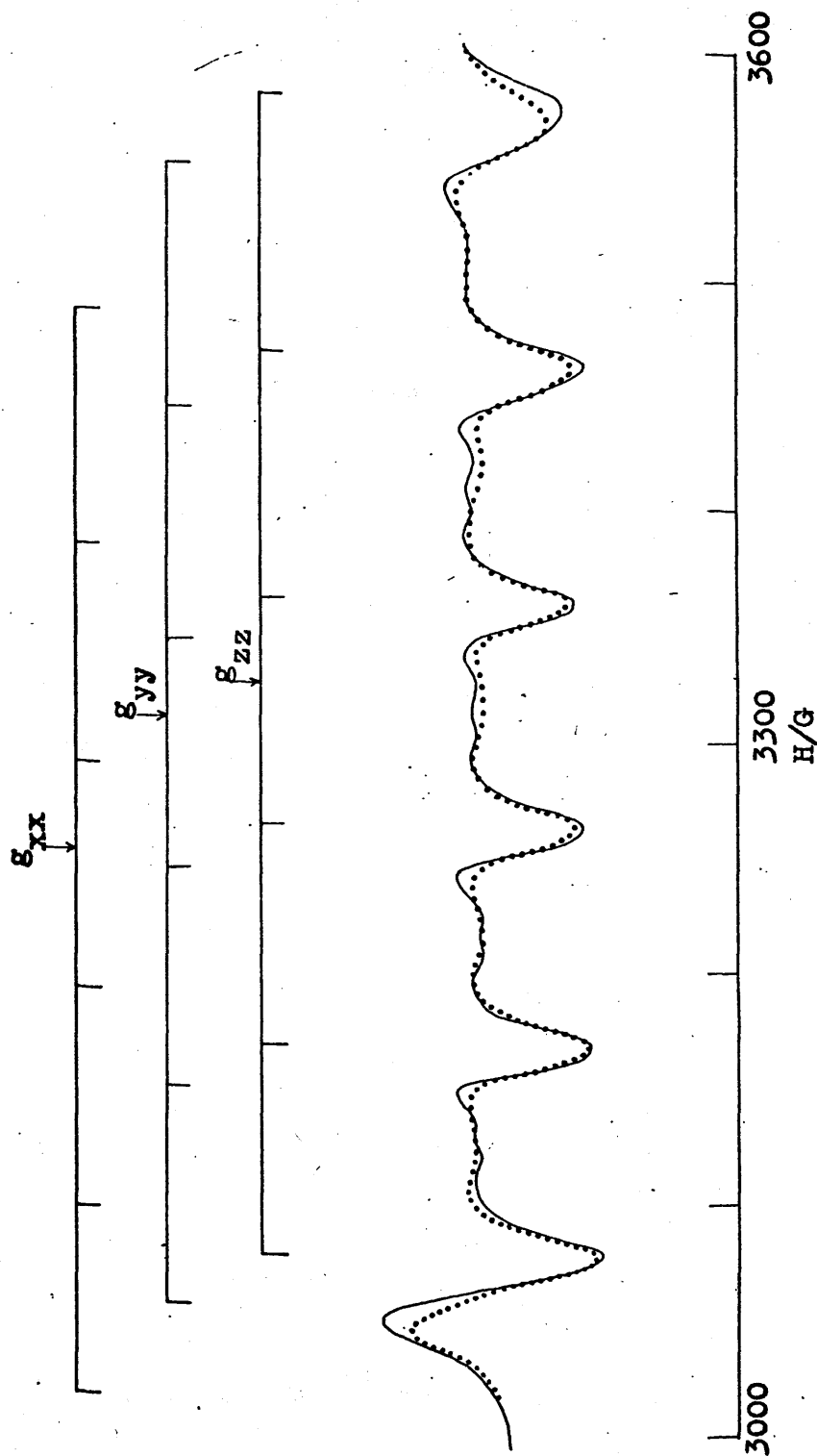


Figure 6.1. Observed (full line) and calculated (dotted line) e.p.r. spectra of magnetically dilute solution of MnO_2Cl_2 in CCl_4 at 77K.

The e.p.r. spectrum was analysed by fitting it to curves of the type ¹⁸ described in Appendix C.

$$S(H') = (2\pi)^{-\frac{1}{2}} \sum_{m_I = -5/2}^{+5/2} \int_{H = -\infty}^{+\infty} \beta^{-1} S_{m_I}(H) \exp \left[-(H' - H)^2 (2\beta^2)^{-1} \right] dH$$

..... 6.4

where $S_{m_I}(H)$ is a Kneubuhl function and β is an appropriate Gaussian broadening factor. Reasonable sets of values of H_x, H_y and H_z for each value of m_I can be taken directly from the experimental spectrum and iterative computational procedures then used to obtain the best match of the derivative of the calculated function $S(H')$ to the observed spectrum. When the resonant field values H_x, H_y and H_z obtained when the magnetic field lies along the principal x, y and z directions are known, then the principal g- and A-tensor components, and the ⁵⁵Mn nuclear quadrupole coupling parameter, Q' , can be obtained from the following relationships ^{17,19} which are derived from general equation B29 of Appendix B.

$$H_z = h\nu_0 (g_{zz} \beta_e)^{-1} - hc (g_{zz} \beta_e)^{-1} A_{zz} m_I -$$

$$hc^2 (4g_{zz} \beta_e \nu_0)^{-1} [A_{xx}^2 + A_{yy}^2] [I(I+1) - m_I^2] \dots\dots 6.5$$

$$H_x = h\nu_0 (g_{xx} \beta_e)^{-1} - hc (g_{xx} \beta_e)^{-1} A_{xx} m_I - hc^2 (4g_{xx} \beta_e \nu_0)^{-1} (A_{yy}^2 + A_{zz}^2) [I(I+1) - m_I^2] - hc (2g_{xx} \beta_e A_{xx})^{-1} Q'^2 [2I(I+1) - 2m_I^2 - 1] m_I$$

..... 6.6

where ν_0 is the frequency of the microwave radiation used in recording the e.p.r. spectrum, and A-tensor components are in units of cm^{-1} . H_y is obtained from 6.6 by interchanging subscripts x and y. The spin-Hamiltonian parameters obtained in this way are listed in Table 6.1 : analysis shows that the signs of A_{xx} , A_{yy} and A_{zz} must all be identical. A spectrum computed from 6.4 using these spin-Hamiltonian parameters is shown in Figure 6.1. Although we have not included them in the computed spectrum, weak formally forbidden transitions, $\Delta m_S = \pm 1$, $\Delta m_I = \pm 1$ and $\Delta m_S = \pm 1$, $\Delta m_I = \pm 2$, can be seen on the observed spectrum on Figure 6.1. Their positions and relative intensities are consistent with the parameters listed in Table 6.1. The large broadening parameter β , and the broad 30 gauss peak-peak lines observed in derivative spectra obtained from this compound at 295 K, both indicate that the unpaired electron interacts markedly with the chlorine nuclei, but we have not been able to resolve these spectra further.

One of the principal components of the g-tensor is larger than the spin-only value, a situation unusual in d^1 complexes. This, as will be explained later, is shown to be due to relatively large spin-orbit coupling at the chlorine atoms.

Table 6.1

Spin-Hamiltonian parameters for MnO_2Cl_2 . Data refer to solutions in CCl_4 at 77 K, except for g_0 and A_0 which are the isotropic g-factor and hyperfine coupling constant obtained from solution spectra at 298 K. All hyperfine tensor components are in units of cm^{-1} and β is in gauss. Limits of error in the principal components of g, A, and Q' are ± 0.002 , ± 0.0002 and $\pm 0.00005 cm^{-1}$ respectively.

	$\underline{g_{xx}}$	$\underline{g_{yy}}$	$\underline{g_{zz}}$	$\underline{A_{xx}}$	$\underline{A_{yy}}$	$\underline{A_{zz}}$	Q'	$\langle g \rangle$	$\langle A \rangle$	$\underline{g_0}$	$\underline{A_0}$	$\underline{\beta}$
MnO_2Cl_2 at 77K	2.031	1.999	1.989	-0.0088	-0.0092	-0.0094	± 0.00045	2.0066	-0.0092	2.0098	-0.0092	10
Rigid MnO_2Cl_2	2.031	-	-	-0.0088	-0.0052	-0.0138	-	2.0098	-0.0093	-	-	-

6.4 Extended Hückel molecular orbital calculation of MnO_2Cl_2

As was described in Part II, in order to use the spin-Hamiltonian parameters to obtain detailed information about the electronic distribution in the compound, estimates of the values of the spin-orbit coupling constant, ξ , and the parameter $P = 2.0023 g_N \beta_e \beta_N \langle \psi | r^{-3} | \psi \rangle$ for the manganese ion with the appropriate charge and configuration were needed. Since no estimates of the charge and configuration of the manganese ion was available, for compound of this type, an extended Hückel molecular orbital calculation was therefore carried out on the MnO_2Cl_2 .

The general procedure used in this calculation is similar to that for ReOCl_4 described in detail in Part II.

The molecular geometry was assumed to be as in CrO_2Cl_2 ²⁰. The Mn-O distances was taken to be 1.57Å and the Mn-Cl distances to be 2.12Å . The angles O-Mn-O, O-Mn-Cl and Cl-Mn-Cl were taken to be 105° , 109° and 113° respectively.

Using the coordinate system in Figure 6.2, molecular orbitals in this compound can be described in terms of basis orbitals derived from

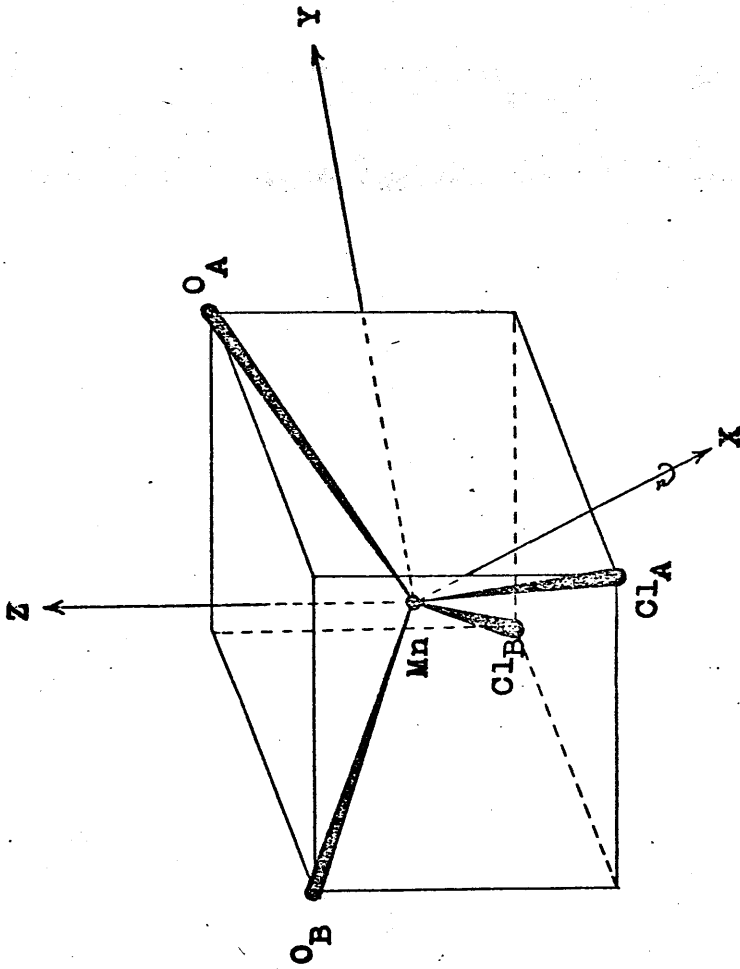


Figure 6.2. Coordinate system of MnO_2Cl_2

- i) the 3d, 4s and 4p orbitals of the manganese ion,
 ii) chloride ion 3s and 3p orbitals,
 iii) oxide ion 2s and 2p orbitals.

In the C_{2v} group these 25 basis orbitals can themselves be grouped as follows:

<u>Class</u>	<u>A₁</u>	<u>A₂</u>
Manganese ion orbitals	4s; 4p _z ; 3d _{z²} ; 3d _{x²-y²}	3d _{xy}
Chloride ion orbitals	3p _x (A ₁) = $\frac{1}{\sqrt{2}}(3p_{x_A} - 3p_{x_B})$ 3p _z (A ₁) = $\frac{1}{\sqrt{2}}(3p_{z_A} + 3p_{z_B})$ 3s(A ₁) = $\frac{1}{\sqrt{2}}(3s_A + 3s_B)$	3p _y (A ₂) = $\frac{1}{\sqrt{2}}(3p_{y_A} - 3p_{y_B})$
Oxide ion orbitals	2p _x (A ₁) = $\frac{1}{\sqrt{2}}(2p_{x_A} - 2p_{x_B})$ 2p _z (A ₁) = $\frac{1}{\sqrt{2}}(2p_{z_A} + 2p_{z_B})$ 2s(A ₁) = $\frac{1}{\sqrt{2}}(2s_A + 2s_B)$	2p _y (A ₂) = $\frac{1}{\sqrt{2}}(2p_{y_A} - 2p_{y_B})$
	<u>B₁</u>	<u>B₂</u>
Manganese ion orbitals	3d _{xz} ; 4p _x	3d _{yz} ; 4p _y
Chloride ion orbitals	3p _x (B ₁) = $\frac{1}{\sqrt{2}}(3p_{x_A} + 3p_{x_B})$ 3p _z (B ₁) = $\frac{1}{\sqrt{2}}(3p_{z_A} - 3p_{z_B})$ 3s(B ₁) = $\frac{1}{\sqrt{2}}(3s_A - 3s_B)$	3p _y (B ₂) = $\frac{1}{\sqrt{2}}(3p_{y_A} + 3p_{y_B})$
Oxide ion orbitals	2p _x (B ₁) = $\frac{1}{\sqrt{2}}(2p_{x_A} + 2p_{x_B})$ 2p _z (B ₁) = $\frac{1}{\sqrt{2}}(2p_{z_A} - 2p_{z_B})$ 2s(B ₁) = $\frac{1}{\sqrt{2}}(2s_A - 2s_B)$	2p _y (B ₂) = $\frac{1}{\sqrt{2}}(2p_{y_A} + 2p_{y_B})$

Slater-type atomic orbitals of the kind described by Cusachs et al. ^{21,22} were used to estimate overlap integrals S_{ij} between basis orbitals i and j . These are single exponents of the form $N r^{n-1} e^{-\xi r}$, where n is the principal quantum number and ξ is the orbital exponent. The chosen value ^{21,23,24} of ξ for various atoms are given below

Manganese	4s	$n = 4$	$\xi = 1.36$
	4p	$n = 4$	$\xi = 0.80$
	3d	$n = 3$	$\xi = 2.22$
Chlorine	3s	$n = 3$	$\xi = 2.20$
	3p	$n = 3$	$\xi = 1.82$
Oxygen	2s	$n = 2$	$\xi = 2.20$
	2p	$n = 2$	$\xi = 1.95$

The group overlap integrals obtained using these values are listed in Table 6.2. The coulomb integrals, H_{ii} were set equal to the valence state ionisation potentials of the appropriate basic atomic orbitals, ionisation potentials for Cl^- and O^{2-} orbitals being derived from data given in reference 25, and ionisation potentials for central metal-ion basis orbitals, corrected to take charge and configuration effects into account ²⁵, being obtained by the methods described in reference 25.

The resonance integrals, H_{ij} , were evaluated using the Wolfsberg-Helmholtz approximation ²⁶

$$H_{ij} = 0.85 (H_{ii} + H_{jj})S_{ij} \quad \dots 6.7$$

Table 6.2

Group overlap integrals for MnO₂Cl₂

	<u>3s [Cl]</u>	<u>3p_z [Cl]</u>	<u>3p_x [Cl]</u>	<u>2s [O]</u>	<u>2p_z [O]</u>	<u>2p_x [O]</u>
A₁ symmetry						
4s	0.453	0.209	-0.313	0.489	-0.107	0
4p _z	-0.331	0.220	0.139	0.255	0.163	0
3d _{x²-y²}	0.108	0.131	-0.079	-0.202	0.212	0
3d _{z²}	-0.007	0.089	0.070	0.019	-0.192	0
A₂ symmetry						
	<u>3p_y [Cl]</u>	<u>2p_y [O]</u>				
3d _{xy}	0.188	0				

Table 6.2 (contd.)

B₁ symmetry

	<u>3s [Cl]</u>	<u>3p_z [Cl]</u>	<u>3p_x [Cl]</u>	<u>2s [O]</u>	<u>2p_z [O]</u>	<u>2p_x [O]</u>
4p _x	0.497	0.139	0.103	0	0	0.197
3d _{xz}	-0.140	-0.053	0.180	0	0	0.166

B₂ symmetry

	<u>3p_y [Cl]</u>	<u>2p_y [O]</u>
4p _y	0.313	0.280
3d _{yz}	-0.078	-0.257

and the secular equations diagonalised using standard techniques. The computed atom charges and orbital populations were then used to estimate new H_{ii} values and the cycle of calculations then repeated until the input and output charge associated with each atom coincided.

The most important results of the molecular orbital calculations of MnO_2Cl_2 are listed below

1. The final estimated electronic configuration and charge at the manganese ion turned out to be $Mn (\dots\dots 3d^{5.821} \quad 4s^{0.357} \quad 4p^{0.336})$ and + 0.486 respectively. The overall charge distribution in units of the proton charge is

Atom	Mn	O	Cl
Charge	+0.486	-0.708	+0.465

The final eigenvalues and eigenfunctions are listed in Table 6.3 and the resultant energy level diagram is shown in Figure 6.3.

2. The unpaired electron is in the antibonding molecular orbital A_1 , numbered 17, in Figure 6.3 and starred in Table 6.3. This orbital is compounded out of the d_{z^2} , $d_{x^2-y^2}$ orbitals of manganese, $3p_z$ orbital of chlorine and $2p_z$ orbital of oxygen, and it is about 55% delocalised on to the chlorine atoms.

Table 6.3

Energy levels and atomic orbital coefficients in the LCAO molecular orbital description of MnO_2Cl_2 . The molecule is assumed to belong to the C_{2v} point group. Energies are in units of eV. The unpaired electron is in the starred A_1 orbital.

<u>A_1 symmetry</u>		<u>Atomic orbital coefficients</u>										
Orbital	Energy	4s	4p _z	$3d_{x^2-y^2}$	$3d_{z^2}$	3s[Cl]	3p _z [Cl]	3p _x [Cl]	3p _x [Cl]	2s [0]	2p _z [0]	2p _x [0]
1	-32.6	-0.085	0.0001	0.062	-0.007	0.012	0.007	-0.014	-0.014	-0.942	-0.013	0.000
3	-25.3	0.119	-0.027	0.074	-0.005	0.922	-0.008	0.021	0.021	-0.055	0.004	0.000
5	-14.9	0.053	0.076	0.356	-0.525	-0.081	0.036	-0.255	-0.255	0.061	0.537	0.000
9	-14.3	0.100	0.095	0.429	0.466	-0.104	0.624	-0.105	-0.105	0.021	-0.011	0.000
10	-13.1	-0.127	0.079	0.084	0.054	0.098	0.065	0.852	0.852	0.076	0.369	0.000
15	-12.6	0.000	0.000	0.000	0.000	0.000	0.000	0.000	0.000	0.000	0.000	1.000
17*	-11.2	0.039	-0.011	-0.381	-0.642	0.028	0.708	0.174	0.174	-0.104	-0.300	0.000
21	- 8.0	0.071	0.159	0.780	-0.375	-0.110	-0.300	0.278	0.278	0.126	-0.752	0.000
23	+ 1.7	0.033	1.147	-0.229	0.050	0.417	-0.280	-0.218	-0.218	-0.371	-0.130	0.000
25	+27.0	1.564	-0.117	-0.091	0.064	-0.806	-0.347	0.577	0.577	-0.808	0.256	0.000

<u>A_2 symmetry</u>		<u>Atomic orbital coefficients</u>		
Orbital	Energy	$3d_{xy}$	3p _y [Cl]	2p _y [0]
8	-14.5	0.711	0.581	0.000
16	-12.6	0.000	0.000	1.000
18	-10.9	0.728	-0.836	0.000

Table 6.3 (contd.)

B₁ symmetryAtomic orbital coefficients

<u>Orbital</u>	<u>Energy</u>	<u>4p_x</u>	<u>3d_{xz}</u>	<u>3s [Cl]</u>	<u>3p_z [Cl]</u>	<u>3p_x [Cl]</u>	<u>2s [O]</u>	<u>2p_z [O]</u>	<u>2p_x [O]</u>
2	-32.4	0.000	0.000	0.000	0.000	0.000	1.000	0.000	0.000
4	-25.1	0.039	-0.086	0.964	-0.005	0.001	0.000	0.000	-0.002
7	-14.7	0.091	-0.642	-0.104	0.122	-0.455	0.000	0.000	-0.377
11	-12.8	0.054	-0.008	-0.032	0.973	0.151	0.000	0.000	0.094
13	-12.7	0.029	0.033	-0.009	0.025	-0.680	0.000	0.000	0.728
14	-12.7	0.000	0.000	0.000	0.000	0.000	0.000	1.000	0.000
20	-9.5	0.055	0.801	0.139	0.153	-0.585	0.000	0.000	-0.579
24	+3.2	1.202	-0.117	-0.653	-0.213	-0.117	0.000	0.000	-0.258

B₂ symmetryAtomic orbital coefficients

<u>Orbital</u>	<u>Energy</u>	<u>4p_y</u>	<u>3d_{yz}</u>	<u>3p_y [Cl]</u>	<u>2p_y [O]</u>
6	-14.9	0.028	-0.682	0.184	0.531
12	-12.8	0.133	0.074	0.927	-0.271
19	-10.3	0.313	0.718	0.034	0.723
22	-2.3	1.057	-0.323	-0.487	-0.555

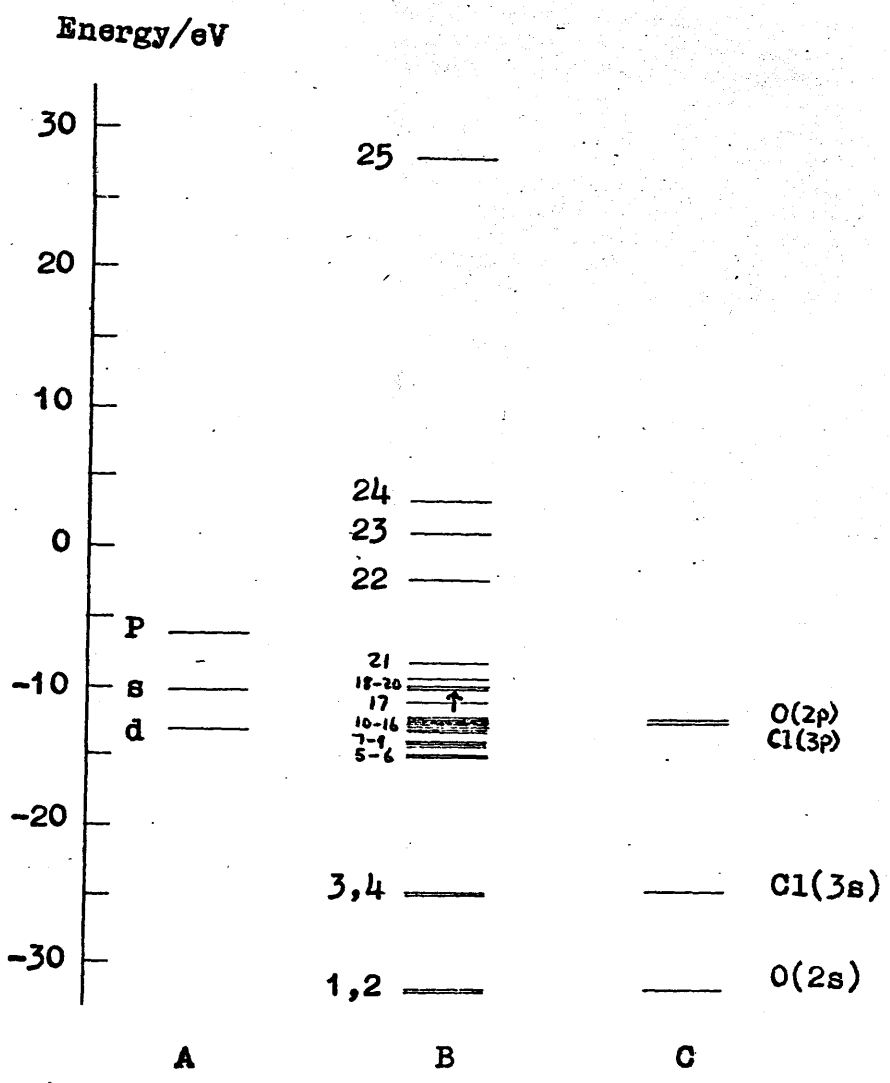


Figure 6.3. Molecular orbital energy-level diagram for MnO₂Cl₂: A, metal-ion orbitals; B, molecular orbitals; and C, ligand orbitals.

3. Knowing the ionic charge and the configuration of the manganese ion, the values of P and the spin-orbit coupling constant ξ , for manganese in MnO_2Cl_2 can now be estimated. The plot of the free ion values of the spin-orbit coupling constants ²⁷, for manganese ions, against the charges on the ions, shown in Figure 6.4 shows that for manganese ion with a charge of 0.486 and a configuration $3d^{6.518}$, $\xi = 212 \text{ cm}^{-1}$. For manganese (0) in a $3d^7$ configuration $\xi = 190 \text{ cm}^{-1}$; for manganese (0) in a $3d^5 4s^2$ configuration, $\xi = 295 \text{ cm}^{-1}$. Promoting of an electron from a $3d$ to a $4s$ orbital therefore increases ξ by 52 cm^{-1} and hence promoting 0.7 of an electron from $\text{Mn}^{+0.486} (3d^{6.518})$ to $\text{Mn}^{+0.486} (3d^{5.821} 4s^{0.357} 4p^{0.336})$ increases ξ by 36 cm^{-1} to 248 cm^{-1} . Figure 6.5 shows a plot of ξ against P for various ions ^{27,28} of manganese, from which it can be seen that the value of P corresponding to $\xi = 248 \text{ cm}^{-1}$ is 0.0172 cm^{-1} . Thus the values of ξ and P for manganese ion in MnO_2Cl_2 are

$$\begin{aligned}\xi &= 248 \text{ cm}^{-1} \\ P &= 0.0172 \text{ cm}^{-1}\end{aligned}$$

6.5 Equations relating the spin-Hamiltonian parameters to the molecular orbital coefficients in MnO_2Cl_2

As can be seen from the molecular orbital energy level diagram the unpaired electron is in the antibonding A_1 molecular orbital. The general form of the A_1 orbital

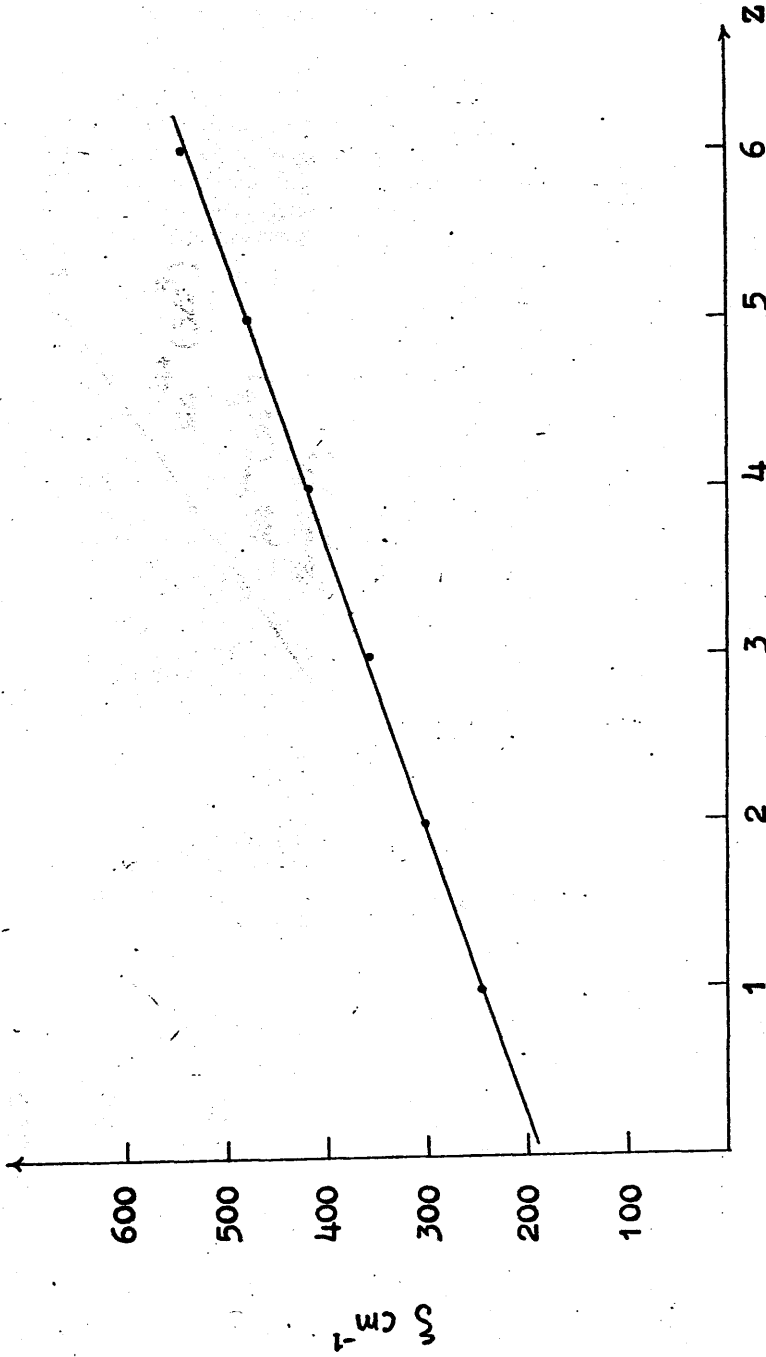


Figure 6.4. Spin-orbit coupling constant ζ for manganese ions as a function of ionic charge Z .

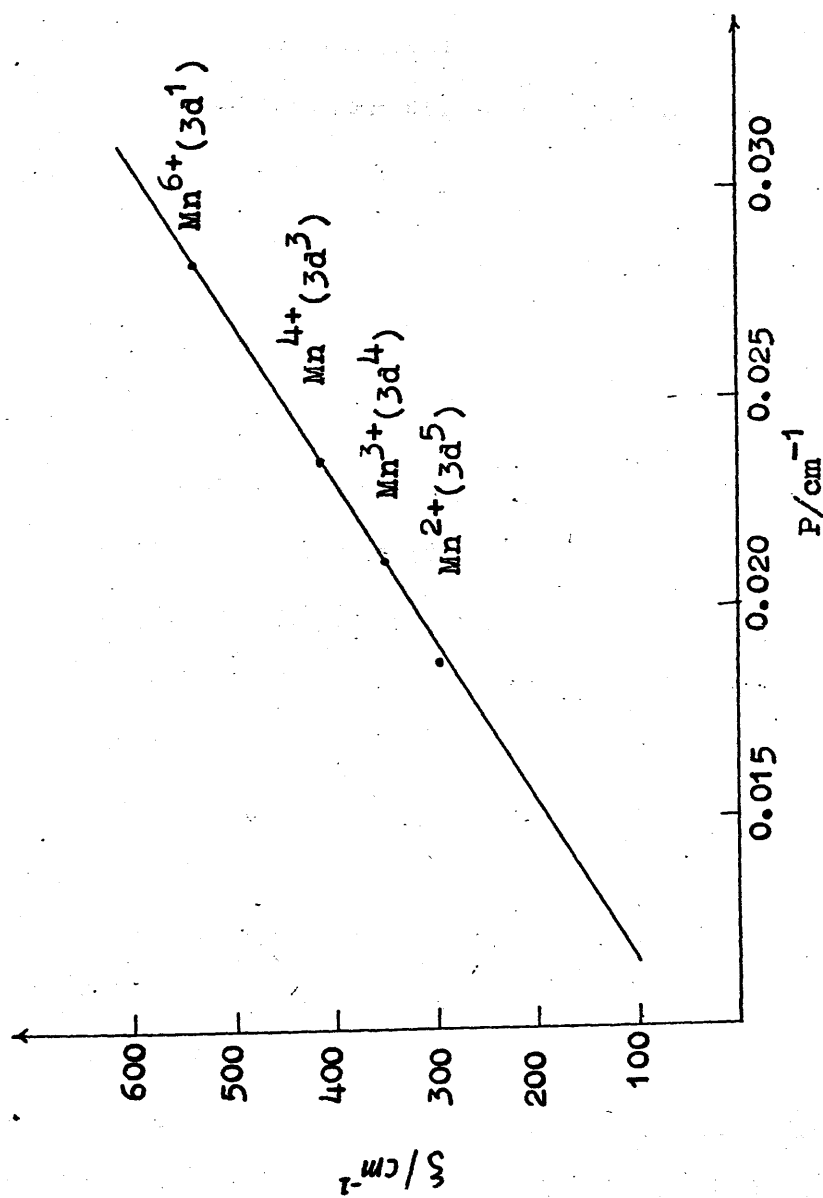


Figure 6.5. Spin-orbit coupling constant ζ for various manganese ion configurations as a function of P .

consists of a linear combination of the ten basis orbitals which belong to this representation, but in fact our molecular orbital calculations show that in this particular compound only contributions from the metal ion $d_{x^2-y^2}$ and d_{z^2} orbitals and from the chloride ion $3p_z$ and the oxide ion $2p_z$ orbitals are important. If the spin-orbit coupling is ignored then this molecular orbital has the form

$$\Psi(A_1) = \alpha_1^* (a d_{x^2-y^2} + b d_{z^2}) + \alpha_1^{*(1)} 3p_z(A_1) + \alpha_1^{*(11)} 2p_z(A_1) \dots 6.8$$

It can be shown that spin-orbit coupling at the central metal ion and at the chloride ions causes considerable mixing of two kinds of excited state into the ground state of this molecule: these excited states are produced either by promoting the unpaired electron into the empty antibonding orbitals of B_1 , B_2 or A_2 symmetry which lie immediately above $\Psi^*(A_1)$ in Figure 6.3, or by promoting an electron into this $\Psi^*(A_1)$ orbital from the filled bonding orbitals of B_1 , B_2 or A_2 symmetry lying immediately below $\Psi^*(A_1)$. Furthermore, only mixing of the molecular orbitals listed in Table 6.3 as 11, 12, 13, 16, 18, 19 and 20 need be considered in this context. Wave functions for these orbitals may be written in the following form

$$\Psi(B_1) = \beta_1 d_{xz} + \beta_1^{(I)} 4p_x + \beta_1^{(II)} 3p_z(B_1) + \beta_1^{(III)} 3p_x(B_1) \\ + \beta_1^{(IV)} 2p_z(B_1) + \beta_1^{(V)} 2p_x(B_1)$$

$$\Psi(B_2) = \beta_2 d_{xy} + \beta_2^{(I)} 4p_y + \beta_2^{(II)} 3p_y(B_2) + \beta_2^{(III)} 2p_y(B_2)$$

$$\Psi(A_2) = \gamma d_{xy} + \gamma^{(I)} 3p_y(A_2) + \gamma^{(II)} 2p_y(A_2)$$

..... 6.9

If the matrix elements of the spin-orbit coupling at the manganese and chloride ions, plus the true Zeeman and hyperfine interactions are now equated to the corresponding matrix elements of the spin-Hamiltonian as described in Appendix A then the following relationships for the principal components of the g- and A-tensors may be deduced from standard perturbation theory ²⁹.

$$g_{xx} = 2.0023 \pm \sum \frac{2\xi_{Mn}}{|\Delta E(B_2)|} \left[(a+b\sqrt{3}) \alpha_1^* \beta_2 + \alpha_1^{*(I)} \beta_2^{(II)} V_{Cl} \right] \left[(a+b\sqrt{3}) \alpha_1^* \beta_2 + \alpha_1^{*(I)} \beta_2^{(II)} \right]$$

..... 6.10

Where molecular orbitals 12 and 19 contribute to the sum and the positive sign refers to orbital 12, and the negative sign to orbital 19: $V_{Cl} = (\xi_{Cl}/\xi_{Mn})$.

$$g_{yy} = 2.0023 \pm \sum \frac{2\xi_{Mn}}{|\Delta E(B_1)|} \left[(a-b\sqrt{3}) \alpha_1^* \beta_1 - \alpha_1^{*(I)} \beta_1^{(III)} V_{Cl} \right] \left[(a-b\sqrt{3}) \alpha_1^* \beta_1 - \alpha_1^{*(I)} \beta_1^{(III)} \right]$$

..... 6.11

Where molecular orbitals 11, 13 and 20 contribute to the sum, the positive sign referring to orbitals 11 and 13, and the negative sign to orbital 20.

$$g_{zz} = 2.0023 - 8a^2 (\alpha_1^*)^2 \xi_{Mn} \left[\frac{P_{md}(A_2)}{|\Delta E(A_2^*)|} - \frac{P_{md}(A_2)}{|\Delta E(A_2)|} \right] \dots\dots 6.12$$

where the first term in the bracket is contributed by orbital 18, and the second by orbital 16. $P_{md}(A_2)$ is the metal-ion d orbital population in $\Psi(A_2)$, and ξ_{Mn} , ξ_{Cl} are the spin-orbit coupling constants of manganese and chloride ions. The hyperfine tensor components are given by

$$A_{xx} = P \left[-K + \frac{2}{7} (a^2 - b^2) (\alpha_1^*)^2 - \frac{4\sqrt{3}}{7} (ab) (\alpha_1^*)^2 + (g_{xx} - 2.0023) + \frac{1}{14} \frac{(3a + b\sqrt{3})}{(a - b\sqrt{3})} (2.0023 - g_{yy}) - \frac{1}{7} \frac{b}{a} (2.0023 - g_{zz}) \right] \dots\dots 6.13$$

$$A_{yy} = P \left[-K + \frac{2}{7} (a^2 - b^2) (\alpha_1^*)^2 + \frac{4\sqrt{3}}{7} (ab) (\alpha_1^*)^2 + (g_{yy} - 2.0023) + \frac{1}{14} \frac{(3a - b\sqrt{3})}{(a + b\sqrt{3})} (2.0023 - g_{xx}) + \frac{1}{7} \frac{b}{a} (2.0023 - g_{zz}) \right] \dots\dots 6.14$$

$$A_{zz} = P \left[-K - \frac{4}{7} (a^2 - b^2) (\alpha_1^*)^2 - \frac{1}{14} \frac{(3a + b\sqrt{3})}{(a - b\sqrt{3})} (2.0023 - g_{yy}) - \frac{1}{14} \frac{(3a - b\sqrt{3})}{(a + b\sqrt{3})} (2.0023 - g_{xx}) + (g_{zz} - 2.0023) \right] \dots\dots 6.15$$

$$\langle A \rangle = -PK - [2.0023 - \langle g \rangle] P \dots\dots 6.16$$

Where $\langle g \rangle = \frac{1}{3} (g_{xx} + g_{yy} + g_{zz})$ and $\langle A \rangle = \frac{1}{3} (A_{xx} + A_{yy} + A_{zz})$ \dots\dots 6.17

- PK is the isotropic contribution to the hyperfine coupling arising from the Fermi contact interaction.

6.6 Molecular orbital coefficients and bonding in MnO_2Cl_2

It follows immediately from equation 6.12 that the value of g_{zz} for d^1 complexes of this type must always be less than 2.0023 and this, combined with the unexpectedly large g -tensor component of 2.031 obtained in analysing the 77 K spectrum, forces us to assign the magnitudes of the principal tensor components to the principal directions shown in Table 6.1.

The isotropic hyperfine coupling constant A_0 observed in the 298 K e.p.r. spectrum of MnO_2Cl_2 shows that the manganese ion orbitals contribute appreciably to the molecular orbital $\Psi^*(A_1)$ which contains the unpaired electron. Equations 6.13 - 6.15 show that the principal values of the manganese hyperfine interaction tensor in the rigid molecule can never be identical, and therefore the value of A_{xx} , A_{yy} , and A_{zz} obtained by analysing the 77 K e.p.r. spectrum, and listed in Tables 6.1, must be those appropriate to the molecule undergoing rotation about its X-axis. The magnitudes of the ^{55}Mn isotropic hyperfine coupling constant, A_0 , and of the hyperfine tensor components A_{xx} and $(A_{yy}+A_{zz})$ in MnO_2Cl_2 are proportional to the hyperfine tensor components for MnO_4^{2-} doped into BaSO_4 ¹⁵. Hence the principal values of the manganese hyperfine interaction

tensor for rigid MnO_2Cl_2 are those listed in the second row of Table 6.1 and the frequency of the motion which averages the spin-Hamiltonian parameters g_{yy} and g_{zz} , A_{yy} and A_{zz} , at 77 K must be greater than 250×10^6 Hz.

Values of K and of the coefficients of $d_{x^2-y^2}$, d_{z^2} metal orbitals a and b respectively, and α_1^* which indicate the degree of delocalisation of the unpaired electron in this compound, involved in the molecular orbital $\Psi^*(A_1)$ estimated from equation 6.13 - 6.17 are

K	a	b	α_1^*
0.527	0.96	0.28	0.67

The relative signs of the coefficients a and b cannot be determined directly from the paramagnetic resonance data but Hückel calculations show that a and b are both negative. In MnO_2Cl_2 the unpaired electron lies essentially in the metal-ion $3d_{x^2-y^2}$ orbital, mixed with a small amount (8%) of the $3d_{z^2}$ orbital, and it is strongly (55%) delocalised on to the ligands. Since we have not been able to resolve chlorine hyperfine splitting in the e.p.r. spectrum we cannot evaluate the coefficients $\alpha_1^{*(1)}$ and $\alpha_1^{*(11)}$ in 6.8 from our magnetic resonance data. The magnetic resonance data show that the molecular orbital model described in 6.4 overestimates the $3d_{z^2}$ contribution to $\Psi^*(A_1)$ and underestimates the $3d_{x^2-y^2}$ contribution.

Charge-transfer transitions make important contributions to the g-tensor components in this compound and result in too many variables in equations 6.10 - 6.12 to enable them to be used to obtain unique solutions for the coefficients in the molecular orbitals 6.9. However, use of the magnetic resonance estimates of a, b, and and the Hückel-calculation estimates of the other coefficients involved in 6.10 - 6.12 results in estimates of the principal g-tensor components of $g_{xx} = 2.01$, $g_{yy} = 2.01$, and $g_{zz} = 1.98$ for the rigid molecule. The values of g_{xx} g_{yy} are unusually large for a d^1 complex as a result of charge-transfer mixing caused by the relatively large spin-orbit interactions at the chlorine atoms. The g-tensor components can only be rationalised by labelling the principal axes directions as in Table 6.1 and by placing the unpaired electron in a molecular orbital derived from the manganese $3d_{x^2-y^2}$ orbital. The molecular orbital calculations show that if the unpaired electron is in a molecular orbital derived from the manganese $3d_{z^2}$ orbital then the principal values of the g-tensor in this compound can never be greater than the spin-only value. Similar reasoning may provide a quick method of identifying the metal-ion orbital involved in other tetrahedral d^1 complexes when there are relatively large spin-orbit interactions at the ligands, and hence may provide a method of distinguishing those complexes where the tetrahedron is distorted by extension along the z-axis, from others in which it is compressed in this direction.

Thus the molecular orbital and magnetic resonance results correspond in that the unpaired electron lies in an orbital of A_1 symmetry and is strongly delocalised on to the ligands. They also essentially agree on the total contribution of the metal ion to this orbital but the molecular orbital calculation overestimates the contribution of the $3d_z^2$ basis orbital and underestimates the contribution of the $3d_{x^2-y^2}$ basis orbital. It therefore appears that there are significant differences in the structures CrO_2Cl_2 and MnO_2Cl_2 , the ligands in the latter being closer to the molecular z-axis.

6.7 Summary of Part VI

X-Band e.p.r. spectra of magnetically dilute solutions of MnO_2Cl_2 in CCl_4 have been recorded at 77 K and 298 K and are analysed in detail. The spin-orbit coupling constant, ζ_{Mn} and the parameter P for the manganese ion in this compound are estimated to be 248 and 0.0172 cm^{-1} respectively. At 77 K, MnO_2Cl_2 rotates about its x-axis in CCl_4 solution. Spin-Hamiltonian parameters are listed for 298 K, for 77 K, and for the rigid molecule, and are equated to the atomic orbital coefficients in the molecular orbitals involved in bonding in this molecule. The unpaired electron lies in the metal ion $3d_{x^2-y^2}$ orbital mixed with a small amount (8%) of the $3d_{z^2}$ orbital, and it is strongly (55%) delocalised on to the ligands. One of the principal components of the g-tensor, g_{xx} , is larger than the spin-only value, a situation unusual in d^1 complexes. This is shown to be due to relatively large spin-orbit coupling at the chlorine atoms. It is pointed out that principal values of the g-tensor may be used to distinguish distorted tetrahedral complexes which are stretched along their z-axis from the corresponding complexes compressed in this direction, provided that spin-orbit interactions at the ligands are relatively large.

References to Part VI

1. G.F. Kokoszka, H.C.Allen Jun. and G. Gordon,
Inorg.Chem., 1966, 5, 91.
2. D.W. Pratt, Nuclear Science Abstracts, 1967, 21,34254.
3. C.E.Halloway, F.E.Mabbs and W.R.Smail, J.Chem.Soc. (A),
1968, 2980.
4. D.C.Bradley, R.H.Moss and K.D.Sales, Chem.Commun.,1969,
1255.
5. E.C.Alyes and D.C.Bradley, J.Chem.Soc.(A),1969,2330.
6. D.P.Bakalik and R.G.Hayes, Inorg.Chem.,1972,11,1734.
7. C.P.Stewart and A.L.Porte, J.Chem.Soc.,Dalton,1973,722.
8. J.L.Peterson and L.F.Dahl,J.Am.Chem.Soc.,1973,96,2248.
9. R.S.Title and M.W.Shafer,Phys.Rev.Letters,1972,28,808.
10. D.C.Bradley and M.H.Chisholm,J.Chem.Soc.(A),1971,1511.
11. A.Carrington,D.J.E.Ingram,D.Schonland and M.C.R.Symons,
J.Chem.Soc.,1956, 4710.
12. R.L.Copper and M.L.H.Green, J.Chem.Soc.(A),1967,1155.
13. A.Carrington, D.J.E.Ingram, K.A.K.Lott, D.S.Schonland
and M.C.R.Symons,Proc.Roy.Soc.,1959,A,254.
14. D.S.Schonland, Proc.Roy.Soc.,1959, A,254,111.
15. C.A.Kosky, B.R.McGarvey and S.L.Holt, J.Chem.Phys.,
1972, 56, 5904.
16. T.S.Briggs, J.Inorg.Nuclear Chem.,1968,30,2866.
17. A.Abragam and M.H.L.Pryce, Proc.Roy.Soc.,1951,A,205,135
18. F.K.Kneubühl, J.Chem.Phys.,1960,33,1074.
19. R.M.Golding, "Applied Wave Mechanics", Van Nostrand,
New York, 1969, 452.

20. K.J. Palmer, J. Am. Chem. Soc., 1938, 60, 2360.
21. L.C. Cusachs, B.L. Trus., D.G. Carroll and S.P. McGlynn, Internat. J. Quantum Chemistry, 1967, 1, 423.
22. L.C. Cusachs and J.H. Carrington, "Sigma Molecular Orbital Theory", eds. O. Sinanoglu and K.W. Wiberg, Yale University Press, Newhaven, 1970, 256.
23. E. Clementi, "Tables of Atomic Functions", I.B.M. Corporation Development Lab. Reports, 1965; I.B.M. J. Res. Dev., 1965, 9, 22.
24. F.A. Cotton and C.B. Harris, Inorg. Chem., 1967, 6, 924.
25. C.J. Ballhausen and H.B. Gray, "Molecular Orbital Theory", Benjamin, New York, 1965, 120.
26. M. Wolfsberg and L. Helmholz, J. Chem. Phys., 1952, 20, 837.
27. T.M. Dunn, Trans. Faraday Soc., 1961, 57, 1441.
28. B.R. McGarvey, J. Phys. Chem., 1967, 71, 51.
29. B.R. McGarvey, "Transition Metal Chemistry", ed. R.L. Carlin, Arnold, London, 1966, 3, 89 and references therein.

APPENDIX ATHE SPIN HAMILTONIAN

The spin-Hamiltonian is an artificial concept, since the true Hamiltonian should contain orbital angular momentum operators as well as spin operators. The advantage of the spin-Hamiltonian, which was first introduced by Abragam and Pryce¹, is that a complete description of the experimental data can be presented. For the systems discussed in this work, the form of the spin-Hamiltonian can be developed as follows:

(a) The Zeeman Interaction^{2,3}

Kramers' theorem⁴ states that a purely electrostatic field acting on a system with an odd number of electrons, can never reduce the degeneracy below two. Therefore the ground state of a molecule with one unpaired electron is a spin doublet.

Let the ground state wavefunction in the absence of spin-orbit coupling ϕ_0^α and ϕ_0^β be real wavefunctions with no orbital magnetic moment. Spin-orbit coupling causes considerable mixing of the characters of excited states ϕ_n^α and ϕ_n^β in the ground state wavefunctions, and it leads to a reintroduction of a certain amount of orbital paramagnetism. The spin-orbit coupling Hamiltonian has the form

$$\mathcal{H}_{LS} = \xi \underline{L} \cdot \underline{S} = \xi (L_z S_z + L_x S_x + L_y S_y) \quad \dots \quad A1$$

where ξ is the spin-orbit coupling constant. The new ground states wavefunctions, which are still degenerate, may be determined by first-order perturbation theory.

$$|+\rangle = |\phi_0\alpha\rangle - \frac{1}{2}\xi \sum_n \frac{\langle\phi_n|L_z|\phi_0\rangle}{E_n - E_0} |\phi_n\alpha\rangle - \frac{1}{2}\xi \sum_n \frac{\langle\phi_n|L_x + iL_y|\phi_0\rangle}{E_n - E_0} |\phi_n\beta\rangle$$

$$|-\rangle = |\phi_0\beta\rangle + \frac{1}{2}\xi \sum_n \frac{\langle\phi_n|L_z|\phi_0\rangle}{E_n - E_0} |\phi_n\beta\rangle - \frac{1}{2}\xi \sum_n \frac{\langle\phi_n|L_x - iL_y|\phi_0\rangle}{E_n - E_0} |\phi_n\alpha\rangle$$

..... A2

A magnetic field will, however, resolve this degeneracy, and the true form of the Zeeman Hamiltonian is

$$\mathcal{H}_Z = \beta_e \underline{H} \cdot (g_e \underline{S} + \underline{L})$$

$$= \beta_e H_z (g_e S_z + L_z) + \beta_e H_y (g_e S_y + L_y) + \beta_e H_x (g_e S_x + L_x)$$

..... A3

where g_e is the g value for the free electron and is equal to 2.00232.

This Hamiltonian has the following matrix elements:

$$\langle+|\mathcal{H}_Z|+\rangle = \beta_e [\langle+|g_e S_z + L_z|+\rangle H_z + \langle+|g_e S_y + L_y|+\rangle H_y + \langle+|g_e S_x + L_x|+\rangle H_x]$$

$$\langle+|\mathcal{H}_Z|-\rangle = \beta_e [\langle+|g_e S_z + L_z|-\rangle H_z + \langle+|g_e S_y + L_y|-\rangle H_y + \langle+|g_e S_x + L_x|-\rangle H_x]$$

$$\langle-|\mathcal{H}_Z|+\rangle = \beta_e [\langle-|g_e S_z + L_z|+\rangle H_z + \langle-|g_e S_y + L_y|+\rangle H_y + \langle-|g_e S_x + L_x|+\rangle H_x]$$

$$\langle-|\mathcal{H}_Z|-\rangle = \beta_e [\langle-|g_e S_z + L_z|-\rangle H_z + \langle-|g_e S_y + L_y|-\rangle H_y + \langle-|g_e S_x + L_x|-\rangle H_x]$$

.... A4

By evaluation and comparison of these matrix elements and by using the Hermitean property of angular momentum operators, the following substitutions can be made

$$\langle + | g_e S_j + L_j | + \rangle = - \langle - | g_e S_j + L_j | - \rangle = \frac{1}{2} g_{jz}$$

$$\langle - | g_e S_j + L_j | + \rangle = \langle + | g_e S_j + L_j | - \rangle^* = \frac{1}{2}(g_{jx} + i g_{jy})$$

..... A5

These substitutions are made from knowing that diagonal matrix elements represent the expectation value of the real variable and so must be real, while the off-diagonal matrix elements may be imaginary.

The matrix elements of the Hamiltonian thus become

$$\langle + | \mathcal{H}_z | + \rangle = \frac{1}{2} g_{zz} \beta_e H_z + \frac{1}{2} g_{yz} \beta_e H_y + \frac{1}{2} g_{xz} \beta_e H_x$$

$$\langle + | \mathcal{H}_z | - \rangle = \frac{1}{2} (g_{zx} - i g_{zy}) \beta_e H_z + \frac{1}{2} (g_{yx} - i g_{yy}) \beta_e H_y + \frac{1}{2} (g_{xx} - i g_{xy}) \beta_e H_x$$

$$\langle - | \mathcal{H}_z | + \rangle = \frac{1}{2} (g_{zx} + i g_{zy}) \beta_e H_z + \frac{1}{2} (g_{yx} + i g_{yy}) \beta_e H_y + \frac{1}{2} (g_{xx} + i g_{xy}) \beta_e H_x$$

$$\langle - | \mathcal{H}_z | - \rangle = -\frac{1}{2} g_{zz} \beta_e H_z - \frac{1}{2} g_{yz} \beta_e H_y - \frac{1}{2} g_{xz} \beta_e H_x \quad \dots A6$$

The matrix elements are exactly the same as those which would be obtained by defining a fictitious spin operator S which would act on the states $| + \rangle$ and $| - \rangle$ in the same way as the true spin operator acts on the α and β states, and by using a Hamiltonian of the form

$$\mathcal{H} = \beta_e \underline{H} \cdot g \cdot \underline{S} \quad \dots A7$$

where g is a second rank tensor.

Expressions for the Zeeman energy of the system thus can be obtained by considering first the starting states to be pure spin states and by using a Hamiltonian containing only spin operators, hence the spin Hamiltonian.

In general it is possible to obtain expressions for the g-tensor by comparing the elements of the spin-Hamiltonian with those of the true Hamiltonian.

$$g_{ij} = g_e \delta_{ij} - 2 \sum_n \frac{\langle \phi_0 | L_i | \phi_n \rangle \langle \phi_n | L_j | \phi_0 \rangle}{E_n - E_0}$$

.... A8

where $g_{ij} = g_{ji}$ from the Hermitean properties of the angular momentum operators, i.e. the g-tensor is symmetric.

(b) The Hyperfine Interaction²

The magnetic hyperfine interactions, as noted earlier, arise in three quite distinct ways.

1. The Fermi contact interaction which is given by the Hamiltonian

$$\mathcal{H}_{\text{contact}} = \frac{8\pi}{3} g_e g_N \beta_e \beta_N \delta(r) \underline{I} \cdot \underline{S} \quad \dots \quad \text{A9}$$

2. The spin-dipolar interaction between the magnetic moments of the electron and the nucleus which is represented by the Hamiltonian

$$\mathcal{H}_{\text{SI}} = - g_e g_N \beta_e \beta_N \left[r^2 \underline{S} \cdot \underline{I} - 3 (\underline{S} \cdot \underline{r})(\underline{r} \cdot \underline{I}) \right] r^{-5}$$

.... A10

This Hamiltonian can be expanded to give

$$\begin{aligned} \mathcal{H}_{SI} = r^{-3} P' & [S_z I_z (3 \cos^2 \theta - 1) + S_x I_x (3 \sin^2 \theta \cos^2 \phi - 1) + \\ & S_y I_y (3 \sin^2 \theta \sin^2 \phi - 1) + 3 S_x I_y \sin^2 \theta \\ & x \sin \phi \cos \phi + 3 I_z S_x \cos \theta \sin \theta \cos \phi + \\ & 3 S_y I_x \sin^2 \theta \sin \phi \cos \phi + 3 S_z I_x \sin \theta \cos \theta \cos \phi \\ & + 3 S_y I_z \sin \theta \cos \theta \sin \phi + 3 S_z I_y \sin \theta \cos \theta \sin \phi] \end{aligned}$$

$$P' = 2.0023 \quad g_N \quad \beta_e \quad \beta_N \quad \dots \quad A11$$

where θ and ϕ are polar coordinate for the electron referred to the nucleus at $[0, 0, 0]$.

3. The orbital-dipolar interaction between the magnetic moment of the nucleus and the electron's orbital moment which is given by the Hamiltonian

$$\mathcal{H}_{LI} = 2 \quad g_N \quad \beta_e \quad \beta_N \quad r^{-3} \quad \underline{L} \cdot \underline{I} \quad \dots \quad A12$$

All these interactions can be combined to give, for the total hyperfine energy, the form

$$\mathcal{H} = A_x I_x + A_y I_y + A_z I_z$$

..... A13

where

$$A_x = r^{-3} p' \left[\frac{8\pi}{3} \delta(r) r^3 S_x + (3 \cos^2 \phi \sin^2 \theta - 1) S_x + \right. \\ \left. 3 \sin^2 \theta \sin \phi \cos \phi S_y + 3 \sin \theta \cos \theta \cos \phi S_{z+L_x} \right]$$

$$A_y = r^{-3} p' \left[\frac{8\pi}{3} \delta(r) r^3 S_y + (3 \cos^2 \theta \sin^2 \phi - 1) S_y + \right. \\ \left. 3 \sin^2 \theta \sin \phi \cos \phi S_x + 3 \sin \theta \cos \theta \sin \phi S_{z+L_y} \right]$$

.... A14

$$A_z = r^{-3} p' \left[\frac{8\pi}{3} \delta(r) r^3 S_z + (3 \cos^2 \theta - 1) S_z + 3 \cos \theta \sin \theta \right. \\ \left. \cos \phi S_x + 3 \sin \theta \cos \theta \sin \phi S_y + L_z \right]$$

Since the Hamiltonian now contains nuclear spin operators, the basic functions are now of the form $|+, m_I\rangle$ and $|-, m_I\rangle$. The matrix elements thus have the form

$$\langle +, m_I | \mathcal{H} | +, m_I' \rangle = \langle +, m_I | A_x I_x | +, m_I' \rangle + \langle +, m_I | A_y I_y | +, m_I' \rangle + \langle +, m_I | A_z I_z | +, m_I' \rangle$$

$$\langle +, m_I | \mathcal{H} | -, m_I' \rangle = \langle +, m_I | A_x I_x | -, m_I' \rangle + \langle +, m_I | A_y I_y | -, m_I' \rangle + \langle +, m_I | A_z I_z | -, m_I' \rangle$$

$$\langle -, m_I | \mathcal{H} | +, m_I' \rangle = \langle -, m_I | A_x I_x | +, m_I' \rangle + \langle -, m_I | A_y I_y | +, m_I' \rangle + \langle -, m_I | A_z I_z | +, m_I' \rangle$$

$$\langle -, m_I | \mathcal{H} | -, m_I' \rangle = \langle -, m_I | A_x I_x | -, m_I' \rangle + \langle -, m_I | A_y I_y | -, m_I' \rangle + \langle -, m_I | A_z I_z | -, m_I' \rangle$$

..... A15

By using similar substitutions to those in equation A5

$$\langle +, m_I | A_j I_j | +, m_I' \rangle = - \langle -, m_I | A_j I_j | -, m_I' \rangle = \frac{1}{2} A_{jz} \langle m_I | I_j | m_I' \rangle$$

..... A16

$$\langle -, m_I | A_j I_j | +, m_I' \rangle = \langle +, m_I | A_j I_j | -, m_I' \rangle^* = \frac{1}{2} (A_{jx} + i A_{jy}) \langle m_I | I_j | m_I' \rangle$$

The matrix elements of the Hamiltonian now becomes

$$\langle +, m_I | \mathcal{H} | +, m_I' \rangle = \frac{1}{2} A_{xz} \langle m_I | I_x | m_I' \rangle + \frac{1}{2} A_{yz} \langle m_I | I_y | m_I' \rangle + \frac{1}{2} A_{zz} \langle m_I | I_z | m_I' \rangle$$

$$\begin{aligned} \langle +, m_I | \mathcal{H} | -, m_I' \rangle &= \frac{1}{2} (A_{xx} - i A_{xy}) \langle m_I | I_x | m_I' \rangle + \frac{1}{2} (A_{yx} - i A_{yy}) \langle m_I | I_y | m_I' \rangle \\ &\quad + \frac{1}{2} (A_{zx} - i A_{zy}) \langle m_I | I_z | m_I' \rangle \end{aligned}$$

$$\langle -, m_I | \mathcal{H} | +, m_I' \rangle = \frac{1}{2} (A_{xx} + i A_{xy}) \langle m_I | I_x | m_I' \rangle + \frac{1}{2} (A_{yx} + i A_{yy})$$

$$\langle m_I | I_y | m_I' \rangle + \frac{1}{2} (A_{zx} + i A_{zy}) \langle m_I | I_z | m_I' \rangle$$

$$\langle -, m_I | \mathcal{H} | -, m_I' \rangle = -\frac{1}{2} A_{xz} \langle m_I | I_x | m_I' \rangle - \frac{1}{2} A_{yz} \langle m_I | I_y | m_I' \rangle - \frac{1}{2} A_{zz} \langle m_I | I_z | m_I' \rangle$$

..... A17

We can obtain as before exactly the same matrix elements by using the fictitious spin operator S , and a spin-Hamiltonian of the form

$$\mathcal{H} = \underline{S} \cdot \underline{A} \cdot \underline{I} \quad \text{..... A18}$$

where A is a second rank tensor.

(c) The Quadrupole Interaction ^{5,6}

The Hamiltonian representing the energy of quadrupole interaction may be written as

$$\mathcal{H}_Q = \frac{e Q}{6 I(2I-1)} \sum_{ij} V_{ij} \left[\frac{3}{2} (I_i I_j + I_j I_i) - \delta_{ij} I^2 \right] \quad \dots A19$$

where $e Q$ is the nuclear quadrupole moment and the V_{ij} are the components of the field gradient tensor,

$$V_{xx} = \frac{\partial^2 V}{\partial x^2}, \quad V_{xy} = \frac{\partial^2 V}{\partial x \partial y}, \quad \text{etc.}$$

This can be expressed more compactly as a tensor coupling of the nuclear spin with itself,

$$\mathcal{H}_Q = \underline{I} \cdot \underline{P} \cdot \underline{I} \quad \dots A20$$

where \underline{P} is the quadrupole coupling tensor, whose components are of the form

$$P_{ij} = \frac{e Q V_{ij}}{2I(2I-1)} \quad \dots A21$$

The field gradient obeys Laplace's equation, so the field gradient tensor is traceless,

$$\sum_i V_{ii} = 0$$

and it follows that the quadrupole coupling tensor is traceless

$$\sum_i P_{ii} = 0$$

i.e. \underline{P} is a symmetric tensor.

If \mathcal{H}_Q is written in its diagonal form, and the following substitutions are made

$$V_{zz} = q \quad V_{xx} = -\frac{1}{2} q (1 - \gamma) \quad \dots \quad A22$$

$$\gamma = \frac{V_{xx} - V_{yy}}{q} \quad V_{yy} = -\frac{1}{2} q (1 + \gamma)$$

where γ is the asymmetry parameter, the Hamiltonian becomes

$$\mathcal{H}_Q = \frac{eQq}{4I(2I-1)} \left[3 I_z^2 - I(I+1) + \gamma(I_x^2 - I_y^2) \right] \dots \quad A23$$

In systems with axial symmetry, γ is equal to zero, and the Hamiltonian may be written as

$$\mathcal{H}_Q = q' \left[I_z^2 - \frac{1}{3} I(I+1) \right] \dots \quad A24$$

where $q' = \frac{3eQq}{4I(2I-1)}$

The total spin-Hamiltonian can thus be most generally written as

$$\mathcal{H} = \beta_e \underline{H} \cdot \underline{g} \cdot \underline{S} + \underline{S} \cdot \underline{A} \cdot \underline{I} + \underline{I} \cdot \underline{P} \cdot \underline{I} \quad \dots \quad A25$$

In solutions where the rotation of the system is able to average out the anisotropic contribution to the various tensors, equation A25 can be written as

$$\mathcal{H} = g_0 \beta_e \underline{H} \cdot \underline{S} + A_0 \underline{S} \cdot \underline{I} \quad \dots \quad A26$$

APPENDIX BEIGENVALUES OF THE SPIN HAMILTONIAN

The eigenvalues of the general spin Hamiltonian derived in Appendix A can be derived by considering first the Zeeman interaction alone and then considering the hyperfine and quadrupole terms as successive perturbation. Two kinds of system will be considered here, (1) an axially symmetric system and (2) systems with lower than axial symmetry.

1. An axially symmetric system ^{2,3,4}

For the axially symmetric case, $A_x = A_y = B$ and $A_z = A$, and $g_z = g_{11}$ and $g_x = g_y = g_1$. The general spin Hamiltonian becomes

$$\mathcal{H} = g_{11}\beta_e H_z S_z + g_1\beta_e (H_x S_x + H_y S_y) + A S_z I_z + B(S_x I_x + S_y I_y) + Q' \left[I_z^2 - \frac{1}{3} I(I+1) \right] \dots B1$$

Here we have assumed that the principal axes of the g , A and Q' tensors coincide. If the applied magnetic field is at an angle θ to the z -axis a general orientation of the magnetic field can always lie in the x - z plane, so we can write

$$H_z = H \cos \theta, \quad H_x = H \sin \theta \quad \text{and} \quad H_y = 0$$

Thus the Hamiltonian B1 without the quadrupole term can be written

$$\mathcal{H} = g_{11}\beta_e \cos \theta H S_z + g_1\beta_e \sin \theta H S_x + A I_z S_z + B(I_x S_x + I_y S_y) \dots B2$$

The basic wavefunctions are of the form $|\frac{1}{2}, m_I\rangle$ and $|\frac{1}{2}, m_I\rangle$. The energy matrix can be diagonalised in the following steps. We first carry out the transformations

$$S_x = S'_z \sin \alpha + S'_x \cos \alpha$$

$$S_y = S'_y$$

$$S_z = S'_z \cos \alpha - S'_x \sin \alpha$$

and

..... B3

$$I_x = I'_z \sin \beta + I'_x \cos \beta$$

$$I_y = I'_y$$

$$I_z = I'_z \cos \beta - I'_x \sin \beta$$

where the new axes of quantisation for the electron and nuclear spins inclined at angle α and β to z axis. With these transformations the Hamiltonian becomes

$$\begin{aligned} \mathcal{H} = & \beta_e H (g_{11} \cos \theta \cos \alpha + g_1 \sin \theta \sin \alpha) S'_z + \beta_e H (g_1 \sin \theta \cos \alpha - \\ & g_{11} \cos \theta \sin \alpha) S'_x + (A \cos \alpha \cos \beta + \\ & B \sin \alpha \sin \beta) S'_z I'_z + (B \sin \alpha \cos \beta - \\ & \cos \alpha \sin \beta) S'_z I'_x + (B \cos \alpha \sin \beta - \\ & A \sin \alpha \cos \beta) S'_x I'_z + (A \sin \alpha \sin \beta + \\ & B \cos \alpha \cos \beta) S'_x I'_x + B I'_y S'_y \end{aligned}$$

..... B4

The large off-diagonal matrix elements of the electron Zeeman term and the fourth term on the right hand side of B4 will be zero if we choose α and β such that

$$g_1 \sin \theta \cos \alpha - g_{11} \cos \theta \sin \alpha = 0$$

.... B5

and

$$B \sin \alpha \cos \beta - A \cos \alpha \sin \beta = 0$$

This condition gives

$$\cos \alpha = \frac{g_{11} \cos \theta}{g} \quad \sin \alpha = \frac{g_1 \sin \theta}{g}$$

.... B6

$$\cos \beta = \frac{A g_{11} \cos \theta}{gK} \quad \sin \beta = \frac{B g_1 \sin \theta}{gK}$$

where

$$g^2 = g_{11}^2 \cos^2 \theta + g_1^2 \sin^2 \theta$$

and

$$g^2 K^2 = A^2 g_{11}^2 \cos^2 \theta + B^2 g_1^2 \sin^2 \theta$$

.... B7

Substituting in B4 leads to the Hamiltonian

$$\mathcal{H} = g \beta_e H S'_z + K S'_z I'_z + (B^2 - A^2) \frac{g_{11} g_1}{g^2 K} \sin \theta \cos \theta S'_x I'_z +$$

$$\left(\frac{AB}{K}\right) S'_x I'_x + B S'_y I'_y$$

.... B8

To calculate the eigenvalues of this Hamiltonian first-order perturbation theory can be used for the second term in the Hamiltonian and second-order perturbation theory for the third, fourth and the fifth terms.

The eigenvalues of the states $|+\frac{1}{2}, m_I\rangle$ and $|-\frac{1}{2}, m_I\rangle$ are thus calculated to be

$$\begin{aligned}
 E (' | +\frac{1}{2}, m_I \rangle ') &= \frac{1}{2} g \beta_e H + \frac{1}{2} K m_I - \frac{A^2 B^2}{4g\beta_e H K} m_I + \frac{B^2(A^2 + K^2)}{8g\beta_e H K^2} \\
 \times [I(I+1) - m_I^2] &+ \frac{(A^2 - B^2)^2}{4g\beta_e H} \left[\frac{g_{11} g_1}{g^2 K} \right]^2 \sin^2 \theta \cos^2 \theta m_I^2 \\
 &\dots B9
 \end{aligned}$$

and

$$\begin{aligned}
 E (' | -\frac{1}{2}, m_I \rangle ') &= -\frac{1}{2} g \beta_e H - \frac{1}{2} K m_I - \frac{A B^2}{4g\beta_e H K} m_I - \frac{B^2(A^2 + K^2)}{8g\beta_e H K^2} \\
 \times [I(I+1) - m_I^2] &- \frac{(A^2 - B^2)^2}{4g\beta_e H} \left[\frac{g_{11} g_1}{g^2 K} \right]^2 \sin^2 \theta \cos^2 \theta m_I^2 \\
 &\dots B10
 \end{aligned}$$

So that the energy of the transitions with $\Delta m_I = 0$ are given by

$$\begin{aligned}
 \Delta E &= g \beta_e H + K m_I + \frac{B^2(A^2 + K^2)}{4g\beta_e H K^2} [I(I+1) - m_I^2] \\
 &+ \frac{(A^2 - B^2)^2}{2K^2} \left(\frac{g_{11} g_1}{g^2} \right)^2 \frac{\sin^2 \theta \cos^2 \theta}{g \beta_e H} m_I^2 \\
 &\dots B11
 \end{aligned}$$

The $(2l+1)$ lines in the spectra are separated by K to the first order. The second-order terms lead to unequal spacing of the hyperfine lines and to displacement of the centre of the spectra from $g \beta_e H$.

The quadrupole term in the general spin Hamiltonian can now be treated by applying second-order perturbation theory to the eigenfunctions of the Zeeman plus hyperfine interaction Hamiltonian. Substituting for I_z from B3 the quadrupole term becomes

$$\mathcal{H} = Q' \left[I_z'^2 \cos^2 \beta - \frac{1}{3} I(I+1) - \sin \beta \cos \beta (I_z' I_x' + I_x' I_z') + I_x'^2 \sin^2 \beta \right]$$

.... B12

This can be written in the usual form

$$\mathcal{H} = \left(\frac{Q'}{2} \right) \left[I_z'^2 - \frac{1}{3} I(I+1) \right] \left[3 \cos^2 \beta - 1 \right] - Q' \left[I_z' I_x' + I_x' I_z' \right] \sin \beta \cos \beta +$$

$$\left(\frac{Q'}{4} \right) \left[I_x'^2 - I_y'^2 \right] \sin^2 \beta$$

.... B13

Substituting for $\cos \beta$ and $\sin \beta$ from B6 we finally obtain the Hamiltonian

$$\mathcal{H} = \left(\frac{Q'}{2} \right) \left[(3A^2 g_{11}^2 / g^2 K^2) \cos^2 \theta - 1 \right] \left[I_z'^2 - \frac{1}{3} I(I+1) \right]$$

$$- Q' (AB g_{11} g_1 / g^2 K^2) \sin \theta \cos \theta \left[I_z' I_x' + I_x' I_z' \right]$$

$$+ \left(\frac{Q'}{4} \right) (B^2 g_1^2 / g^2 K^2) \sin^2 \theta \left[I_x'^2 - I_y'^2 \right]$$

.... B14

The eigenvalues of this Hamiltonian for our basis state

$|m_S, m_I\rangle$ can be written

$$E = \left(\frac{Q'}{2} \right) \left[(3A^2 g_{11}^2 / g^2 K^2) \cos^2 \theta - 1 \right] \left[m_I^2 - \frac{1}{3} I(I+1) \right]$$

$$- \frac{Q'^2}{2K m_S} (AB g_{11} g_1 / g^2 K^2)^2 (\sin^2 \theta \cos^2 \theta) m_I \left[4I(I+1) - 8m_I^2 - 1 \right]$$

$$+ \frac{Q'^2}{8K m_S} (B^2 g_1^2 / g^2 K^2)^2 (\sin^4 \theta) m_I \left[2I(I+1) - 2m_I^2 - 1 \right]$$

.... B15

The spectrum shows no effects from the first term because the energy of states connected by $\Delta m_I = 0$ transitions are shifted equally. The second and third terms of B15 mix respectively states $|m_S, m_I \pm 1\rangle$ and $|m_S, m_I \pm 2\rangle$ with $|m_S, m_I\rangle$ and both $\Delta m_I = \pm 1$ and $\Delta m_I = \pm 2$ transitions become weakly allowed so that the energy of the states are shifted unequally. The analysis of quadrupole splitting is helped by the appearance of forbidden transitions making no difficulty of sorting out the effect of the quadrupole coupling from those of second-order hyperfine interactions. The frequency increments arising from quadrupole effects for transitions with $\Delta m_I = 0$ are given by

$$\Delta E = - \frac{2Q'{}^2}{K} (ABg_{11}g_1/g^2K^2)^2 (\sin^2\theta \cos^2\theta) m_I [4I(I+1) - 8m_I^2 - 1]$$

$$+ \frac{Q'{}^2}{2K} (B^2g_1^2/g^2K^2)^2 (\sin^4\theta) m_I [2I(I+1) - 2m_I^2 - 1]$$

.... B16

Combining B16 with B11 the result gives ΔE for the allowed $\Delta m_S = \pm 1$, $\Delta m_I = 0$ transitions, including quadrupole effects and second-order hyperfine interactions

$$\begin{aligned}
\Delta E = & g\beta_e H + K m_I + \frac{B^2(A^2+K^2)}{4g\beta_e HK^2} [I(I+1) - m_I^2] \\
& + \frac{(A^2-B^2)^2}{2K^2} \left(\frac{g_{11} g_1}{g^2}\right)^2 \frac{\sin^2\theta \cos^2\theta}{g\beta_e H} m_I^2 \\
& - \frac{2Q'^2}{K} (AB g_{11}g_1/g^2K^2)^2 (\sin^2\theta \cos^2\theta)_{m_I} [4I(I+1)-8m_I^2-1] \\
& + \left(\frac{Q'^2}{2K}\right) (B^2 g_1^2/g^2K^2)^2 (\sin^4\theta)_{m_I} [2I(I+1)-2m_I^2-1]
\end{aligned}$$

.....B17

or, in terms of the usual experimental arrangement, the resonant fields are given by

$$\begin{aligned}
H=H^0-Km_I - & \frac{B^2 g_1^2}{4Hg^2} \left[\frac{A^2 g_{11}^2 + K^2 g^2}{K^2 g^2} \right] [I(I+1) - m_I^2] \\
& - \frac{1}{2H} \left[\frac{A^2 g_{11}^2 - B^2 g_1^2}{Kg^2} \right]^2 \left[\frac{g_{11} g_1}{g^2} \right]^2 \sin^2\theta \cos^2\theta m_I^2 \\
& + \frac{2Q'^2 g_1^2 \cos^2\theta \sin^2\theta}{Kg^2} \left[\frac{ABg_{11}^2 g_1^2}{K^2 g^4} \right]^2_{m_I} [4I(I+1)-8m_I^2-1] \\
& - \frac{Q'^2 g_1^2 \sin^4\theta}{2Kg^2} \left[\frac{B g_1^2}{Kg^2} \right]^4_{m_I} [2I(I+1)-2m_I^2-1]
\end{aligned}$$

..... B18

where all coupling constants are expressed in gauss.

2. A system with symmetry lower than axial^{1,4}

In this case the magnetic field is in any arbitrary direction. We use the same procedure as before. The general spin-Hamiltonian now can be written

$$\begin{aligned} \mathcal{H} = & g_x \beta_e H_x S_x + g_y \beta_e H_y S_y + g_z \beta_e H_z S_z + A_x I_x S_x + A_y I_y S_y \\ & + A_z I_z S_z + P_x I_x^2 + P_y I_y^2 + P_z I_z^2 \end{aligned}$$

..... B19

Again we have assumed that the principal axes of the g , A and P tensors coincide.

The direction of the applied field H will be given by the direction cosines l , m and n with respect to the principal tensors axes, x , y and z , i.e., $H_x = lH$, $H_y = mH$, and $H_z = nH$. The problem can be examined by considering first the Zeeman interaction alone.

$$\mathcal{H} = g \beta_e H \cdot S = g_x \beta_e l S_x H + g_y \beta_e m S_y H + g_z \beta_e n S_z H$$

..... B20

The energy matrix can be diagonalised with respect to the Zeeman term by carrying out the transformation

$$\begin{aligned} S_x &= a_{11} S'_x + a_{12} S'_y + a_{13} S'_z \\ S_y &= a_{21} S'_x + a_{22} S'_y + a_{23} S'_z \\ S_z &= a_{31} S'_x + a_{32} S'_y + a_{33} S'_z \end{aligned}$$

..... B21

If the direction cosines of z' with respect to the x , y and z axes are defined to be $g_{xx}^{-1} l g^{-1}$, $g_{yy}^{-1} m g^{-1}$ and $g_{zz}^{-1} n g^{-1}$ the Zeeman term becomes

$$\mathcal{H} = g \beta_e H S'_z$$

If the electron spin functions are quantised with respect to the z' axis, these functions can become eigenfunctions

of the Zeeman part of the Hamiltonian, with energies of $\pm \frac{1}{2} g \beta_e H$. Where g is given by the direction cosines

$$g = g_{xx}^2 l^2 + g_{yy}^2 m^2 + g_{zz}^2 n^2 \quad \dots B22$$

The transformed hyperfine term in the Hamiltonian now becomes

$$\begin{aligned} &= S'_x (a_{11} A_{xx} I_x + a_{21} A_{yy} I_y + a_{31} A_{zz} I_z) + S'_y (a_{12} A_{xx} I_x + a_{22} A_{yy} I_y + \\ &\quad a_{32} A_{zz} I_z) + S'_z (a_{13} A_{xx} I_x + a_{23} A_{yy} I_y + a_{33} A_{zz} I_z) \end{aligned} \quad \dots B23$$

We shall now return and consider the hyperfine term using non-degenerate perturbation theory. Similarly the energy matrix can be diagonalised by carrying out a second transformation for the nuclear spin of the form

$$\begin{aligned} I_x &= b_{11} I'_x + b_{12} I'_y + b_{13} I'_z \\ I_y &= b_{21} I'_x + b_{22} I'_y + b_{23} I'_z \\ I_z &= b_{31} I'_x + b_{32} I'_y + b_{33} I'_z \end{aligned} \quad \dots B24$$

If we define the coefficients in B24 so that z'' has direction cosines with respect to the x , y and z axes of $a_{13} A_{xx} A^{-1}$, $a_{23} A_{yy} A^{-1}$ and $a_{33} A_{zz} A^{-1}$, the term in S'_z in the transformed Hamiltonian has the form $AS'_z I'_z$.

If the nuclear spin functions are quantised with respect to the z' axis, the term $AS'_z I'_z$ has only diagonal matrix elements, and to first order the hyperfine terms reduce to $Am_S m_I$. Where A is given by direction cosines

$$A^2 = (g_{xx}^2 l^2 A_{xx}^2 + g_{yy}^2 m^2 A_{yy}^2 + g_{zz}^2 n^2 A_{zz}^2) g^{-2}$$

.... B25

The quadrupole term in the Hamiltonian can be treated by the same technique as before by using second-order perturbation theory.

With all these transformations we can derive expressions for the energy of the state $|m_S, m_I\rangle$ and for the allowed transitions of the form $\Delta m_S = \pm 1$,

$$\Delta m_I = 0$$

$$\begin{aligned} \Delta E = g \beta_e H + Am_I + \frac{1}{4g\beta_e H} \left\{ [A_1(m_I^2 - I(I+1))] + 2 A_2 m_I^2 \right\} \\ + \frac{1}{2A} \left\{ [P_1(18I(I+1) - 34m_I^2 - 5)] + P_2 [2I(I+1) - 2m_I^2 - 1] \right. \\ \left. - P_3 [20 I (I+1) - 36 m_I^2 - 6] \right\} \end{aligned} \quad \text{.... B26}$$

where

$$A_2 A^2 g^2 = (A_{xx}^2 - A_{yy}^2)^2 g_{xx}^2 g_{yy}^2 l^2 m^2 + (A_{yy}^2 - A_{zz}^2)^2 g_{yy}^2 g_{zz}^2 m^2 n^2 \\ + (A_{xx}^2 - A_{zz}^2)^2 g_{xx}^2 g_{zz}^2 l^2 n^2$$

$$A_1 A^2 g^4 = (A_{xx}^2 A_{yy}^2 g_{zz}^2 n^2 + A_{yy}^2 A_{zz}^2 g_{xx}^2 l^2 + A_{xx}^2 A_{zz}^2 g_{yy}^2 m^2) \\ - g^2 (A_{xx}^2 A_{yy}^2 + A_{xx}^2 A_{zz}^2 + A_{yy}^2 A_{zz}^2)$$

$$P_1 A^4 g^4 = (A_{xx}^2 P_{xx} g_{xx}^2 l^2 + A_{yy}^2 P_{yy} g_{yy}^2 m^2 + A_{zz}^2 P_{zz} g_{zz}^2 n^2)$$

$$P_2 = (P_{xx}^2 + P_{yy}^2 + P_{zz}^2) - 2 (P_{xx}^2 P_{yy}^2 A_{zz}^2 g_{zz}^2 n^2 + P_{yy}^2 P_{zz}^2 A_{xx}^2 g_{xx}^2 l^2 \\ + P_{zz}^2 P_{xx}^2 A_{yy}^2 g_{yy}^2 m^2) A^{-2} g^{-2}$$

$$P_3 A^2 g^2 = (P_{xx}^2 A_{xx}^2 g_{xx}^2 l^2 + P_{yy}^2 A_{yy}^2 g_{yy}^2 m^2 + P_{zz}^2 A_{zz}^2 g_{zz}^2 n^2)$$

..... B27

In the case where the applied field lies along the direction of principal axes equation B26 reduces to

$$\Delta E = g_{ij} \beta_e H + A_{ii} m_I + \frac{(A_{jj}^2 + A_{kk}^2)}{4g_{ii} \beta_e H} [I(I+1) - m_I^2] \\ + m_I \frac{(P_{kk} - P_{jj})^2}{2A_{ii}} [2I(I+1) - 2m_I^2 - 1] m_I \quad \text{..... B28}$$

and the resonance fields are given by

$$H_i = H_0 - a_{ii} m_I - \frac{(a_{jj}^2 + a_{kk}^2)}{4H_i} [I(I+1) - m_I^2] \\ - \frac{(P_{jj} - P_{kk})^2}{2a_{ii}} [2I(I+1) - 2m_I^2 - 1] m_I \quad \text{..... B29}$$

where the various parameters are in gauss.

APPENDIX CLINE SHAPES FOR ELECTRON PARAMAGNETIC RESONANCE
SPECTRA OF MAGNETICALLY DILUTE GLASSES OR POLY-
CRYSTALLINE SAMPLES

In glasses or in magnetically dilute polycrystalline samples, there are a large number of crystallites randomly oriented with respect to the applied magnetic field. Thus the observed e.p.r. spectrum is the summation of all possible spectra, each one weighted by the probability of obtaining that particular orientation. As a result of the anisotropy in the g and hyperfine tensor, magnetic resonance absorption therefore occurs over a wide range of magnetic fields. The analytical expressions describing the forms of the spectra obtained in these cases have been deduced by Kneubühl.¹

Kneubühl assumes that the probability of any e.p.r. transition occurring is independent of the orientation of the crystallite in the magnetic field. This approximation is not valid in general² but it is satisfactory for rhenium and manganese complexes. With this assumption the probability that an electron absorbs microwave radiation at a given field H is proportional to the probability of finding this species in a suitable orientation with respect to the magnetic field such that it undergoes a transition when this

value of H is reached. The problem then reduces to an estimation of the probability that a crystallite lies in each orientation.

Different types of characteristic spectra are obtained from different kinds of system. Consider first the e.p.r. spectra of polycrystalline samples of ions with $S = \frac{1}{2}$ and no hyperfine interaction present. Two kinds of system will be discussed: (i) an axially symmetric system and (ii) systems with symmetry lower than axial.

1. An axially symmetric system

The probability that the axis of symmetry lies in the angular range θ to $\theta + d\theta$ with respect to the applied field H is $d(\cos \theta)$. Let the normalised line shape function which describes the intensity of the absorption as a function of H be $S(H)$. Then, for resonance, it can be shown that

$$h\nu = \beta_e g_{\text{eff}} H = \beta_e H [g_{11}^2 \cos^2 \theta + g_1^2 \sin^2 \theta]^{\frac{1}{2}}$$

i.e.
$$\cos \theta = (g_{11}^2 - g_1^2)^{-\frac{1}{2}} [(h\nu)^2 (\beta_e H)^{-2} - g_1^2]^{\frac{1}{2}}$$

..... C1

A crystallite whose axis of symmetry lies in the angular range θ to $\theta + d\theta$ contributes to the e.p.r. absorption spectrum within H and $H + dH$. Hence if $S(H)$ and the probability are both normalised,

$$S(H) dH = d(\cos \theta)$$

$$\begin{aligned} \therefore S(H) &= \frac{d(\cos \theta)}{dH} \\ &= - (g_{11}^2 - g_1^2)^{-\frac{1}{2}} \left[(h\nu)^2 (\beta_{eH})^{-2} - g_1^2 \right]^{-\frac{1}{2}} (h\nu)^2 \beta_e^{-2} H^{-3} \end{aligned}$$

..... C2

$$\text{when } \theta = 0^\circ \text{ then } h\nu = g_{11} \beta_{eH_{11}}$$

$$\therefore g_{11} = \frac{h\nu}{\beta_{eH_{11}}}$$

$$\text{when } \theta = 90^\circ \text{ then } h\nu = g_1 \beta_{eH_1}$$

$$\therefore g_1 = \frac{h\nu}{\beta_{eH_1}}$$

$$\text{So that } S(H) = H_{11}^2 (H_1^2 - H^2)^{-\frac{1}{2}} H^{-2} (H_1^2 - H^2)^{-\frac{1}{2}} \quad \text{..... C3}$$

The line shape function $S(H)$ and its derivatives are plotted below, in Figure C1

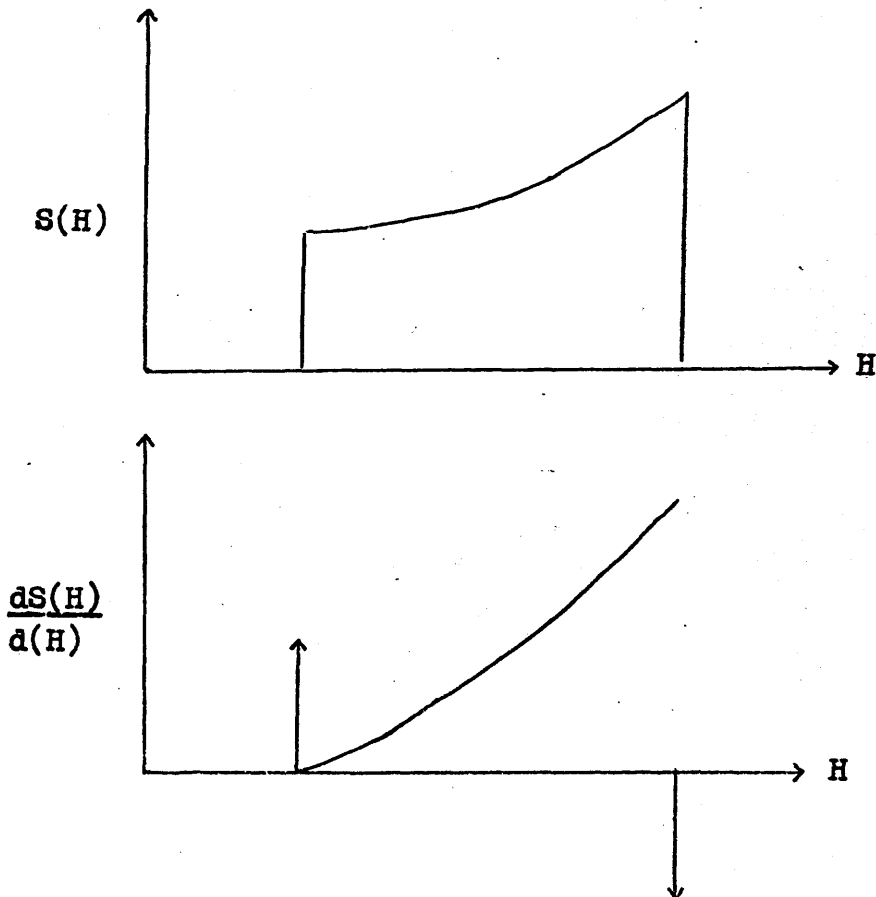


Figure C1.

So far it has been assumed that

- i) the probability that a transition takes place is independent of the orientation of a crystallite in the field, and
- ii) the absorption lineshape function for each crystallite is a delta function i.e. infinitely sharp absorption.

In fact it can be shown³ that the probability that a given transition will take place is proportional to

$$g_1^2 \left[g_{11}^2 g^{-2} + 1 \right]$$

Absorption lineshape functions are not delta functions, but may be Lorentzian or Gaussian in nature. It is a reasonably good approximation to take the lineshape function for polycrystalline samples to be Gaussian. This has the form

$$Y(H - H_0) = (2\pi)^{-\frac{1}{2}} \beta^{-1} \exp \left[-(H-H_0)^2 / 2\beta^2 \right]$$

.... C4

where the width of the line is controlled by the broadening parameter β . The effect of this is to broaden the lines in the absorption spectrum so that a resonance centred at H contributes to the absorption at H' , an amount given by

$$S(H) dHY(H'-H)$$

Hence the total absorption intensity at H' is the sum

of all these contributions, i.e.

$$\begin{aligned}
 S(H') &= \sum_{H=H_{11}}^{H=H_1} S(H) Y(H'-H) dH \\
 &= \int_{H=H_{11}}^{H=H_1} S(H) Y(H'-H) dH \\
 &= (2\pi)^{-\frac{1}{2}} \beta^{-1} \int_{H=H_{11}}^{H=H_1} S(H) \exp[-(H'-H)^2 (2\beta^2)^{-1}] dH \quad \dots\dots C5
 \end{aligned}$$

The derivative of this function can easily be shown to be

$$\frac{dS(H')}{dH'} = (2\pi)^{-\frac{1}{2}} \beta^{-3} \int_{H_{11}}^{H_1} (H-H') S(H) \exp[-(H'-H)(2\beta^2)^{-1}] dH \quad \dots\dots C6$$

The lineshape function $S(H')$ and its derivative are shown in Figure C2.

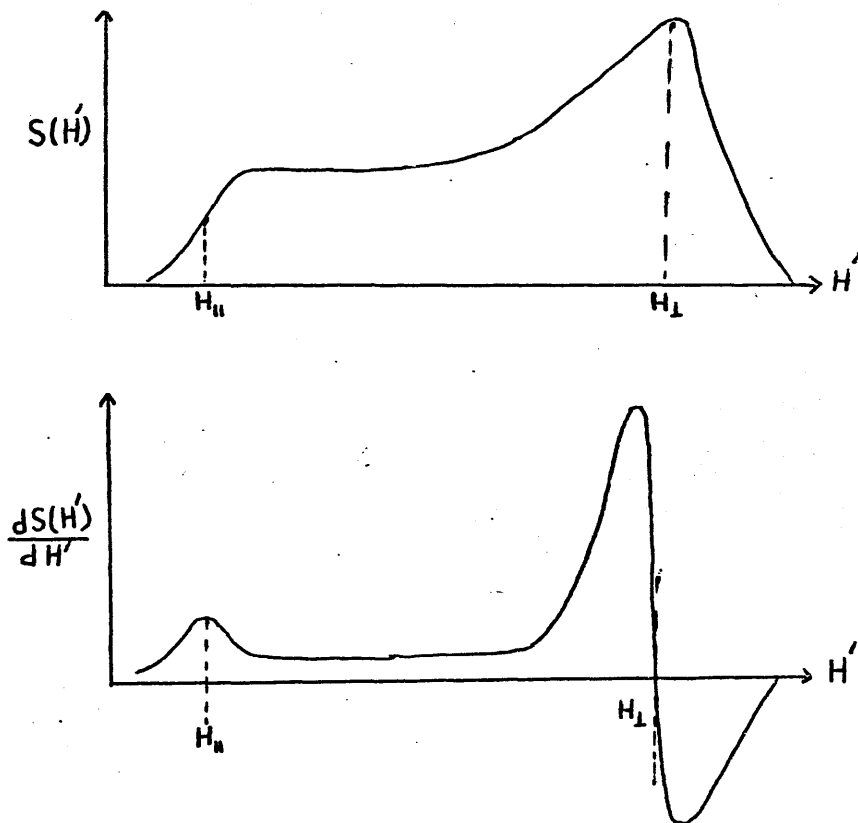


Figure C2.

Thus it is possible from such spectra to obtain values of the absorption fields H_{11} and H_1 , and hence to obtain values of g_{11} and g_1 .

Effects of hyperfine interaction

If the electron now interacts with a nucleus of spin quantum number (say) $I = \frac{1}{2}$, the resonance spectrum is a superposition of two curves of the type shown in Figure C2. When $A_{11} \neq A_1$ the broadened absorption curve, and its derivative are shown in Figure C3.

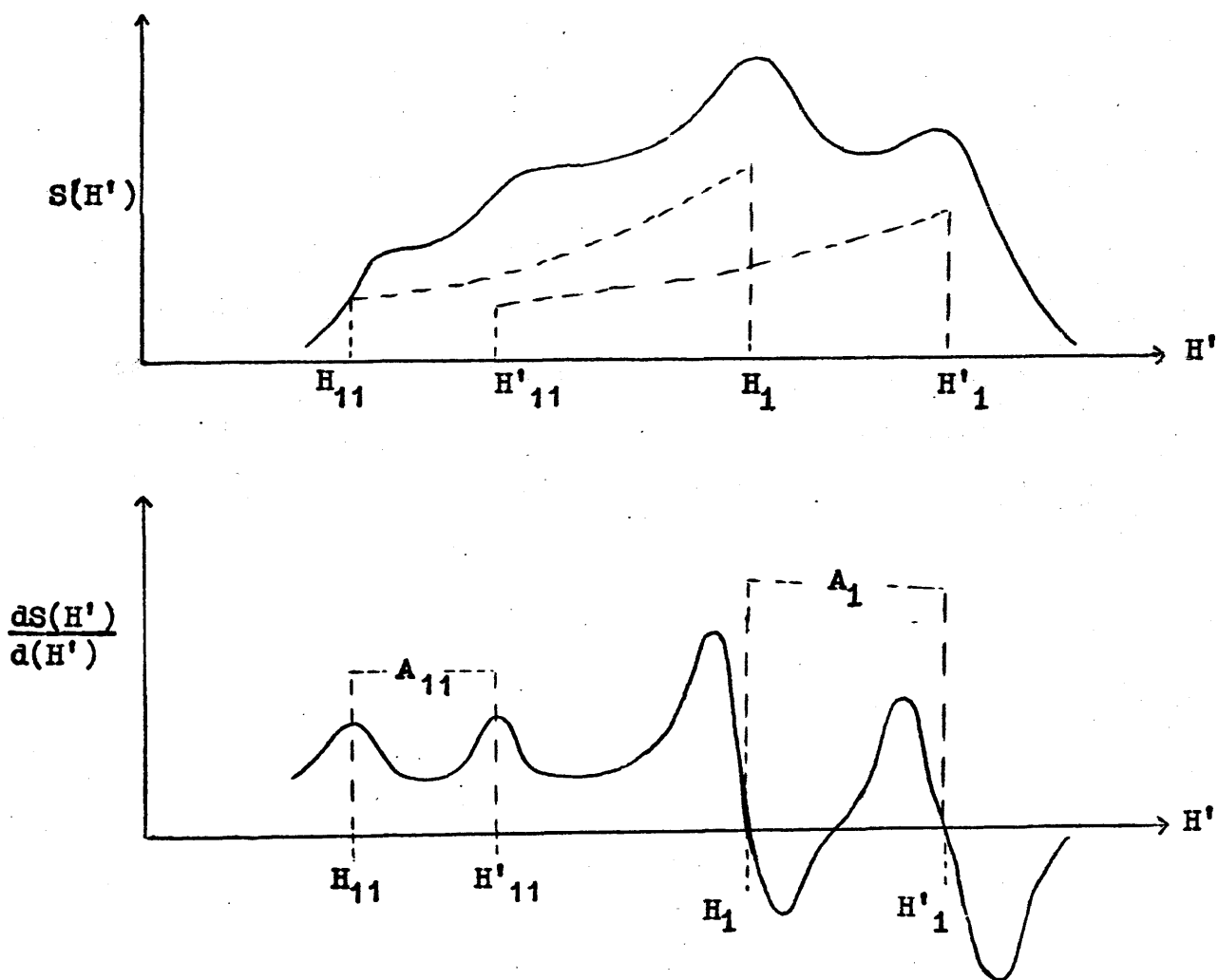


Figure C3

In more complicated systems it has been shown, that certain combinations of g-factors and hyperfine coupling constants cause singularities to appear in the function

$S(H')$ and hence cause extra peaks, "polycrystalline peaks" to appear in the derivative spectrum ^{4,5}.

2. A system with symmetry lower than axial

For a system with less than axial symmetry the analysis has a similar form although now two orientation angles are required to specify the field direction with respect to the x, y and z axes of the g-tensor. This leads to a considerable increase in the complexity of the expressions obtained for the lineshape.

As a result, there is a range of combinations of the two orientation angles which lead to resonance at a particular field, and consequently the amplitude of absorption depends on the probability of the molecule having any one of a combination of orientation angles which lead to resonance at a particular field.

The lineshape function has the form below for $H_{33} < H_{22} < H_{11}$

1. In the interval $H_{11} \geq H \geq H_{22}$

$$S(H) = \frac{2H_{11} H_{22} H_{33}}{\pi H^2 (H_{11}^2 - H_{22}^2)^{\frac{1}{2}} (H^2 - H_{33}^2)^{\frac{1}{2}}} K(1') \quad \dots C7$$

2. In the interval $H_{22} \geq H \geq H_{33}$

$$S(H) = \frac{2 H_{11} H_{22} H_{33}}{\pi H^2 (H_{22}^2 - H_{33}^2)^{\frac{1}{2}} (H_{11}^2 - H^2)^{\frac{1}{2}}} K(1) \quad \dots C8$$

Where $K(l)$ is the standard elliptic integral

$$K(l) = \int_0^{\pi/2} \frac{dx}{(1-l^2 \sin^2 x)^{1/2}}$$

$$= \frac{\pi}{2} \left[1 + \left(\frac{1}{2}\right)^2 l^2 + \left(\frac{1 \cdot 3}{2 \cdot 4}\right) l^4 + \dots \right]$$

.... C9

and

$$(l')^2 = \frac{1}{l^2} = \frac{(H_{11}^2 - H_{22}^2)(H^2 - H_{33}^2)}{(H_{11}^2 - H^2)(H_{22}^2 - H_{33}^2)}$$

.... C10

Thus the function $S(H)$ has discontinuities at $H=H_{11}$ and at H_{33} for absorption between H_{11} and H_{33} . The function becomes infinite at $H=H_{22}$, where l and l' both equal one, and the elliptic integrals expand to infinity. Again the function $S(H)$ gives the form of the unbroadened lineshape. The broadened lineshape function, $S(H')$, and its derivative are shown in Figure C4.

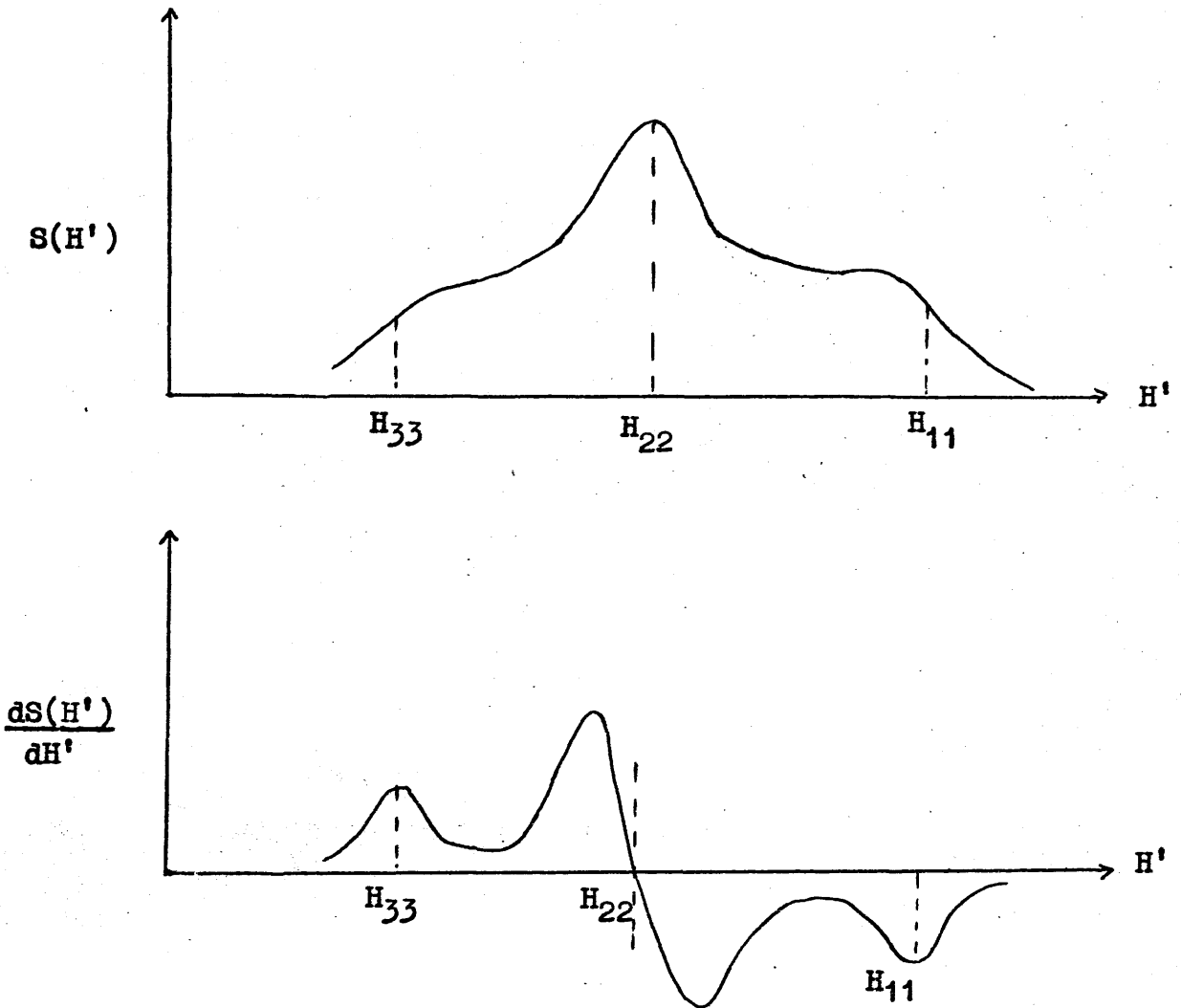


Figure C4

By measurements of H_{11} , H_{22} and H_{33} from the spectrum, the g -tensor components can be obtained.

Effect of hyperfine interaction

As before, if the electron interacts with a nucleus of spin quantum number I , $(2I+1)$ patterns of the above type will be obtained from which it may be possible to obtain the principal components of the hyperfine tensor if they are resolved.

ReferencesAppendix A

1. A. Abragam and M.H.L.Pryce, Proc.Roy.Soc.(A), 1951, 205, 135.
2. B.R.McGarvey, "Transition Metal Chemistry", R.L.Carlin ed., Edward Arnold, London, 1966, 3, 97.
3. A. Carrington and A.D. McLachlan, "Introduction to Magnetic Resonance", Harper and Row, 1967, Chapter 9.
4. H.A. Kramers, Proc.Acad.Sci. Amsterdam, 1930, 33, 953.
5. N.M. Atherton, "Electron Spin Resonance", Ellis Horwood, London, 1973.
6. C.P.Slichter, "Magnetic Resonance", Harper and Row, New York, 1963, 160.

Appendix B

1. P.M.Golding, "Applied Wave Mechanics", Van Nostrand, New York, 1969, 452.
2. N.M. Atherton, "Electron Spin Resonance", Ellis Horwood, London, 1973, Chapter 7.
3. B.Bleaney, Phil.Mag., 1951, 42, 441.
4. A. Abragam and B.Bleaney, "Electron Paramagnetic Resonance in Transition Ions", Clarendon Press, Oxford, 1970, Chapter 3.

Appendix C

1. F.K. Kneubühl, J.Chem.Phys., 1960, 33, 1074.
2. J.R.Pilbrow, Mol.Phys., 1969, 16, 307.
3. B.Bleaney, Proc.Phys.Soc.(London), 1960, 75, 621.
4. R.Neiman and D.Kivelson, J.Chem.Phys., 1961, 35, 156.
5. H.R.Gersmann and J.D. Swalen, J.Chem.Phys., 1964, 36, 3221.